DOE/ET-53088-334

IFSR #334

Trapped Particle Instability and Flute Instability in Tandem Mirror; Scale Separation Closure in Alfvén Wave Turbulence

Changye Chen

Institute for Fusion Studies
The University of Texas at Austin
Austin, Texas 78712

August 1988

Trapped Particle Instability and Flute Instability in Tandem Mirror; Scale Separation Closure in Alfven Wave Turbulence

APPROVED BY

SUPERVISORY COMMITTEE:

Robert L Berger

Swadesh M Mahajan

John D. Ballard

Dedicated to

my wife and my daughters

Trapped Particle Instability and Flute Instability in Tandem Mirror; Scale Separation Closure in Alfven Wave Turbulence

by

Changye Chen

DISSERTATION

Presented to the faculty of the Graduate school of

The Uneversity of Texas at Austin

in Partial fulfillment

of the Requirements

for the Degree of

DOCTOR OF PHILOSOPHY

THE UNIVERSITY OF TEXAS AT AUSTIN

(August 1988)

Acknowledgments

It has been a great honor and privilege to collaborate with and learn from Prof. Herbert Berk and Dr. Swadesh Mahajan. Without their many productive suggestions during numerous discussions, this dissertation would not have been possible. Their guidance, patience and knowledge are deeply appreciated.

I am very grateful to Prof. Marshall Rosenbluth, Prof. Richard Hazeltine, Prof. Wendell Horton, Prof. John Dollard, Prof. Patrick Diamond, Dr. Vernon Wong and Dr. James Van Dam for giving me a chance to learn from them during their various classroom lectures.

I wish to thank Dr. Yang-Zhong Zhang, Ms. Marcia Engquist, Dr. G.Y. Fu Mr. Wann-Quan Li as well as many other fellow graduate students for their warm friendship and support over the last several years.

I also wish to express my gratitude towards technical staff members of the Institute for Fusion Studies for all the assistance they have given me. In particular, I thank Carolyn Valentine, Salalyn Stewart and Joyce Patton.

I would like to thank Dr. T.D. Lee for his initiation of the CASPEA program, that brought me to UT at Austin to enter the Graduate School.

Finally I would like to express my indebt to my wife and daughters for their continuous support and comprehension during all these years.

TABLE OF CONTENTS

Part A

Trapped Particle Instability and Flute Instability

in Tandem Mirror

Part B

Scale Closure Scheme in Alfven

Wave Turbulence

LIST OF FIGURES

Trapped Particle Instability and Flute Instability in Tandem Mirror; Scale Separation Closure in Alfvén Wave Turbulence

Changye Chen

ABSTRACT NOT AVAILABLE

Part A:

Trapped Particle Instability and Flute Instability In Tandem Mirror

Chapter I. Introduction

Tandem mirrors have been one of the major concepts on which fusion research is carried out. The idea of tandem mirrors is aimed at providing significant improvements over simple axisymmetric mirror machines. This part of the dissertation is devoted to investigate the underlying physics of tandem mirrors, particularly the stability properties.

It has been well-known that simple axisymmetric mirrors have obvious shortcomings. A device having the open magnetic field and axisymmetric configuration must have convex magnetic curvature at its mid-plane[1], so the equilibrium structure of the machines does not satisfy the fundamental MHD stability principle[2], which demands the confined plasma have min-B configuration (at least in the average sense). Both theoretical analysis and experimental data have indicated the existence of the MHD fast-growing interchange modes in the machines[3-5]. In addition to the instability problem, a single-cell mirror machine loses its plasma in a relatively fast time scale even as in a min-B mirror field. Particles in the loss-cone are not trapped by the equilibrium field and the collisions constantly scatter more particles into the loss-cone. The particle-loss process has to be compensated by particle injection from the outside machine. The detailed calculation[6] shows that the factor Q

(roughly defined as a ratio of the energy output to the energy input) is at best maginally bigger than 1, which makes the mirrors economically not acceptable.

The concept of the tandem mirror was proposed[7,8] as an attempt to overcome the particle lifetime problem. Magnetic quadrupoles, which have favorable concave curvature, are added at both ends of a long conventional mirror to anchor the inside plasma against MHD instability. The positive ambipolar potential, which is created by more rapid electron loss, peaks in the added anchor cells and "plugs" the ions inside the central cell to avoid further loss. For the whole machine the particle loss can be lowered to a much more acceptable level and the factor Q enhanced about an order of magnitude. Favorable MHD stability features arises because the global curvature averaged over the whole field line can be concave, which can help to suppress the most dangerous MHD interchange modes.

Many innovative ideas were also put forward to gain further improvements on the basic tandem mirror configuration. Among them, employing a thermal barrier and having hot particle ring were investigated.

The quadrupole field cells, although they effectively form min-B configurations, require rather complicated external coils (like ying-yang coils or baseball-shape coils). Since the fields are not axisymmetric, the induced radial transport deteriorates the energy confinement of the machines[9-11]. One promising alternative is to utilize the energetic particles, particularly hot electrons, to create a min-B configuration for the

background plasma. As their rapid drift motion through the plasma does not allow them to respond to slow MHD motion, the mechanism of the hot electrons might decouple from the core plasma. Since the energetic particles have diamagnetic nature, a concave magnetic field can be established inside the plasma without breaking the axisymmetry. The initial approach was promoted by Christofilis[12] for the Astron concept, and continued by Fleischmann.[13] The application to tandem mirrors has also been proposed and evaluated.[14]

It is trivial to show the MHD stable system can be achieved if the hot electron current is treated as a rigid non-interacting ring[15,16]. However, the complete picture is not that simple. Krall[17] and Berk[18] studied the interchange modes with the existence of the hot particles and concluded that the ratio n_h/n_i can not be too large for stability. Lee-Van Dam[19] and Nelson[20] observed that there is an upper limit for the background plasma beta to keep the decoupling condition valid. It is also pointed out[21] that negative energy wave related to the energetic particles may exist and be excited. However, a thorough investigation is beyond the context of this dissertation and refered to the references (for instance, see Ref. 22). In this thesis, we check the decoupling condition simply by calculating the grad-B drift frequency of hot electrons to see whether it exceeds the typical MHD frequency. After justifying this condition, we take full credit of stabilizing effects of hot electrons, which include the curvature enhancement and charge uncovering mechanism.

Physics in the tandem mirrors has its own characteristics compared to that in the closed (toroidal) system. The density gradient and temperature gradient exist along the field line as well as across the field line. The longitudinal physics appears to be very important in tandem mirror analysis. The ambipolar potential, though desirable for confinement, leads to a major density difference between the central cell and anchor cells. It was concluded[23-25] that the density of the plasma inside follows a Boltzmann-type law. Then the density of the anchor cells has to be higher than that of the central cell by an order of magnitude or more. With a motivation to ease the critical requirements for the machine, Baldwin and Logan[26] proposed to set up a negative potential well between the central cell and the anchor cells. The potential is supposed to reduce the passing electrons so as the thermal contact between the cells. Combining the "thermal barrier" operation with appropriate electron heating in the anchor cell, the requirements for the tandem mirror can be lowered significantly. The schemes to form the thermal barrier were studied both theoretically and experimentally.

Experimental devices like TARA and TMX-U are designed to be the tandem mirror configurations and can be used to study the fundamental physics of the tandem mirror and the relavent innovative ideas (the basic configurations of both machines are in the Fig. 2 and Fig. 3). In both the devices, the so-called "sloshing" ion injection has been employed to create the thermal barrier and the electron cyclotron heating in the anchor

region is also arranged with motivation to verify the stabilizing effects of of hot electron ring.

Observation[27,28] in both experiments shows that the plasma in the machine is sometimes subject to a low frequency oscillation. In TMX-U, the modes, coherent $m = 1$ and the mode frequency $f \approx 3 - 7KHz$, appear particularly when the ion cyclotron heating or neutral beam injection heating in the central cell are on. Experimental data exhibits the modes during the electrostatic plugged and unplugged operation and the disturbance can be detected in the central cell as well as in the anchor cell. However, in most operations, these oscillations were purposely avoided by reducing the heating of the central cell ions.

To investigate the origin of this mode is quite important. The operation at high central cell density requires increasing the heating to reduce Coulomb collisional filling of the thermal barrier. Thus, it is crucial to know whether there is intrinsic conflict between controlling this mode and having an effective "thermal barrier".

There were two approaches to study the instability. One is to assume the modes are basicly a flute-like oscillation, and then the MHD theory (sometimes including a few kinetic corrections) is employed to examine the mode features. Another one is to speculate the modes can be the trapped particle modes and then a kinetic formalism is used.

Previous MHD investigations[29,30] concluded that the conventional interchange modes has been stabilized in the tandem mirror and can not

account for the observed instability. Except near the maximum central-cell beta, the ratio of the central-cell beta to the anchor hot-ion beta was not a constant at the stability limit and was smaller than the theoretical limit. Usually, the hot-electron beta greatly exceeded the ion beta in the anchor, further increasing the discrepancy with MHD theory. Neglecting the hot-electron beta, the data at higher central-cell beta (therefore higher density and lower potential) were consistent with stability limited by MHD interchange, but much of the data were unstable at as much as an order of magnitude below the MHD limit.

Recently, there was an attempt[31] to interprete the modes based on a MHD stability analysis. By including the decoupling effect of the energetic particles and $E \times B$ rotation effect, the theory seemingly finds the results which are relatively consistent with the experimental observations in the TMX-U machine . The major driving force to the $m = 1$ flute-like mode is $E \times B$ rotation and the central-cell unfavorable curvature. The modes can be destablized when ion charge uncovering caused by the finite Larmor radius cancel the negative effects of the hot-electron charge uncovering. The theory predicts a mode frequency and instability threshold, which is somewhat larger than experimental results by a factor 2.

Nonetheless, the possibility of the trapped particle modes can not be excluded. Theoretically, if the number of passing particles is too small and the connection between the central cell and anchor cells is too weak, the convex curvature in the central cell will definitely drive an instability.

The increase of the central cell beta by heating puts more weight on unfavorable curvature of the central cell so that the instability is more likely. In the observation of TMX-U experiments, the modes really tends to be strong when the ambipolar potential in the anchor cells becomes higher.

In the early classical paper on the trapped particle modes by Berk et al[32], a variational structure of the linear dispersion for tandem mirrors has been used to study the relation between the MHD flute modes and trapped particle modes. The discussion was developed to analyze the tandem mirrors where axicells are interposed to produce the thermal barrier. The paper shows that in tandem mirrors with the axicell thermal barrier the growth rate of the trapped particle modes can approach that of the MHD instability. In addition, the study uncovers several specific effects such that the kinetic charge uncovering dynamics can provide a potential stabilization for the system and that the equilibrium $E \times B$ drift, if large enough, may cause a flute-like instability. Those analyses, though based on the collisionless theory, remain instructive and qualitatively correct in our discussion.

The theory was extended into the collisional regime.[33,34] Introducing the collisional effect alters the quantitative characteristics of the modes and, more importantly, revealed a dissipative mechanism, in which the negative energy modes can be destabilized, and a relaxing mechanism which can equilibrate the microdistribution of the different cells. The

analyses definitely show more complexities of the tandem mirror system.

On the other hand, Berk and Lane[35] developed Wong's work[36] and achieved an appropriate variational form which is particularly suitable to analyze machines such as the tandem mirrors. In the approach, though the collisional effects are not covered, the ion Landau-damping effects are explicitly evaluated.

In this dissertation, basicly following the approaches in the Ref. 32-35, a more comprehensive variational quadratic form is constructed, and then used to analytically and numerically study the dissipative trapped particle modes as well as the flute modes. As for evaluating the collisional effects, the approach in Ref. 37 is extended to cover cases of arbitrary-length anchor cells. In the numerical study, special attention is paid to understand the physics behind the instability features. To achieve that we often compare our results with the those the previous theories obtained and study limiting cases.

The parameters used in our numerical investigations are collected from the TMX-U machine. However, there is seemingly no , in principle, difficulty to apply the calculations to other type of tandem mirrors, though some modification may be necessary.

The terminology of the instabilities in this dissertation should not be misleading. The flute modes or the trapped particle modes only exhibit their typical features when the parameters are taken to unrealistic extremes. In the context of this thesis, the name of an instability mode

is based on which branch it belongs to in the parameter space.

Numerical study reveals many features of the collisional trapped particle modes as well as the flute modes. The conclusions are summarized briefly as the follows.

1) Flute mode theory gives predictions of frequency and instability threshold which are reasonably consistent with the experimental results. Destabilizing effects of the central-cell heating and the $E \times B$ drift are confirmed. Higher m-modes which have higher frequency are also predicted and detected.

2) Trapped particle mode theory reveals that the mode has many features which are similar to those of the flute mode. Factors like favorable curvature in the anchor cells and the hot electron diamagnetic current tends to stabilize the mode as it does to flute modes. Factors like $E \times B$ drift and central-cell heating tends to destabilize both the modes. The oscillation frequency does not differ from that of the flute mode. As realistic parameters are considered, even the disturbance of the mode spreads into the anchor region, which is the characteristic of flute modes. Those similarities result in difficulties to distinguish those two modes.

3) Diamagnetism provided by energetic particles does stabilize the mirror system. For the flutelike modes it raises the instability threshold a substantial amount. However, for the trapped particle modes the stabilization is not very effective.

4) It turns out that the flute mode theory gives more optimistic

predictions than the experiments suggest. The oscillation persists in situations where the flute mode is supposed to be suppressed by limiting the central-cell beta and lowering the $E \times B$ drift. The trapped particle mode theory, though having difficulties to give an adequate stability region, seemingly provides an explanation for the instability. The features of the modes revealed by this study serve hints to understand the experimental observations.

The structrure of the remainder of this part is as follows: in Chapter II, general review on the variational form with collisional effects is given. The collisional effects in tandem mirrors are analyzed. Particle loss rate and energy loss rate for simple mirrors and tandem mirrors are estimated. In Chapter III, the experimental device in TMX-U is described. Then, various numerical studies are conducted and their results are discussed. In Chapter IV, we summarize the results.

Chapter II Variational Dispersion Relation

II.1 Introduction

The use of the variational dispersion functional is an elegant and powerful way to analyze the linear response of a plasma systerm. Due to the compactness of the formalism, the variational form is often a better physical mean to gain insight into the stability properties of a system without solving the normal mode equations. As far as numerical works are concern, the variational form is even more desirable. Based on the variational form approximation procedures are usually easier to be developed.

In this chapter, we first review the general formalism of the variational principle and discuss its application to the plasma physics briefly. The foundation of the method is established basicly on the self-adjoint operator theory. For the ideal MHD system, since the normal mode equation has been proved to be self-adjoint, the method was well developed to be a powerful energy principle (see review paper by Freidberg[38]), which is very effective to analyze the stability features of a MHD system.

For kinetic systems, following the approach in Ref. 33, it is shown that the variational dispersion relation for the electostatic perturbation can be described by a relatively simple expression $Q = -\sum_j \int \frac{ds}{B} q_j \tilde{n}_j \tilde{\phi}^\dagger$. Starting from this expression, we derive an appropriate variational form for analyzing the instabilities of tandem mirrors.

The collision effects as well as many other kinetic effects are included

in deriving the variational quadratic form. To evaluate the collision term in the quadratic dispersion relation, we will discuss the Fokker-Planck collision operator and calculate the endloss in mirror machines. The endloss problem with the existence of the ambipolar potential was solved classically by Pastukhov[39]. The method is based on squre-well assumption and by introducing a fictitious source (sink) of particles. The particle loss rate and energy loss rate are given in terms of the density , ambipolar potential and mirror ratio. The solution is used to determine the collision effects on the trapped particle modes.

II. 2 Variational Formalism

In this section we briefly review the general principle of the variational form. Then we actually derive a variational form for analyzing tandem mirrors.

II.2.1 General Principle

From a rather mathematical point of view, the dynamics of many physical systems can often be described by a self-adjoint operator equation

$$L\phi = \lambda\phi, \tag{2.2.1}$$

where the variable ϕ is the eigenfunction of the system and the parameter λ the eigenvalue, where both the quantities need to be determined.

The definition of self-adjoint operators is related to an appropriately inner-product which may be defined differently . For now, we use

$$(\phi, \psi) = \int \phi^* \psi d\tau. \tag{2.2.2}$$

The operator being self-adjoint means that

$$(\phi, L\psi) = (L\phi, \psi). \tag{2.2.3}$$

Then, a variational form

$$S(\phi, \phi) = (\phi, L\phi) - (\phi, \lambda\phi) \tag{2.2.4}$$

can be constructed. By requiring the form to be extreme and applying the Euler-Langrange equation, one simply reobtains the eigenequation (2.2.1). So, one can analyze the variational form to study the system instead of solving the individual equations obtained from the variation of the quadratic form.

An important advantage of the method is that one can develop a trial function procedure to obtain approximate solutions. Assuming a test function ψ has a first-order error $\delta\psi$ compared to the exact eigenfunction ψ_0

$$\psi = \psi_0 + \delta\psi, \tag{2.2.5}$$

one can substitute the test function into the form and require the form to be stationary to calculate the parameter λ. The virtue of this method is that the determined λ has only a second order error from the exact eigenvalue λ_0. To see that, one has, from S being stationary ($\delta S = 0$),

$$S = S(\psi_0) + o(|\delta\psi|^2). \tag{2.2.6}$$

The expression (2.2.6) implies that the error $\delta\lambda$ can be expressed by

$$\delta\lambda \propto o(|\delta\psi|^2), \tag{2.2.7}$$

which is second-order.

For the non-self-adjoint operators, the situation may not be as simple as above. However, if one assume the operator can be explicitly separated into two parts, one is Hermitian and another one anti-Hermitian, a variational form can be established[40].

Using the variational form to study instability features of a plasma system is very productive[41].

In the ideal MHD stage, the method was successfully developed to be a very powerful and effective energy principle[38]. In the energy principle,

the variation form may be rewritten in terms of the perturbation type, which is very intuitive itself. Besides that, if one has some speculation about the expression of an unstable perturbation, this expression, which needs not be too close to the real eigenfunction, can be substituted into the variational form. By minimizing the variational form to see under what condition the form varies from negative to positive, one can determine how the system can be stable in terms of the perturbation. Some important stability criteria for plasma systems were derived with this method[42].

In kinetic theories, sometimes it is not very obvious that dynamics of a system can be described by self-adjoint operators. However, Dominguez and Berk[43] explicitly showed that for Vlasov system with desirable property being described by self-adjoint operator can still be maintained if one takes broader definition for the selt-adjointness.

In the next sections, a variational form which is suitable to analyze the mirror machines will be derived and discussed. The derivation assumes that the quadratic form with collisions still maintains a self-adjoint operator. The self-adjointness of the system was shown in Ref. 33.

II.2.2 Variational form for Electrostatic Perturbation

To analyze the instability problems in tandem mirrors we construct a variational form from the gyro-kinetic equation and quasineutrality condition.

In the derivation, we assume that the perturbations (both field and distribution) can be characterized as having relatively short wavelength across the confining magnetic field and relatively long wavelength along the magnetic field. Thus, the perpendicular variation of the modes is described by the eikonal description and the parallel variation by the non-eikonal description.

The perturbed electric field is described by

$$\begin{aligned} \tilde{\phi} &= \phi(s)\exp(i\mathbf{k}_\perp \cdot \mathbf{r} - i\omega t) \\ \tilde{\phi}^\dagger &= \phi(s)\exp(-i\mathbf{k}_\perp \cdot \mathbf{r} + i\omega t), \end{aligned} \tag{2.2.11}$$

where s is the length along a field line. The perpendicular wavenumber $k_\perp$ in the eikonal approximation is

$$\mathbf{k}_\perp = \nabla S(\alpha,\beta) = \frac{\partial S}{\partial \alpha}\nabla\alpha + \frac{\partial S}{\partial \beta}\nabla\beta \tag{2.2.12}$$

with $B = \nabla\alpha \times \nabla\beta$. In mirror machines, if the axisymmetry is roughly kept, then

$$\alpha \approx \frac{\Phi}{2\pi}, \quad \beta \approx \theta,$$

where Φ is flux of magnetic field and θ is azimuthal angle. So,

$$k_\perp \approx Br\frac{\partial S}{\partial \alpha}\hat{e}_r + \frac{m}{r}\hat{e}_\theta, \tag{2.2.13}$$

where m is the azimuthal wave number.

From the standard gyro-kinetic theory[44,45], the linearized perturbed distribution function $f_j(\mathbf{v})$ takes the form

$$f_j = -q_j[\phi(s)/T_j]F_j + h_j F_j \tag{2.2.14a}$$

with F_j being local Maxwelliam distribution

$$F_j = \frac{n_{0j}}{(2\pi T_j/M_j)^{\frac{3}{2}}} \exp\left(\frac{-[M_j v^2/2 + q_j\Phi(s)]}{T_j}\right). \tag{2.2.14b}$$

Here M_j, q_j and n_{0j} are the mass, charge and density factor of the j-th species and Φ is the equilibrium electric potential along the field line. The function h_j satisfies the equation

$$\begin{aligned} -i(\omega - \omega_{dj})h_j - \frac{\partial}{\partial \mathbf{v}} \cdot \mathrm{D}_j F_j \cdot \frac{\partial}{\partial \mathbf{v}}\left(\frac{h_j}{F_j}\right) = \\ - i(\omega - \omega_j^*)(q_j\phi/T_j)J_0(k_\perp \rho_j), \end{aligned} \tag{2.2.15}$$

where D_j is the velocity space diffusion coefficient of the species j, ρ_j is the gyroradius, J_0 is the Bessel function of zeroth order, and

$$\omega_j^* = \frac{cT_j \mathbf{k} \times \mathbf{b} \cdot \nabla F_j}{q_j B F_j} \tag{2.2.16}$$

is the diamagnetic drift frequency which is a constant along a field line $\mathbf{b} = \mathbf{B}/B$.

The appropriate expression of the drift frequency ω_{dj} is

$$\begin{aligned} \omega_{dj} = \frac{c}{q_j B}(\mathbf{k} \times \mathbf{b} \cdot \kappa)(2E - \mu B - \Phi) \\ - \frac{c\mu}{q_j B^2} \sum_j \mathbf{k} \times \mathbf{b} \cdot (\nabla P_{\perp j} - B^2 \kappa), \end{aligned} \tag{2.2.17}$$

with

$$\kappa = (\mathbf{b}\cdot\nabla)\mathbf{b}, \quad \mu = \frac{1}{2}M_j v_\perp^2/B, \quad E = \frac{1}{2}M_j v^2 + q_j\Phi$$

and $P_{\perp j}$ is the perpendicular pressure of the jth species.

Since the mode frequency is significantly lower than the plasma characteristic frequency, the quasineutrality condition is considered to be valid, which demands

$$\sum_j q_j \int d^3v \left(-q_j\phi\frac{F_j}{T_j} + h_j J_0(k_\perp\rho_j) \right) = 0 \tag{2.2.18}$$

where the Bessel function J_0 stems from that the function h_j is given in the guiding center coordinate system.

Now, we can introduce the following quadratic form[33]

$$\begin{aligned} Q(g,\phi,\omega) = -\sum_j \int \frac{dl}{B} \int d^3v \frac{F_j}{T_j} \times \Bigg(& q_j\phi^2 + \frac{(\omega-\omega_{dj})T_j^2 g_j^2}{(\omega-\omega_j^*)} \\ & + \frac{iT_j^2(\partial/\partial\mathbf{v})g_j\cdot \mathrm{D}_j\cdot(\partial/\partial\mathbf{v})g_j}{(\omega-\omega_j^*)} - 2q_j\phi J_0(k_\perp\rho_j)g_j T_j \Bigg), \end{aligned} \tag{2.2.19}$$

where $g_j = h_j/F_j$.

It is readily shown that varying the form with respect to g and ϕ reproduces the gyro-kinetic equation (2.2.15) and quasineutrality equation (2.2.18). The quadratic form is also equivalent to the following form

$$Q = -\sum_j \int \frac{ds}{B} q_j \tilde{n}_j \tilde{\phi}^\dagger \tag{2.2.20}$$

where $\tilde{n}_j$ is related to the perturbed distribution f_j. The equation (2.2.20) is symbolicly more concise and will be used to obtain more explicit formulae in the next sections.

II.3 Collision Effects

As far as the dissipative mechanism in a plasma system is concerned, two processes are needed to be considered: collisional effect and the Landau damping effect. For electrons, collisional effects tends to dominate the dissipative mechanism. For ions, the Landau damping is more important For ion Landau-damping, the Berk-Lane formulas will be used[35]. The electron collisional effects will be discussed in this section.

The collisions provide a dissipative mechanism which can be a damping factor to many waves. However, for a negative energy wave, the mechanism may become the destabilizing factor. In mirror machines, particularly, when rotational modes are potentially important, this kinetic effect can be essential.

The connection between the different cells in tandem mirrors are kept by collisions between passing particles and particles trapped in the central cell and anchor cells. Without this connection (or if the connection is too weak), the different cells in the tandem mirrors become isolated ones and the interchange modes driven by unfavorable curvature of the central cell will occur in a fast time scale.

In this section, we investigate the collisional operator and discuss the particle loss and energy loss of a mirror which will be used to determine collisional term in the variational form.

II.3.1 Time Scale of Collisions

It is useful to briefly discuss the time scale for the involved collisions in tandem machines.

The fatest collision process in the mirror confinement is that of electron-electron scattering. From Spitzer[46] we can take the average "relaxation" time for a 90° deflection in a velocity phase space as the following

$$\tau_{ee} = \frac{1.1 \times 10^{10} T_e^{3/2}}{n_e n^* \ln \Lambda} s, \qquad (2.3.1)$$

here $n_e(\mathrm{cm}^{-3})$ is the electron density and T_e (KeV) electron kinetic temperature. The parameter $\ln\Lambda$ is typically about 20 for magnetic fusion plasma. Thus, for a mirror fusion plasma in TMX-U device with $T_e = 0.1\mathrm{KeV}$ and $n_e = 10^{12} cm^{-3}$,

$$\tau_{ee} \approx 0.017ms \quad \nu_{e-e} \approx 60KHz.$$

For singly charged ions, electron-ion scattering occurs on virtually the same time scale i.e. $\tau_{ei} \approx \tau_{ee}$.

The ion-ion 90° scattering time is much longer than that of electrons of the same mean energy, since the ratio $(M/m)^{1/2} \approx 60$ or deuterons. In this dissertation, we omit the ion-ion collision effects when analyzing instability modes.

II.3.2. Fokker-Planck Collision Operator

The Fokker-Planck collision equation has been long recognized as classical means of evaluating the collisional effects. The equation is essentially equivalent to the kinetic equation derived by Landau[47]

$$C(F_i) \equiv \left(\frac{\partial F_i}{\partial t}\right)_{\text{col}} = \int d^3v' \sum_j \frac{b_j}{m_i} \frac{\partial}{\partial \mathbf{v}} \cdot \frac{\mathbf{I}g^2 - \mathbf{gg}}{g^3} \cdot \left(\frac{1}{m_i}\frac{\partial}{\partial \mathbf{v}} - \frac{1}{m_j}\frac{\partial}{\partial \mathbf{v}'}\right) F_i(\mathbf{v}) F_j(\mathbf{v}'). \tag{2.3.2}$$

where

$$\mathbf{g} = \mathbf{v} - \mathbf{v}'$$

$$b_j = 2\pi Z_i^2 Z_j^2 e^4 n^* \ln \Lambda_{ij}$$

After the early pioneer work by Rosenbluth et al[48] the collision term in the Fokker-Planck equation can be conveniently written as the following

$$\left(\frac{\partial F_i}{\partial t}\right)_{\text{col}} = -\frac{\partial}{\partial \mathbf{v}}(F_i \Gamma_i \frac{\partial h_i}{\partial \mathbf{v}}) + \frac{1}{2}\frac{\partial^2}{\partial \mathbf{v}\partial \mathbf{v}} : F_i \Gamma_i \frac{\partial^2 g_i}{\partial \mathbf{v}\partial \mathbf{v}} \tag{2.3.3}$$

where

$$\Gamma_i = \frac{2\pi Z_i^4 e^4 n^* \ln \Lambda_{ij}}{m_i^2}$$

and the functions h and g are called "Rosenbluth potential" and defined as

$$h_i = \sum_j (\frac{Z_j}{Z_i})^2 \frac{m_i}{m_{ij}} \int d^3v' \frac{F_j(\mathbf{v}')}{|\mathbf{v} - \mathbf{v}'|}$$

and

$$g = \sum_j (\frac{Z_j}{Z_i})^2 \int d^3v' F_j(\mathbf{v}') |\mathbf{v} - \mathbf{v}'|$$

The formalism is very useful to calculate the collisional effects, when certain symmetries of particle distributions can be utilized.

When the distributions in the operator are not too far from the Maxwellian one, the collision operator can be linearized. In particular, if the electrons and ions are considered to satisfy the gyro-kinetic equation

$$f_j = -e[\phi/T_j]F_j + hF_j. \quad (j = e, i) \tag{2.3.4}$$

The linearized Fokker-Planck operator C_l operating on the electron distribution f_e is given by

$$C_l(h_e) = \int d^3v' \sum_e \frac{b_j}{m_i} \frac{\partial}{\partial \mathbf{v}} \cdot \frac{\mathbf{I}g^2 - \mathbf{gg}}{g^3} \cdot \left(\frac{1}{m_e} \frac{\partial h(\mathbf{v})}{\partial \mathbf{v}} - \frac{1}{m_j} \frac{\partial h_j(\mathbf{v}')}{\partial \mathbf{v}'} \right) F_e(\mathbf{v}) F_j(\mathbf{v}'). \tag{2.3.5}$$

Now, we observe several properties of the linearized operator. Noticing that $m_i^{-1} << m_e^{-1}$ so that the electron-ion energy exchange rate is negligible and $\mathbf{g} \approx \mathbf{v} - \mathbf{v}'$, we can easily prove

$$C_l(v^2) = 0, \quad C_l(\frac{m_e v^2}{2} + e\Phi) = 0, \tag{2.3.6}$$

which will be used to assure that the mode solution in the work is consistent with the global energy conservation of the collision operator.

II.3.3 Loss Rate of Mirrors

Estimating the particle loss has been a classical problem for both simple mirrors and tandem mirrors. The solutions can also be used to determine the number of passing electrons in tandem mirrors, which will greatly effect the stability problem.

The electron scattering-loss rate in a mirror configuration without an ambipolar potential can be evaluated in the way described in Ref. 49. The method is based on treating the background particle distribution as Maxwellian. As the mirror ratio $R \equiv B_{\max}/B_{\min}$ goes high, the distribution function of the trapped particles tends to approach Maxwellian. As far as the collisional effect on lifetime of a test particle is concerned, the distribution function of the background particles can be taken as Maxwellian without introducing too large errors. So, by introducing a source term S, we have a simplified Fokker-Planck equation

$$\frac{D_\perp}{v^2 \sin\theta}\frac{\partial}{\partial\theta}\sin\theta\frac{\partial f}{\partial\theta} + \frac{1}{v^2}\frac{\partial}{\partial v}[v^2(D_\parallel\frac{\partial f}{\partial v} - Af)] = -S, \qquad (2.3.7)$$

where

$$D_\perp = \sum{}^* \frac{\pi(ee^*)n^* \ln\Lambda}{m_e^2 v}[\phi(b^*v) - \frac{\phi_1(b^*v)}{2b^{*2}v^2}]$$

$$D_\parallel = \sum{}^* \frac{\pi(ee^*)n^* \ln\Lambda}{m_e^2 v}\frac{\phi_1(b^*v)}{b^{*2}v^2}$$

$$A = -\frac{m_e v D_\parallel}{T^*}$$

with

$$\theta = \arccos\frac{\mathrm{v}\cdot\mathrm{B}_0}{vB_0}$$

$$b^* = (m^*/2T^*)^{1/2}$$

$$\phi(x) = \frac{2}{\pi^{1/2}}\int_0^x \exp(-\xi^2)d\xi$$

$$\phi_1(x) = \phi(x) - \frac{2x}{\pi^{1/2}}\exp(-x^2).$$

where "*" refers to the background particles.

For a simple mirror, the general solution of Eq. (2.3.7) can be expressed as

$$f = \Theta(\theta, v)\exp(-\frac{m_e v^2}{2T}) \tag{2.3.8}$$

As the large mirror ratio is assumed, the distribution f can be relaxed to near Maxwellian in terms of the speed v, and then, the function Θ can be expected to depend on θ mainly. Thus, the Eq. (2.3.7) can be further simplified to be

$$\frac{D_\perp}{v^2\sin\theta}\frac{\partial}{\partial\theta}\sin\theta\frac{\partial f}{\partial\theta} = -S. \tag{2.3.9}$$

Assuming that the source term S can expressed by

$$S = \chi(v)\psi(\theta), \tag{2.3.10}$$

we can integrate the equation and obtain

$$f = C\int_{\theta_0}^{\theta}\frac{d\theta'}{\sin\theta'}\int_{\theta'}^{\pi/2}\psi(\theta'')\sin\theta''d\theta'', \tag{2.3.11}$$

where θ_0 is the loss-cone angle, C a constant independent of v, θ. The source θ-dependence can explicitly be assumed to satisfy[49]

$$\psi(\theta) = \delta(\theta - \frac{\pi}{2}). \tag{2.3.12}$$

From Eq. (2.3.9)-(2.3.12), the function $\chi(v)$ can be expressed as

$$\chi(v) = C\frac{D_\perp}{v^2}\exp(-\frac{m_e v^2}{2T}). \tag{2.3.13}$$

Now, we have

$$f = C\ln\frac{\tan(\theta/2)}{\tan(\theta_0/2)}\exp(-\frac{m_e v^2}{2T}). \tag{2.3.14}$$

The electron loss rate ν can be obtained by calculating the following expression

$$\nu = \frac{\int S d^3v}{\int f d^3v}. \tag{2.3.15}$$

For future use, we explicitly calculate the electron loss rate ν_{e-e} which is defined as the loss rate due to electron-electron collisions. After substituting Eq. (2.3.12)-(2.3.14) into Eq. (2.3.15), we have

$$\begin{aligned}\nu_{e-e} &= \frac{\int S_{e-e} v^2 \sin\theta dv d\theta}{\int f v^2 \sin\theta dv d\theta} \\ &= \frac{4\pi}{(2\pi T/m_e)^{3/2}\ln\frac{1}{\sin\theta_0}}\int_0^\infty D_\perp^{ee}\exp(-\frac{m_e v^2}{2T})dv \\ &= 0.615\Gamma_e,\end{aligned} \tag{2.3.16}$$

with

$$\Gamma_e = \frac{2^{5/2}\pi^{1/2}e^4 n_e \Lambda_{ee}}{T^{3/2}m_e^{1/2}\ln R}$$

$$R = B_{\max}/B_{\min} = (\frac{1}{\sin\theta_0})^2.$$

Similarly, the electron loss rate ν_{e-i} due to electron-ion collisions is

$$\nu_{e-i} = \frac{8\pi}{(2\pi T/m_e)^{3/2}\ln R}\int_{(\frac{2e^4}{m_e})^{1/2}}^\infty D_\perp^{ei}\exp(-\frac{m_e v^2}{2T})dv.$$

where we have introduced a small negative barrier $\bar{\Phi}$ to prevent an overescaping problem. Noticing that $(m_i/m_e)(e\bar{\Phi}/T_i) \gg 1$ and $e\bar{\Phi}/T_e \ll 1$, we find

$$\begin{aligned}\nu_{e-i} &\approx \Gamma_i \int_{(\frac{2e\bar{\Phi}}{m_e})^{1/2}}^{\infty} \frac{\phi(b_i v)}{v} \exp(-\frac{m_e v^2}{2T}) dv, \\ &\approx \frac{1}{2}\Gamma_i [\frac{1}{2}\ln(\frac{T_e}{e\bar{\Phi}}) - \gamma],\end{aligned} \tag{2.3.17}$$

with γ being Euler constant and

$$\Gamma_i = \frac{2^{5/2}\pi^{1/2}e^4 n_i \Lambda_{ei}}{Z_i^2 T^{3/2} m_e^{1/2} \ln R}.$$

Similarly, we define two related energy loss rates as following

$$\begin{aligned}\nu_{Ee-e} &\equiv \frac{1}{E}(\frac{dE}{dt})_{e-e} \\ &= \frac{\int \left(\frac{mv^2}{2}\right) S_{e-e} d^3v}{\int \left(\frac{mv^2}{2}\right) f d^3v}.\end{aligned} \tag{2.3.18}$$

With straitforward calculations, we have

$$\begin{aligned}\nu_{Ee-e} &= \frac{8\pi}{(3T/2m_e)(2\pi T/m_e)^{3/2}\ln R} \int_0^{\infty} v^2 D_{\perp}^{ee} \exp(-\frac{m_e v^2}{2T}) dv \\ &= 0.178\Gamma_e.\end{aligned} \tag{2.3.19}$$

We also have

$$\begin{aligned}\nu_{Ee-i} &\equiv \frac{1}{E}(\frac{dE}{dt})_{e-i} \\ &\approx 0.33\Gamma_i.\end{aligned} \tag{2.3.20}$$

We also symbolicly define the following quantity for the future use in

Sec. II.5.2.

$$\begin{aligned}\nu_{E^2 e-e} &= \frac{1}{E^2}\left(\frac{dE^2}{dt}\right)_{e-e} \\ &= \frac{8\pi}{(15T^2/4m_e^2)(2\pi T/m_e)^{3/2}\ln R}\int_0^\infty v^4 D_\perp^{ee}\exp\left(-\frac{m_e v^2}{2T}\right)dv \\ &\approx 0.088\Gamma_e.\end{aligned} \tag{2.3.21}$$

When the ambipolar potential has an effect on the trapped particles, the particle loss rate and related energy loss rate are a little harder to evaluate. The first essential calculation done by Pastukhov is instructive and useful[38].

Following his approach, the Fokker-Planck operator for electrons can be rewritten in the dimensionless manner

$$\begin{aligned}\tau_e\left(\frac{\partial f_e}{\partial t}\right)_{\text{col}} = \frac{1}{x^2}\frac{\partial f_e}{\partial x} + \frac{1}{x^2}\frac{\partial}{\partial x}\frac{1}{2x}\frac{\partial f_e}{\partial x} \\ + \frac{Z_e}{x^3}\frac{\partial}{\partial \mu}(1-\mu^2)\frac{\partial f_e}{\partial \mu},\end{aligned} \tag{2.3.22}$$

where

$$\tau_e = \frac{2^{\frac{1}{2}} m_e^{\frac{1}{2}} T_e^{\frac{3}{2}}}{\pi e^4 n_e n^* \ln \Lambda_{ee}}$$

$$Z_e = \frac{1}{2}\left(1 + \frac{\sum Z_i^2 n_i n^* \ln \Lambda_{ei}}{n_e n^* \ln \Lambda_{ee}}\right)$$

with

$$x = \frac{v}{v_e}, \quad v_e = \left(\frac{2T_e}{m_e}\right)^{\frac{1}{2}}$$

$$f_e = \left(\frac{T_e}{m_e}\right)^{\frac{3}{2}}\frac{F_e}{n_e}, \quad f_e|_{x\to 0} \to \pi^{-3/2}e^{-x^2}$$

$$f_e|_{\mu=\mu_0} = 0, \quad (\mu^2 = \mu_0^2, \text{ or } x > \frac{e\phi_m}{T})$$
$$\mu_0 = 1 + R_m^{-1} + R_m^{-1}\frac{e\phi_m}{Tx^2}$$

Notice that the first term in Eq. (2.3.22) represents the energy drag term, the second one energy diffusion term and third pinch angle scattering term. The boundary condition is that the distribution function has to be vanished at the separatrix as shown as in Fig. 2.1.

By introducing a fictitious (but physically reasonable) source of the particles in the form

$$S_p = -q\delta(1-\mu^2)\eta(x-a)e^{-x^2},$$

where η is the step function, one obtains a nearly solvable equation. After a few approximations, Pastukhov found out that the loss rates of particles and energy are

$$\begin{aligned}
\nu_p &= 2(\frac{1}{\pi})^{\frac{1}{2}}\nu_e\frac{(\frac{e\phi}{T})^{\frac{1}{2}}(1+Z)\exp(-\frac{|e\phi|}{T})}{\ln[2R(1+Z)]} \\
\nu_{pE} &= \left(1+\frac{|e\phi|}{T}\right)\nu_p \qquad (2.3.23) \\
\nu_e &= \frac{2^{\frac{1}{2}}\pi n_0 e^4\lambda_e}{m_e^{\frac{1}{2}}|e\phi|^{\frac{3}{2}}}.
\end{aligned}$$

The results with their related boundary condition will be used to determine the collision effects of the trapped particle modes.

For future use, we point out the insensitivity of ν_p and ν_{pE} to the precise form of the source term S_p as long as S_p is not too peaked near the

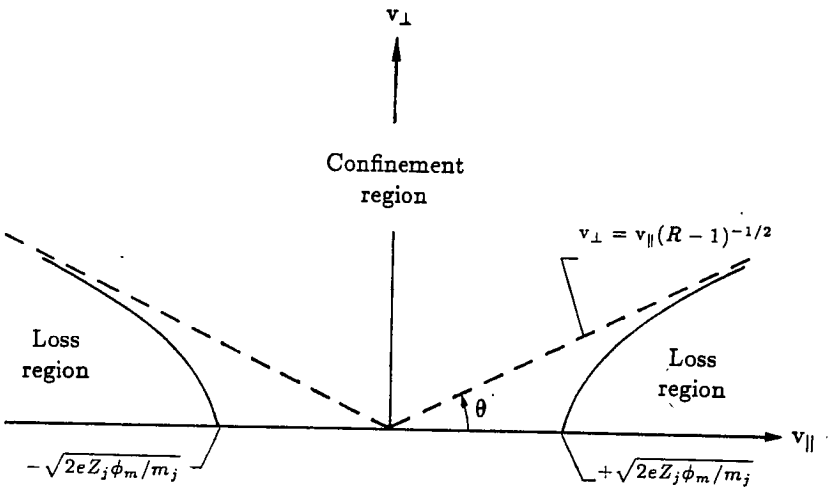

Fig. 2.1. Velocity-space loss boundary for particles in an electrostatically plugged magnetic-mirror trap.

separatrix. Consider a particle 'injected" into the machine by the source term. The particle having energy below the separatrix energy can not escape by pitch angle scattering, but just by energy diffusion. However, initially the drag term dominates energy diffusion, and the particle can go to the separatrix with very low probability. Only after several 90° scattering times, when the distribution has relaxed to near a Maxwellian and is highly peaked at low energy, there is a significant probability that the initial particle will obtain enough energy to exceed the separatrix energy and then escape out of the machine.

The proceding arguments can also be applied to the simple-mirror scattering if large mirror ratio is assumed, which makes particles go to separatrix with low probability. A direct calculation in Ref. 49 also shows that introducing different source term does not substantially change the loss ratio.

II.4 Derivation of the Dispersion For Tandem Mirrors

In this section, we start with Eq. (2.2.20),

$$Q = -\sum_j \int \frac{ds}{B} q_j \tilde{n}_j \tilde{\phi}^\dagger \tag{2.4.1}$$

and bounce-averaged gyro-kinetic equation to construct the quadratic dispersion relation for tandem mirrors.

The electron bounce-averaged kinetic equation is

$$-i(\omega - \overline{\omega}_d)h - \overline{C}_l(h) = -ie\left[\frac{(\omega - \omega_T^*)\overline{\phi}}{T(\alpha)}\right], \tag{2.4.2}$$

where $h(E, \mu, \alpha)$ is related to the perturbed electron distribution f_e in the following way

$$f_e = (-e\phi/T)F_e + hF_e, \tag{2.4.3}$$

The other quantities in Eqs. (2.4.2) and (2.4.3) are given

$$\bar{q} = \frac{1}{\tau}\int q d\tau,$$

$$\tau(E,\mu) = \int_{-s_0}^{s_0} \frac{ds}{|v_\parallel(E,\mu,s)|},$$

$\pm s_0 \equiv$ turning points of particle,

$$\omega_T^* = \omega_e^*\left(1 + \eta\frac{m_e v^2/2 + e\Phi}{T} - \frac{3}{2}\eta\right),$$

$$\omega_e^* = \frac{Tm}{q_e n_0}\frac{\partial n_0}{\partial \alpha},$$

$$\eta = \left(\frac{T\partial n_0}{\partial \alpha}\right)^{-1}\frac{\partial T}{\partial \alpha},$$

$$\omega_{en}^* = \omega_e^* - \omega_E + \eta\omega_e^*\frac{e\Phi}{T}$$

$$= \frac{Tm}{en_e}\frac{\partial}{\partial \alpha}\left[n_0(\alpha)\exp\left(\frac{-e\Phi(s,\alpha)}{T(\alpha)}\right)\right],$$

$$\omega_d = m\frac{\partial \Phi}{\partial \alpha} + \frac{m\kappa}{\omega_{ce} r m_e}(2E - \mu B - 2e\Phi) \equiv \omega_E + \omega_\kappa,$$

$$\omega_{ce} = eB/m_e,$$

$$\mu = m_e v_\perp^2/2B, \quad \kappa = \mathbf{b}\cdot\nabla\mathbf{b}\cdot\nabla\alpha/|\nabla\alpha|,$$

Note that ω_{en}^* is proportional to the gradient of the real particle density, while ω_e^* is a parameter that is a constant on a flux surface.

In the expression for the curvature drift we have neglected geodesic curvature for convenience of presentation, and we assumed sufficiently small β so that $\nabla_\perp B/B \approx \kappa$.

The linearized electron collision operator $C_l(h)$ is defined by Eq. (2.3.5). We observe from Eq. (2.3.6) that $\bar{C}_l(m_e v^2/2 + e\Phi) = 0$.

We now define h_ξ ($\xi = c, a, p$) where subindex 'c', 'a' and 'p' refer to particles in the central cell, anchor cells and passing particles respectively. Then, we define the g_ξ through the relation

$$h_\xi = \frac{e(\omega - \omega_T^*)}{T}\frac{\overline{\psi(\omega - \omega_E)}}{\omega - \bar{\omega}_E} + g_\xi, \tag{2.4.4}$$

where the amplitude ψ is given by

$$\psi = \phi/(\omega - \omega_E). \tag{2.4.5}$$

It is noticed that the first term in Eq. (2.4.4) is nearly independent of E and μ for the particles trapped in the central cell or the anchor cells if they sample a nearly constant ψ and ω_E. For the passing particles, the first term on the right-hand side of Eq. (2.4.4) generally depends on E and μ. However, if the length of the central cell is relatively long compared to the anchor region, the term can nearly be independent of E and μ. Now, taking a test function in which ψ is a piecewise constant and an equilibrium model where ω_E is also a piecewise constant, we find that g_ξ is given by

$$\begin{aligned}
(\omega-\omega_{Ec})g_c &= i\bar{C}_l(g_c)+\bar{\omega}_{\kappa c}\left(\frac{e(\omega-\omega_T^*)}{T}\psi_c+g_c\right),\\
(\omega-\omega_{Ea})g_a &= i\bar{C}_l(g_a)+\bar{\omega}_{\kappa a}\left(\frac{e(\omega-\omega_T^*)}{T}\psi_c+g_a\right),\\
(\omega-\bar{\omega}_E)g_p &= i\bar{C}_l(g_p)+i\bar{C}_l\left(\frac{e(\omega-\omega_T^*)\overline{\psi(\omega-\omega_E)}}{(\omega-\bar{\omega}_E)}\right)\\
&\quad+\bar{\omega}_\kappa\left(\frac{e(\omega-\omega_T^*)\overline{\phi(\omega-\omega_E)}}{T(\omega-\bar{\omega}_E)}+g_p\right),
\end{aligned}\tag{2.4.6}$$

where the equations $\overline{C}_l(\text{const})=0$ and $\overline{C}_l(m_e v^2/2+e\Phi)=0$ have been used.

Roughly, we estimate

$$g_{c,a}\approx\frac{\overline{\omega}_{\kappa c,a}}{(\omega-\overline{\omega}_{Ec,a})}\frac{e(\omega-\omega_T^*)}{T}\psi_{c,a}\approx\epsilon h,\tag{2.4.7}$$

where$\epsilon\approx\overline{\omega}_{\kappa c,a}/(\omega-\overline{\omega}_{Ec,a})$. Thus we treat $g_{c,a}\approx o(\epsilon)$. We shall take the ratio of the passing particles to the trapped particles to be $o(\epsilon)$.

We substitute the electron contribution into Eq. (2.4.1), using Eqs.

(2.4.3) and (2.4.4), to find

$$
\begin{aligned}
Q_e(\omega) &= e\int_{-\infty}^{\infty}\frac{ds}{B}n_e^{(1)}(\omega-\omega_E)\psi \\
&= \frac{4\pi e^2}{Tm_e^2}\int_{-\infty}^{\infty}ds\psi^2(\omega-\omega_E)^2\int\frac{dEd\mu}{|v_\parallel|}F_e \\
&\qquad + \frac{4\pi e}{m_e^2}\int_{-\infty}^{\infty}ds\psi(\omega-\omega_E)\int\frac{dEd\mu}{|v_\parallel|}F_e h \\
&= -\frac{4\pi e^2}{Tm_e^2}\int dEd\mu\tau F_e\left(\overline{\psi^2(\omega-\omega_E)^2}-(\omega-\omega_T^*)\frac{\overline{[\psi(\omega-\bar{\omega}_E)]^2}}{(\omega-\bar{\omega}_E)}\right) \\
&\qquad + \frac{4\pi e}{m_e^2}\int dEd\mu\tau F_e\overline{g(\omega-\omega_E)\psi}.
\end{aligned}
\tag{2.4.8}
$$

Now, we write $\psi = \psi_c + \delta\psi$, and use Eq. (2.4.6) and the particle conservation property of the collision operator which implies for arbitrary $q(v)$ that

$$
\int dEd\mu\tau F_e\overline{C}(q) = 0. \tag{2.4.9}
$$

Then, using Eqs. (2.4.6) and (2.4.9), we find exactly

$$
\begin{aligned}
\delta Q_e &= \frac{4\pi}{m_e^2}\int dEd\mu\tau F_e\overline{g(\omega-\omega_E)(\psi_c+\delta\psi)} \\
&= \frac{4\pi}{m_e^2}\int dEd\mu\tau F_e\overline{\omega}_\kappa\left(\frac{e^2}{T}\frac{\overline{(\omega-\omega_E)\psi^2}}{(\omega-\overline{\omega}_E)^2}(\omega-\omega_T^*)+\right. \\
&\left. e\frac{\overline{(\omega-\omega_E)\psi g}}{(\omega-\overline{\omega}_E)}\right)+\frac{4\pi ei}{m_e^2}\int dEd\mu\tau F_e\delta\psi\overline{C}_l(h).
\end{aligned}
\tag{2.4.10}
$$

In the last term we note that there is no contribution from the particles trapped in the central cell where $\delta\psi = 0$. Also, in this term we neglect the contribution from passing particles as their contribution is smaller than from the anchor region by the ratio of passing to trapped particle

density which is of order to be $o(\epsilon)$. Then note that $C_l(h_a) = C_l(g_a)$ as $C_l(h_a - g_a) = 0$ as $h_a - g_a = \alpha + \beta E$, with α and β constant.

We now use that the charge density

$$\rho = \sum_j \frac{4\pi q_j}{m_j^2} \int \frac{dE d\mu B}{|v_\parallel|} F_j = 0$$

to obtain the following identities that follow after appropriate parts integrating:

$$m \int ds \psi^2 (\omega - \omega_E) B \frac{\partial \rho / B^2}{\partial \alpha}$$
$$= \sum_j \frac{4\pi q_j^2}{m_j^2} \int dE d\mu \tau \overline{(\hat{\omega}_s^* - \omega_E - \omega_\kappa) \psi^2 (\omega - \omega_E)} \frac{\partial F_j}{\partial E} = 0, \tag{2.4.11a}$$

$$m \int \frac{ds}{B} \psi^2 (\omega - \omega_E) \frac{\partial \rho}{\partial \alpha}$$
$$= \sum_j \frac{4\pi q_j^2}{m_j^2} \int dE d\mu \tau \overline{\omega_{\kappa\parallel} \psi^2 (\omega - \omega_E)} \frac{\partial F_j}{\partial E} = 0, \tag{2.4.11b}$$

where

$$\hat{\omega}_j^* \frac{\partial F_j}{\partial E} = -(m/q_j) \frac{\partial F_j}{\partial \alpha}$$

and

$$\omega_{\kappa\parallel} = \frac{2m\kappa(E - \mu B - q_j \Phi)}{\omega_{cj} r m_j}$$

and at low beta $\kappa = r \partial B / \partial \alpha$. These identities follow exactly from charge neutrality. We add these terms into our quadratic form, and for the electron contribution we have

$$\hat{\omega}_e^* \frac{\partial F}{\partial E} = -\frac{\omega_T^* F}{T}.$$

Now substituting Eqs. (2.4.10), (2.4.11) and (2.4.8) yields

$$Q_e(\omega) = -\frac{4\pi e^2}{Tm_e^2}\int_p dE d\mu F_e \Bigg[\overline{\psi^2(\omega-\omega_E)(\omega-\omega_T^*)} - \overline{\psi(\omega-\omega_E)}^2\frac{\omega-\omega^*}{\omega-\bar{\omega}_E} - \bar{\omega}_\kappa\frac{\overline{(\omega-\omega_E)\psi^2}}{\omega-\omega_E} + \overline{\omega_\kappa(\omega-\omega_E)\psi^2} + \frac{\overline{(\omega-\omega_E)\psi^2}}{(\omega-\bar{\omega}_E)^2}\bar{\omega}_\kappa(\omega_T^*-\bar{\omega}_E) - \frac{i}{e}T_e\overline{C}_l(g)\delta\psi\Bigg] + o(\epsilon^2). \tag{2.4.12}$$

Now substituting $\psi = \psi_c$ in the central cell, $\psi = \psi_a$ in the two anchor regions, define $\Delta\psi = \psi_a - \psi_c$ and find

$$\begin{aligned} Q_e(\omega) &= -\frac{8\pi e^2}{Tm_e^2}\int_p dE d\mu F_e\frac{\tau_a\tau_c}{\tau}\times \\ &\frac{\Delta\psi^2(\omega-\omega_{Ec})(\omega-\omega_{Ea})(\omega-\omega_T^*)}{\omega-(\omega_{Ec}\tau_c+\omega_{Ea}\tau_a)/\tau}\left[1+o\left(\frac{\omega_\kappa}{\omega-\omega_E}\right)\right] \\ &- 2m^2\int_c\frac{ds}{B^2r}\kappa\frac{\partial P_e}{\partial\alpha}\psi_c^2 - 4m^2\int_a\frac{ds}{B^2r}\kappa\frac{\partial P_e}{\partial\alpha}\psi^2 \\ &+ \frac{8\pi e\Delta\psi}{m_e^2}i\int dE d\mu\tau\overline{C}_l(g_a)F_e + o(\epsilon^2), \end{aligned} \tag{2.4.13}$$

where $\Delta\psi = \psi_a - \psi_c$, P_e is the electron pressure. The notation $\int_\xi$ $(\xi = c, a, p)$ refers to integration over the particles in the center, anchor and passing particles respectively. In the equation, the integrals is over just one anchor region, since a factor of 2 has alredy been added to account for both anchor cells. In obtaining the result the following equation has been used

$$\begin{aligned} &\frac{4\pi}{m_e^2}\int dE d\mu\tau_{c,a}F_e\overline{\omega}_\kappa(\omega_T^*-\omega_{Ec,a}) \\ &= 2\int_{c,a}\frac{ds}{B^2r}\kappa\frac{\partial P_e}{\partial\alpha}[1+o(\epsilon)]. \end{aligned} \tag{2.4.14}$$

With $\overline{C}_{(}g_a) = 0$ the dispersion is the correct response for the collisionless theory. For the collisional theory we need to calculate g_a and g_c.

We observe that the boundary condition for g is that it is continuous on the separatrix between the trapped and passing particles, i.e.,

$$h_a = h_p, \quad h_c = h_p. \tag{2.4.15}$$

Thus we have

$$\begin{aligned} h_{a,c} &= g_{a,c} + \frac{e\psi_{a,c}(\omega - \omega_T^*)}{T} \\ h_p &= g_p + \frac{e}{T}\frac{(\psi_c\Omega_c\tau_c + \psi_a\Omega_a\tau_a)(\omega - \omega_T^*)}{(\Omega_c\tau_c + \Omega_a\tau_a)}, \end{aligned} \tag{2.4.16}$$

where $\Omega_{c,a} = (\omega - \omega_{Ec,a})$. We obtain

$$\begin{aligned} g_a - g_p &= \frac{-e}{T}\frac{\Omega_c\tau_c\Delta\psi(\omega - \omega_T^*)}{(\Omega_c\tau_c + \Omega_a\tau_a)} \\ g_c - g_p &= \frac{-e}{T}\frac{\Omega_a\tau_a\Delta\psi(\omega - \omega_T^*)}{(\Omega_c\tau_c + \Omega_a\tau_a)}. \end{aligned} \tag{2.4.17}$$

As there is only one separatrix contour of passing particles separating the trapped anchor region and the trapped central region, the E and μ dependence of Ω_c and Ω_a are at the same energy and magnetic moment. Then, subtracting the two equations yield the boundary condition

$$g_a - g_c = -\frac{e\Delta\psi}{T}(\omega - \omega_T^*). \tag{2.4.18}$$

To solve for g_a and g_c we have from Eqs. (2.4.6)

$$\begin{aligned} \Omega_c g_c &= i\overline{C}_l(g_c) + o(\epsilon) \\ \Omega_a g_a &= i\overline{C}_l(g_a) + o(\epsilon). \end{aligned} \tag{2.4.19}$$

If $\nu > \Omega_{Ec,a}$, where ν is the electron collision frequency, the solution is dominated by the collision frequency term, so that g has the form over most of the phase space

$$g_a = \frac{e\Delta\psi\omega_e^*}{T}\left[\lambda_{1a} + \lambda_{2a}\left(\frac{1}{2}\frac{m_e v^2}{T} - \frac{3}{2}\right)\right], \qquad (2.4.20a)$$

$$g_c = \frac{e\Delta\psi\omega_e^*}{T}\left[\lambda_{1c} + \lambda_{2c}\left(\frac{1}{2}\frac{m_e v^2}{T} - \frac{3}{2}\right)\right], \qquad (2.4.20b)$$

where $\lambda_{1a}, \lambda_{2a}, \lambda_{1c}$ and λ_{2c} are constant coefficients that need to be determined. In fact, the validity of Eq. (2.4.20) may be larger than our estimation. For examples, in Ref. 37 the valid range of collisional frequency was found to be $\nu/\Omega\ (|e\Phi|/T + B_{max}/B_a)^{-1}$. Eq. (2.4.20) is not necessarily satisfied in a boundary layer near the separatrix. However, we shall assume that passing particles equilibrate primarily with the central cell particles, a condition that implies

$$\frac{L_a}{L_c}\left(\frac{T}{|e\Phi|}\right)^2 \exp\left(\frac{|e\Phi|}{T}\right) \ll 1. \qquad (2.4.21)$$

This condition limits the validity of the calculation if $|e\Phi|/T$ is too large. However, when Eq. (2.4.21) is satisfied, we can expect (2.4.20b) to be valid near the separatrix (as the combined passing and central cell traped distribution are described to lowest order by the same Maxwelliam distribution function), but (2.4.20a) to break down near the separatrix as the distribution of particles trapped near the separatrix in the anchor has a distribution that is strongly affected by both the central cell distribution

and the anchor distribution, which are distributions of different functional forms, than in the bulk of the anchor region.

We can eliminate the condition Eq. (2.4.21) by employing a more complicated boundary condition. The evaluation of the collision term then becomes more complicated and will be discussed in the next section.

The relationships among the four unknown constants can be obtained if we use the particle and energy conservation properties of the collision operator. We take the zeroth moment and an energy moment $(2/3)(E-T)$ of Eq. (2.4.19) and sum the expression (thereby annihilating the collisional contribution) and have

$$\Omega_c N_c \lambda_{1c} + 2\Omega_a N_a \lambda_{1a} = 0, \tag{2.4.22a}$$

and

$$N_c \Omega_c \left(\frac{2}{3} \frac{\lambda_{1c} e\Phi_c}{T} + \lambda_{2c} \right) + 2N_a \Omega_a \left(\frac{2}{3} \frac{\lambda_{1a} e\Phi}{T} + \lambda_{2a} \right) = 0$$

or with the use of Eq. (2.4.22a),

$$\frac{2}{3} N_c \omega_c \tilde{\Phi} \lambda_{1c} + N_c \Omega_c \lambda_{2c} + 2N_a \Omega_a \lambda_{2a} = 0, \tag{2.4.22b}$$

where

$$\tilde{\Phi} \equiv -\frac{e}{T}(\Phi_a - \Phi_c) > 0, \quad N_{a,c} = \int_{a,c} \frac{ds}{B} n_e .$$

Further, Eq. (2.4.19) yields

$$\frac{8\pi i}{m_e^2} \int dE d\mu \tau_a F_e \overline{C}(g_a) = 2\lambda_{1a} \omega_e^* \Omega_a N_a \frac{e\Delta\psi}{T}$$

$$= \lambda_{1c} \omega_e^* \Omega_c N_c \frac{e\Delta\psi}{T}. \tag{2.4.23}$$

Substituting Eq. (2.4.19) into Eq. (2.4.9) then yields

$$Q_e(\omega) = \frac{-8\pi e^2}{Tm_e^2}\int_p dE d\mu F_e \Delta\psi^2 \frac{\tau_a\tau_c}{\tau}\frac{\Omega_a\Omega_c(\omega-\omega_T^*)}{\omega-\bar{\omega}_E}$$
$$- 2m^2\int_c \frac{ds}{B^2 r}\kappa\frac{\partial p_e}{\partial\alpha}\psi_c^2 - 4m^2\int_a \frac{ds}{B^2 r}\kappa\frac{\partial p_e}{\partial\alpha}\psi_a^2 \qquad (2.4.24)$$
$$+ \frac{2\lambda_{1a}e^2}{T}N_a\Omega_a\Delta\psi^2\omega_e^*.$$

By using the results of the previous approaches[32-35], we can add the response of collisionless ions and the contribution from hot electrons to Eq. (2.4.24), and obtain the complete quadratic form $Q(\omega)$ as following

$$-Q(\omega) = R\psi_c^2 + S\psi_a^2 + W\Delta\psi^2, \qquad (2.4.25)$$

where

$$R = \int_0^{L_c}\frac{ds}{B_c^2}\frac{n_i m_i}{\alpha_p}\left\{\Omega_c^2(1+m^*) + \Omega_c[2\omega_{Ec} - m^*\omega_{ic}^*(1+\eta_i)] + \omega_{Ec}^2\right\} + \hat{\gamma}_c^2 m^2$$

$$S = 2\int_{L_c}^{\infty}\frac{ds}{B_a^2}\frac{n_i m_i}{\alpha_p}\left\{\Omega_a^2(1+m^*) + \Omega_a[2\omega_{Ea} - m^*\omega_{ia}^*(1+\eta_i)] + \omega_{Ea}^2\right\}$$
$$+ \hat{\gamma}_a^2 m^2 + \omega_i^*\Omega_a\Theta_h$$

$$W = \sum_j \frac{8\pi q_j^2}{T_j m_j^2}\int dE d\mu F_j \frac{\tau_a\tau_c}{\tau}\frac{\Omega_a\Omega_c(\omega-\omega_{Tj}^*)}{\omega-\hat{\omega}_E}$$
$$- 2\lambda_{1a}N_a\Omega_a\omega_e^*\frac{e^2}{T_e} + D_{\text{Landau}}$$

with

$$\alpha_p = Br_p^2$$
$$m^* = k_\perp^2 r_p^2 - 1, \quad \left(\frac{1}{r}\frac{\partial}{\partial r} \to \frac{1}{r_p^2}\right),$$
$$\Omega_{c,a} = \omega/m - \omega_{Ec,a},$$
$$\hat{\gamma}_c^2 = \int_0^{L_c}\frac{ds}{B_c^2}\frac{\kappa}{r}\frac{\partial}{\partial\alpha}(P_\parallel + P_\perp),$$
$$\hat{\gamma}_a^2 = \sum_j 2\int_{L_c}^{\infty}\frac{ds}{B_a^2}\frac{\kappa_{\text{eff}}}{r}\frac{\partial}{\partial\alpha}(P_{\parallel j} + P_{\perp j}),$$

which reflects the contribution from the hot electrons. And the charge uncovering term is given by

$$\Theta_h = \int_{-\infty}^{\infty} \frac{ds}{B^2} \frac{n_i m_i}{\alpha_p} \frac{\alpha_p q_i^2 \int \frac{ds}{B} n_h(s)}{\sum_j \int \frac{ds}{B^2} n_j T_j m_j}. \tag{2.4.26}$$

and

$$\omega_i^* = \frac{T_{c\perp}}{\alpha_p} \left[\frac{1 + \frac{2L_{si} n_{si} T_{si} B_c^2}{L_c n_c T_{c\perp} B_a^2}}{1 + \frac{2L_{si} n_a B_c^2}{L_c n_c B_a^2}} \right], \tag{2.4.27}$$

where 'si' refers to the sloshing ions. The ion Landau damping terms are

$$\begin{aligned} D_{\text{Landau}} = \frac{q_i^2}{T_i} N_i(\text{passing}) \times \\ \Big\{ & i\Omega_a^2 \Omega_c^2 [\omega - \omega_{Ec} - \hat{\omega}_{ic}^* (1 - \frac{3}{2}\eta_i)] \frac{L_c^2 L_\phi}{(T_i/m_i)^{\frac{3}{2}}} \alpha_1 G1 \\ & + \Omega_a [\omega - \omega_{Ea} - \hat{\omega}_{ic}^* (1 - \frac{1}{2}\eta_j)](1 + i\Omega_a \alpha_2) G2 \\ & + i[\omega - \omega_{Ec} - \hat{\omega}_{ic}^* (1 + \frac{1}{2}\eta_i)] \frac{(T_i/m_i)^{\frac{1}{2}}}{L_\phi} \alpha_3 G3 \Big\}, \end{aligned} \tag{2.4.28}$$

where

$$\hat{\omega}_{ic}^* = \frac{m T_j}{q_j n_{cj}} \frac{\partial n_{cj}}{\partial \alpha} [1 + \eta_{cj} (\frac{m_j v^2/2 + q_j \Phi}{T_j}) - \frac{3}{2})]$$

with n_{cj} being the factor of Maxwellian distribution as we defined in Eq. (2.2.4). And the coefficients α_1, α_2 and α_3 are

$$\begin{aligned} \alpha_1 &= 0.05 \ln \left(\frac{B_m - B_c}{B_m - B_a} \right) \{ (1 - \frac{B_c}{B_a}) [1 - (1 - \frac{B_a}{B_m})^{\frac{1}{2}}] \}^{-1}, \\ \alpha_2 &= (2\pi)^{-\frac{1}{2}} \ln \left(\frac{B_m}{B_m - B_a} \right) [1 - (1 - \frac{B_a}{B_m})^{\frac{1}{2}}]^{-1} \\ \alpha_3 &= (2\pi)^{-\frac{1}{2}} [1 - (1 - \frac{B_a}{B_m})^{\frac{1}{2}}]^{-1} \end{aligned}$$

And, the interpolation functions $G1, G2$ and $G3$ satisfy the following conditions

$$G1 = 1 \quad \text{if } |\tau_c(\omega - \omega_{Ec}) + 2\tau_a(\omega - \omega_{Ea})| < 1,$$

$$G2 = 1 \quad \text{if } |\tau_c(\omega - \omega_{Ec}) + 2\tau_a(\omega - \omega_{Ea})| > 1 \quad \text{and}$$

$$|2\tau_a(\omega - \omega_{Ea})| < 1,$$

$$G3 = 1 \quad \text{if } |2\tau_a(\omega - \omega_{Ea})| > 1,$$

otherwise they smoothly go to zero.

II.5 Evaluation of the Collisional Term

II.5.1 Case 1: Short Anchor Cells

We still need to evaluate the coefficient λ_{1a}, for which it is necessary to solve Eq. (2.4.15) with the boundary condition given by Eq. (2.4.14). The solution for the perturbed distribution of the central cell is taken as a Maxwellian up to the separatrix, which is justified if Eq. (2.4.17) is satisfied. Then we define $\tilde{g}_a$ from the relation

$$g_a = \frac{e\Delta\psi}{T}\omega_e^*\left[\lambda_{1c} - \frac{\omega-\omega_T^*}{\omega_e^*} + \lambda_{2c}\left(\frac{m_e v^2}{2T} - \frac{3}{2} - \tilde{\Phi}\right) + \tilde{g}_a\right], \qquad (2.5.1)$$

where we have used that, $m_e v_a^2/2 = m_e v_c^2/2 - \tilde{\Phi}T$, in which v_a and v_c are the electron speed in the anchor and central cell respectively. The relation follows from the energy conservation at the separatrix. By using Eqs. (2.4.14) and (2.4.16), we find that on the separatrix

$$\tilde{g}_a(\text{separatrix}) = 0. \qquad (2.5.2)$$

From Eq. (2.4.15), we find that the function $\tilde{g}_a$ satisfies the following equation

$$\overline{C}_l(\tilde{g}_a) = -S_{\text{wave}}, \qquad (2.5.3)$$

where

$$S_{wave} = i\Omega_a\left[\tilde{g}_a + S_1 + S_2\left(\frac{m_e v^2}{2T} - \frac{3}{2}\right)\right],$$

with

$$S_1 = \lambda_{1c} - \lambda_{2c}\tilde{\Phi} - \frac{\omega}{\omega_e^*} + 1 - \eta\tilde{\Phi}_c - \eta\tilde{\Phi},$$

$$S_2 = \lambda_{2c} + \eta,$$

$$\tilde{\Phi}_c = -\frac{e\Phi_c}{T}.$$

Here S_{wave} serves as an effective source of the particles and energy. The solution can be expressed in terms of the linearized Pastukhov problem.

Now, it is essential to relate Eq. (2.5.3) to the known solution of the Pastukhov problem . For simplicity, we limit ourself to the assumption that the electrons are confined in the square-well potential of magnitude $|e\Phi|$ so that the Pastukhov problem has analytic solutions.

Following the standard definitions, the particle loss rate ν_p and energy loss rate ν_{pE} are given respectively by

$$\nu_p = \frac{\int d^3v S_{eo}(v)}{\int d^3v F_p(v)} \tag{2.5.4}$$

and

$$\nu_{pE} = \frac{\int d^3v v^2 S_{eo}(v)}{\int d^3v v^2 F_p(v)}, \tag{2.5.5}$$

where $F_e(v)$ satisties the Fokker-Planck equation

$$C(F_p) = -S_{eo}(v), \tag{2.5.6}$$

with $C(F_p)$ defined by Eq. (2.3.2) and we have the boundary condition that $F_p(v)$ vanishes on the separatrix.

As long as $S_{eo}(v)$ is not too peaked near the separatrix, the values of ν_p and ν_{pE} are insensitive to the precise form of $S_{eo}(v)$ if $\frac{|e\Phi|}{T} > 1$. The reason or this assertion was explained in Sec. II.3.3. We further note that the distribution $F_p(v)$ for the bulk of particles is a Maxwellian with a density n_0 and temperature T. It only deviates from the Maxwellian

near the separatrix, which does not change the moments of F_p to an exponential small factor. Thus, we write

$$F_p(\mathbf{v}) = F_0(v)G(\mathbf{v}), \tag{2.5.7}$$

where F_0 is a standard Maxwellian

$$F_0 = \frac{n_0}{(2\pi T/m_e)^{\frac{3}{2}}} \exp(-\frac{m_e v^2}{2T})$$

related to n_0 and T and the function G is the unity except near the separatrix.

Then we have

$$\begin{aligned} \nu_p &= \frac{1}{n_0}\int d^3v S_{eo}(\mathbf{v}), \\ \nu_{pE} &= \frac{m_e}{3n_0T}\int d^3v v^2 S_{eo}(\mathbf{v}). \end{aligned} \tag{2.5.8}$$

If we substitute Eq. (2.5.7) into Eq. (2.3.2) we find

$$\begin{aligned} C(F_p) = \int d^3v' \sum_j \frac{b_j}{m_e}\frac{\partial}{\partial \mathbf{v}} F_0(v)F_{0j}(v') \\ \cdot \frac{\mathbf{I}g^2 - \mathbf{gg}}{g^3}\cdot\frac{\partial}{\partial \mathbf{v}} G(\mathbf{v}) = -S_{eo}(\mathbf{v}), \end{aligned} \tag{2.5.9}$$

where we have neglected the term $F_0(v')\partial G(\mathbf{v}')/\partial \mathbf{v}'$ as $\partial G(\mathbf{v}')/\partial \mathbf{v}'$ vanishes except near the separatrix. The contribution near the separatrix can be neglected since the Maxwellian weighting in the $\mathbf{v}'$ integration produces an exponential small error. The equation (2.5.9) is also the form of the collision operator used by Pastukhov and subsequent investigators in solving the scattering coefficients ν_p and ν_{pE}.

For the actual density and temperature we must solve the nonlinear algebraic problems posed by Eqs. (2.5.8) and (2.3.8) that can be rewritten as

$$n_0 = \frac{\int d^3v S_{eo}}{\nu_p(n_0, T)},$$
$$\frac{3}{2} n_0 T = \frac{m_e \int d^3v v^2 S_{eo}}{2(|e\Phi|/T + 1)\nu_p(n_0, T)}. \tag{2.5.10}$$

These two nolinear equations determine n_0 and T.

Now we assume that the source $S_{eo}(\mathbf{v})$ has small deviation δS from the initial function, and that the separatrix does not change. The density and temperature will change by δn and δT, and Eq. (2.5.10) becomes

$$n_0 + \delta n = \frac{\int d^3v S_{eo} + \int d^3v \delta S}{\nu_(n_0, T) + \delta T(\partial\nu_p/\partial\nu_p/\partial T) + \delta n(\partial\nu_p/\partial n)},$$
$$\frac{3}{2}(n_0 T + \delta n T + n_0 \delta T) = \frac{m_e \int d^3v v^2 (S_{eo} + \delta S)/2}{\nu_{pE}(n_0, T) + \delta T(\partial\nu_{pE}/\partial T) + \delta n(\partial\nu_{pE}/\partial n)}. \tag{2.5.11}$$

Noticing the equilibrium relations, we can linearize all the small quantities and find

$$2\nu_p \delta n + n_0 \delta T \frac{\partial \nu_p}{\partial T} = \int d^3 \delta S, \tag{2.5.12a}$$

$$2\nu_p \delta n + n_0 \delta T \frac{\partial \nu_p}{\partial T} + \nu_p \frac{n_0 \delta T}{T(1+\tilde{\Phi})} = \frac{m_e}{3T(1+\tilde{\Phi})} \int d^3 v v^2 \delta S, \tag{2.5.12b}$$

where $\tilde{\Phi} \equiv -e\Phi/T$ has been used. Substituting Eq. (2.5.12a) into Eq. (2.5.12b) yields

$$\frac{\nu_p n_0 \delta T}{T(1+\tilde{\Phi})} = \frac{m_e}{3T(1+\tilde{\Phi})} \int d^3 v v^2 \delta S - \int d^3 v \delta S. \tag{2.5.12b}$$

Thus, the two quantities δn and δT are determined in terms of the source variation δS, which can be related to the linearized Pastukhov problem.

If we linearize the Fokker-Planck operator given in Eq. (2.5.9) about $F_p = F_0(v)G(\mathbf{v})$, we have

$$F(\mathbf{v}) = F_0(v)G(\mathbf{v}) + \delta F,$$

$$\delta F = F_0(v)h(v).$$

Then

$$C(F_p + \delta F) - C(F_p) \equiv C_{lp}(h(v)) = -\delta S, \tag{2.5.13}$$

with

$$\begin{aligned} C_{lp}(h(v)) &= \int d^3v' \sum_j \frac{b_j}{m_e}\frac{\partial}{\partial \mathbf{v}} \cdot \frac{\mathbf{I}g^2 - \mathbf{gg}}{g^3}\left(\frac{1}{m_e}\frac{\partial}{\partial \mathbf{v}} - \frac{1}{m_j}\frac{\partial}{\partial \mathbf{v}'}\right) \\ &\quad \times [F_0(v)G(\mathbf{v})F_{0j}(v')h_j(\mathbf{v}') + F_{0j}(v')G_j(\mathbf{v}')F_0(v)h(\mathbf{v})] \\ &= \int d^3v' \sum_j \frac{b_j}{m_e}\frac{\partial}{\partial \mathbf{v}} \cdot \left(F_0(v)F_{0j}(v')\frac{\mathbf{I}g^2 - \mathbf{gg}}{g^3}\right) \\ &\quad \cdot \left(\frac{h_j(\mathbf{v}')}{m_e}\frac{\partial}{\partial \mathbf{v}}G_e(\mathbf{v}) - \frac{G_e(\mathbf{v})}{m_j}\frac{\partial h_j(\mathbf{v}')}{\partial \mathbf{v}'}\right. \\ &\quad \left. + \frac{G_j(\mathbf{v}')}{m_e}\frac{\partial h_e(\mathbf{v})}{\partial \mathbf{v}} - \frac{h_e(\mathbf{v})}{m_j}\frac{\partial}{\partial \mathbf{v}'}G_j(\mathbf{v}')\right). \end{aligned} \tag{2.5.14}$$

We note that over most of the phase space the solution for the elecron distribution

$$C_{lp}\big((h_e(\mathbf{v})\big) = -\delta S \tag{2.5.15}$$

will be the form

$$h_e(v) = \frac{\delta n_e}{n_0} + \frac{\delta T_e}{T}\left(\frac{m_e v^2}{2T} - \frac{3}{2}\right), \tag{2.5.16}$$

where $\delta n_e = \delta n_i = \delta n$ with δn, and $\delta T_e = \delta T$ with δT are defined in Eq. (2.5.11). We find that for the ion term we can have $h_i(\mathbf{v})$ as any arbitrary function since only the zeroth-order moment of $h_i(\mathbf{v})$ couples into the problem as the electron-ion energy exchange in the collision operator is negligible. This solution fails near the separatrix where $h_j(v)$ vanishes. Nonetheless, Eq. (2.5.16) is suitable for determining moments, as the deviation of the solution near the separatrix only introduces an exponentially small error if $\tilde{\Phi} \gg 1$. For similar reasons, we can set $\partial G_(\mathbf{v})/\partial \mathbf{v}' = 0$ and $G(\mathbf{v}) = 1$, in the last two terms in the large parenttheses of Eq. (2.5.14). The function $G(\mathbf{v})$ in the second term in the parenttheses is 1 nearly everwhere except near the separatrix. As $G(\mathbf{v})$ is equal to zero on the separatrix this term does not directly produce particle flux. when $G(\mathbf{v})$ is replaced by unity, there is direct particle flux from this term, but it can be easily shown to be small by a factor $1/\tilde{\Phi}$ compared to the direct flux of the third term. Hence to the order $1/\tilde{\Phi}$ we can replace $G(\mathbf{v})$ by unity in the second term. In the first term, we can replace $h(v')$ by

$$h(\mathbf{v}') = \frac{\delta n}{n_0} + \frac{\delta T}{T}\left(\frac{m_e v'^2}{2T} - \frac{3}{2}\right). \tag{2.5.17}$$

The first term in the last set of the large parentheses of Eq. (2.5.14) then becomes (notice that the δT term in the eletron contribution vanishes to the leading order, as $v^2 \sim \Phi/m_e \gg v'^2 \approx T/m_e$, $\mathbf{g} \approx \mathbf{v}$),

$$\frac{\delta n}{n_0}\int d^3v' \sum_j \frac{b_j}{m_j}\frac{\partial}{\partial \mathbf{v}} F_0(v)F_{0j}(v') \cdot \frac{\mathbf{I}g^2 - \mathbf{gg}}{g^3} \cdot \frac{\partial G_e(\mathbf{v})}{m_e \partial \mathbf{v}} = -\frac{\delta n}{n_0} S_{eo}(\mathbf{v}), \tag{2.5.18}$$

where we used Eq. (2.5.9) to obtain the right-hand side. We thereby find

$$C_{lp}(h) = C_l(h) - \frac{\delta n}{n_0} S_{eo}(v) = -\delta S, \tag{2.5.19}$$

where $C_l(h)$ is given in Eq. (2.3.5) and is the linearized Fokker-planck operator we are interested in for the wave problem. Comparing Eq. (2.5.19) and Eq. (2.5.3) shows that

$$\delta S = S_{\text{wave}} + \frac{\delta n}{n_0} S_{eo}(v). \tag{2.5.20}$$

Observe that the equation and boundary conditions for h are identical to that for $\tilde{g}_a$ if S_{wave} is given by Eq. (2.5.3), and hence $h = \tilde{g}_a$.

Now we find the expression for the source term. Combining Eqs. (2.5.20) and (2.5.12), and, using $T(\partial\nu_p/\partial T) = \tilde{\Phi}\nu_p[1 + o(1/\tilde{\Phi})]$ and Eq. (2.3.23), we have

$$\begin{aligned} \nu_p \delta n + \frac{n_0 \delta T}{T} \tilde{\Phi} \nu_p &= \int S_{\text{wave}} d^3 v \\ \frac{\delta T}{T} \frac{\nu_p}{\tilde{\Phi}} n_0 &= \int d^3 v \left(\frac{m_e v^2}{3\tilde{\Phi} T} S_{\text{wave}} - S_{\text{wave}} \right) + o(\frac{1}{\tilde{\Phi}}). \end{aligned} \tag{2.5.21}$$

Then, using Eqs. (2.5.3) and (2.5.16) for $h(v)$ we find

$$\begin{aligned} \nu_p \delta n + n_0 \frac{\delta T}{T} \tilde{\Phi} \nu_p &= i\Omega_a (\delta n + n_0 S_1) \\ \frac{\delta T}{T} \frac{\nu_p}{\tilde{\Phi}} n_0 &= i\Omega_a \left[-\delta n - n_0 S_1 + \frac{n_0}{\tilde{\Phi}} \left(\frac{\delta T}{T} + S_2 \right) \right] \\ &\quad \times \left[1 + o\left(\frac{1}{\tilde{\Phi}} \right) \right]. \end{aligned} \tag{2.5.22}$$

Solving for δn and δT we have

$$\begin{aligned} \frac{\delta n}{n_0} &= -\frac{-\Omega_a(\Omega_a + i\nu_p) - i\tilde{\Phi}^2 \nu_p \Omega_a + i\tilde{\Phi} S_2 \nu_p \Omega_a}{(\Omega_a + i\nu_p)^2 + i\tilde{\Phi}^2 \nu_p \Omega_a} \\ \frac{\delta T}{T} &= \frac{i\Omega_a [\nu_p S_1 \tilde{\Phi} + i S_2 (\Omega_a + i\nu_p)]}{(\Omega_a + i\nu_p)^2 + i\tilde{\Phi}^2 \nu_p \Omega_a}. \end{aligned} \tag{2.5.23}$$

The distribution, which we are interested in, g_a for the anchor response is

$$g_a = \omega_e^* \frac{e\Delta\psi}{T}\left[S_1 + S_2\left(\frac{m_e v^2}{2T} - \frac{3}{2}\right) + \frac{\delta n}{n_0} + \frac{\delta T}{T}\left(\frac{m_e v^2}{2T} - \frac{3}{2}\right)\right]. \quad (2.5.24)$$

Combining Eqs. (2.5.23) and (2.5.24) we have

$$g_a = \frac{i\nu_p e\Delta\psi\omega_e^*}{T}\times$$
$$\frac{S_1(\Omega_a + i\nu_p) + \tilde{\Phi}S_2\Omega_a + (\frac{m_e v^2}{2T} - \frac{3}{2})[S_2(\Omega_a + \Omega_a\tilde{\Phi}^2 + i\nu_p) + S_1\Omega_a\tilde{\Phi}]}{(\Omega_a + i\nu_p)^2 + i\tilde{\Phi}^2\nu_p\Omega_a}. \quad (2.5.25)$$

Comparing Eq. (2.5.25) with Eq. (2.4.20) determines the two additional relations

$$\begin{aligned}\lambda_{1a} &= i\nu_p[S_1(\Omega_a + i\nu_p) + S_2\Omega_a\tilde{\Phi}]/U \\ \lambda_{2a} &= i\nu_p[S_2(\Omega_a + i\nu_p + \Omega_a\tilde{\Phi}^2) + S_1\Omega_a\tilde{\Phi}]/U,\end{aligned} \quad (2.5.26a)$$

where

$$U = (\Omega_a + i\nu_p)^2 + i\nu_p\Omega_a\tilde{\Phi}^2.$$

Adding Eq. (2.4.22)

$$\begin{aligned}&\Omega_c N_c\lambda_{1c} + 2\Omega_a N_a\lambda_{1a} = 0 \\ &\frac{2}{3}N_c\omega_c\tilde{\Phi}\lambda_{1c} + N_c\Omega_c\lambda_{2c} + 2N_a\Omega_a\lambda_{2a} = 0\end{aligned} \quad (2.5.26b)$$

to Eq. (2.5.26a), we have a complete set of equations for λ coefficients.

We can rewrite Eq. (2.5.26) in the following way

$$\begin{aligned}\lambda_{1c}X + \lambda_{2c}Y &= -(a_1 Q + \eta b_1) \\ \lambda_{1c}Z + \lambda_{2c}X &= -(a_2 Q + \eta b_2),\end{aligned} \quad (2.5.27)$$

with

$$X = 2iN_a\Omega_a\nu_p(\Omega_a + i\nu_p) + N_c\Omega_c[(\Omega_a + i\nu_p)^2 + i\tilde{\Phi}^2\nu_p\Omega_a],$$

$$Y = 2\nu_p^2 N_a\Omega_a\tilde{\Phi},$$

$$Z = 2i\nu_p N_a\Omega_a^2\tilde{\Phi} + 2N_c\Omega_c\tilde{\Phi}[(\Omega_a + i\nu_p)^2 + i\tilde{\Phi}^2\nu_p\Omega_a]/3$$

$$Q = \omega/\omega_e - 1 + \eta\tilde{\Phi}_c$$

$$a_1 = -2iN_a\Omega_a\nu_p(\Omega_a + i\nu_p)$$

$$a_2 = -2iN_a\Omega_a\Omega_a^2\nu_p\tilde{\Phi}$$

$$b_1 = 2N_a\Omega_a\nu_p^2\tilde{\Phi}$$

$$b_2 = 2iN_a\Omega_a\nu_p(\Omega_a + i\nu_p).$$

Now solving for λ_{1c}, and using $-N_c\Omega_c\lambda_{1c} = 2N_a\Omega_a\lambda_{1a}$, which is the quantity explicitly needed in the functional disperional relation, we find

$$2N_a\Omega_a\lambda_{1a} = -2i\nu_p N_a N_c\Omega_a\Omega_c UV/(X^2 - YZ), \tag{2.5.28}$$

where

$$V = (\omega/\omega_e^* - 1 + \eta\tilde{\Phi}_c)[2i\nu_p N_a\Omega_a + N_c\Omega_c(\Omega_a + i\nu_p)] + i\eta\Omega_c\nu_p N_c\tilde{\Phi}$$

II.5.2 Case 2: Anchor Cells with Arbitrary Length

Now, the distribution of the passing particles has to be evaluated explicitly. In order to do so, it is assumed that the characteristic electron collision frequency is larger than the typical mode frequency and then the distribution function for the trapped particles can still be described by Eq. (2.4.16). By the similar arguments, one can express the distribution of passing particles as the following

$$h_p = \frac{e\Delta\psi\omega_e^*}{T}[\lambda_{1p} + \lambda_{2p}(\frac{\varepsilon}{T} - \frac{3}{2}) + \frac{e(\omega - \omega_e^*)}{T}\psi_c], \qquad (2.5.29)$$

where $\varepsilon = m_e v^2/2 + e\Phi(s)$ with $\Phi(s)$ being the equilibrium potential which the passing particles experience. The last term is introduced for mathematical convenience. Actually, the final result is independent of the form of the term.

In order to evaluate the collisional effects in this situation, there are two more parameters λ_{1p} and λ_{2p}, which have to be determined.

As we take the zeroth moment and energy moment, Eq. (2.4.18) remains correct if the number of the passing particles is assumed to occupy a small population of the total particles.

For the scattering from the anchor cells to the central cell, the process is very similar to that in the case 1. At the separatrix, we have

$$h_p = h_a|_{\mu,\varepsilon,\alpha}. \qquad (2.5.30)$$

Exactly following the procedure in the case 1, we find

$$\lambda_{1a} = i\nu_p[S_1(\Omega_a + i\nu_p) + S_2\Omega_a\tilde{\Phi}]/U \qquad (2.5.31a)$$

and

$$\lambda_{2a} = i\nu_p[S_2(\Omega_a + i\nu_p + \Omega_a\tilde{\Phi}^2) + S_1\Omega_a\tilde{\Phi}]/U, \qquad (2.5.31b)$$

where

$$U = (\Omega_a + i\nu_p)^2 + i\nu_p\Omega_a\tilde{\Phi}^2$$

$$S_1 = \lambda_{1p} - \lambda_{2p}\tilde{\Phi} - \frac{\omega}{\omega_e^*} + 1 - \eta\tilde{\Phi}_a$$

$$S_2 = \lambda_{2p} + \eta.$$

For the scattering from the central region to the anchor regions, the situation is different. It is considered that the electrons in the central cell are trapped mainly by the magnetic trapping. The scattering coefficients due to electron-electron and electron-ion collisions were calculated in Sec. II.3.3. Now, we try to construct two more equations for the unknown parameters λ_{1p} and λ_{2p}.

The collisional operator is the same as Eq. (2.5.14). However, the distributioin of particles shows slightly different features from that in Pastukhov problem. We assume the total distribution has the following form

$$\begin{aligned} F(\mathrm{v}) &= F_p + \delta F \\ &= F_e G(\mathrm{v}) + F_e h(\mathrm{v}), \end{aligned} \qquad (2.5.32)$$

where

$$G(v) = G(\theta) = \begin{cases} 1 & \theta < \theta_0 \text{ or } \theta > \pi - \theta_0 \\ 0 & \text{otherwise} \end{cases} \qquad (2.5.33)$$

The last three terms in Eq. (2.5.14) can be similarly evaluated as in Sec.II.5.1. The first term has to be treated differently. We have perturbed

distributions for ions and electrons

$$h_e(v') = \frac{\delta n}{n_0} + \frac{\delta T}{T}(\frac{m_e v'^2}{2T} - \frac{3}{2})$$
$$h_i(v') = \frac{\delta n}{n_0}. \tag{2.5.34}$$

The heating effects on ions have been neglected. Substituting Eq. (2.5.34) into Eq. (2.5.14) yields

$$\begin{aligned} C_{lp}(h(v)) &= -[S_{\text{wave}} + \frac{\delta n}{n_0} S_{eo}(v) + \frac{\delta T}{T}\frac{\partial D_\perp}{\partial T} D_\perp^{-1} S_{e-e}(v)] \\ &= -\delta S, \end{aligned} \tag{2.5.35}$$

where S_{eo} has been defined in Eq. (2.5.18) and $D_\perp$ is defined in Sec.II.3. The following calculation has been employed to obtain Eq. (2.5.35)

$$\begin{aligned} &\int d^3v' \frac{b_e}{m_e}\frac{\partial}{\partial v} F_{0e}(v) F_{0e}(v') \frac{\mathbf{I}g^2 - \mathbf{g}\mathbf{g}}{g^3}\frac{\partial}{\partial v} G(v) \\ =&\frac{D_\perp}{v^2}\frac{1}{\sin\theta}\frac{\partial}{\partial\theta}\sin\theta\frac{\partial}{\partial\theta} F_0(v) G(\theta) \\ =&S_{e-e}(v). \end{aligned} \tag{2.5.36}$$

Plugging Eq. (2.5.35) into Eq. (2.5.12) and using the scattering coefficients evaluated in Sec.II.3.3, we find

$$\begin{aligned} \frac{\delta n}{n_0} &= \frac{i\Omega_c}{R_c}[\lambda_{1p}(\frac{5}{2}\nu_{E^2e-e} - \nu_{Ee-e} - \frac{\nu_E}{2} - i\Omega_c) - \lambda_{2p}(\frac{3}{2}\nu_{Ee-e} - \frac{3}{2}\nu_p)] \\ \frac{\delta T}{T} &= \frac{i\Omega_c}{R_c}[\lambda_{2p}(\nu_p - i\Omega_c) - \lambda_{1p}\nu_E], \end{aligned} \tag{2.5.37}$$

where

$$\nu_p = \nu_{e-e} + \nu_{e-i}$$

$$\nu_E = \nu_{Ee-e} + \nu_{Ee-i}$$

$$\begin{aligned} R_c = &-\nu_p\nu_{Ee-e} + \nu_p\nu_E + \frac{5}{2}\nu_p\nu_{E^2e-e} - i\nu_p\Omega_c + i\Omega_c\nu_{Ee-e} + \frac{1}{2}i\Omega_c\nu_E \\ &- \frac{5}{2}i\Omega_c\nu_{E^2e-e} - \Omega_c^2 + \frac{3}{2}\nu_p\nu_E - \frac{3}{2}\nu_E\nu_{Ee-e}. \end{aligned}$$

where ν_{e-e}, ν_{e-i}, ν_{Ee-e}, ν_{Ee-i} and ν_{E^2e-e} are defined and calculated through Eq. (2.3.16) to Eq. (2.3.21). As that in case 1, we can express g_c as the following

$$g_c = \frac{e\Delta\psi\omega_e^*}{T}[\lambda_{1p} + \lambda_{2p}(\frac{mv^2}{2T} - \frac{3}{2}) + \tilde{g}_c], \tag{2.5.38}$$

where $\tilde{g}_c = 0$ at the separatrix. Noting that $\tilde{g}_c$ is identical with h_e in Eq. (2.5.34), we have from comparing with Eq. (2.4.16b)

$$\begin{aligned}
\lambda_{1c} &= \lambda_{1p} + \frac{i\Omega_c}{R_c}[\lambda_{1p}(\frac{5}{2}\nu_{E^2e-e} - \nu_{Ee-e} - \frac{\nu_E}{2} - i\Omega_c) \\
&\qquad - \lambda_{2p}(\frac{3}{2}\nu_{Ee-e} - \frac{3}{2}\nu_p)] \\
\lambda_{2c} &= \lambda_{2p} + \frac{i\Omega_c}{R_c}[\lambda_{2p}(\nu_p - i\Omega_c) - \lambda_{1p}\nu_E] \\
&\Omega_c N_c\lambda_{1c} + 2\Omega_a N_a\lambda_{1a} = 0 \\
&\frac{2}{3}N_c\omega_c\tilde{\Phi}\lambda_{1c} + N_c\Omega_c\lambda_{2c} + 2N_a\Omega_a\lambda_{2a} = 0 \\
&\lambda_{1a} = i\nu_p[S_1(\Omega_a + i\nu_p) + S_2\Omega_a\tilde{\Phi}]/U \\
&\lambda_{2a} = i\nu_p[S_2(\Omega_a + i\nu_p + \Omega_a\tilde{\Phi}^2) + S_1\Omega_a\tilde{\Phi}]/U.
\end{aligned} \tag{2.5.39}$$

where S_1 and S_2 is defined in Eq. (2.5.31) instead of Eq. (2.5.3) as in the case 1. However, it is now explicit that in low frequency limit $\Omega_c \ll R_c$ Eq. (2.5.39) reduces to Eq. (2.5.26).

In our numerical work, we will compare the collisional effects given by Eqs. (2.5.26) and (2.5.39). The results shown in Fig. 3.18. illustrate a relatively small quantitative difference for the cases I and II.

II.6 Summary

The quadratic variational form, which is suitable to study the instabilities in tandem mirrors, have been derived. Various physical effects are included in the relatively compact variational form. Particularly, the collision term is evaluated analytically. In the next chapter, we will use it to achieve a simplified dispersion relation and study two important instability modes: flute mode and trapped particle mode. We will find that the two modes are just two branches of the dispersion relation.

Chapter III. Investigation of Instabilities

III.1. Introduction

In this chapter we utilize the dispersion relation obtained in the last chapter to investigate two major instabilities in the tandem mirrors: flute modes and trapped particle modes.

It should be noticed that the features of those two modes described by the dispersion relation are not as distinguishable as their terminology suggests. Literally, the typical trapped particle modes are supposed to appear only in the central cell where the magnetic field curvature is not favorable, while the flute modes to spread along the total machine. But, when studying the dispersion relation one finds out that though those two modes belong to different branches of solutions of the dispersion their features are often mixed together.

To compare our theory with several previous theories, we pay extra attention to examining the limiting situation where the parameters are taken maximum or minimum values (sometimes artificially). For instance, when assuming the contribution of the passing particles are high the instability modes obtained by solving the dispersion relation must be flute modes since the passing particles carry the all perturbation throughout the magnetic field line. Whereas, when the magnetic and electrostatic plugs are too effective the trapped particle modes are obtained. After studying these situations, we slowly vary all the parameters until they

approach the realistic values. Since the modes are continous in the parameter space we are able to name those mode branches in terms of the behaviors at the limiting situations. In this way, we not only explicitly obtain the solution branches but also gain more insight about the mode origins.

The parameters used in this dissertation are based on data collected in the TMX-U experimental machine. We use them to do our numerical investigations and do not see, in principle, difficulties to apply the method to the similar machines though some minor modification seems inevitable. Due to some experimental uncertainties, some parameters are not as well-defined as others. As a remedy of those kinds of deficiency, we take a "scan"of the variables in a reasonable range to make sure there are no major physical effects being omitted.

The flute modes were not the major subject of this research. However, it turns out that the parallel research of the flute mode is very important. The flute modes are one very possible candidate to explain the instabilities which are observed in TMX-U device. To some extent, it seemingly gives even better predictions on the mode frequency and instability threshold. Furthermore, the trapped particle modes have some similarities and dissimilarities compared with the flute modes. It is hoped that by comparing them analytically and numerically one can pinpoint the instability origin of the observed modes or even achieve some ideas to suppress the instabilities. When studying the trapped particle modes,

we also compare our results with those the previous collisionless theory and collisional theory. The ion Landau-dampling terms derived by Berk et al[35] is also considered in order to extract more accurate and more physical conclusions. The derivation was basicly conducted in the short wavelength limit, but the applicabability to the long-wavelength sitation is manifested in the discussion.

III.2. Experimental Devices and Observations

The TMX-U device in Lawrence Livermore National Laboratory has been built with the basic tandem mirror magnetic structure and can run with the electrostatic plug on or off. The equilibrium electric and magnetic configuration and various heating schemes are shown in Fig. 3.1 (as a comparison another tandem mirror structure in TARA is also shown in Fig. 3.2).

The device parameters in the central cell and anchor cells are listed in Table I. Note that when the central cell heating (ICH or Neutral Beam Heating) is on the ion distribution is more nonisotropic and the plasma length of the central cell will be longer which both have effects on the other parameters. We will use the data to calculate the parameters in the dispersion relation.

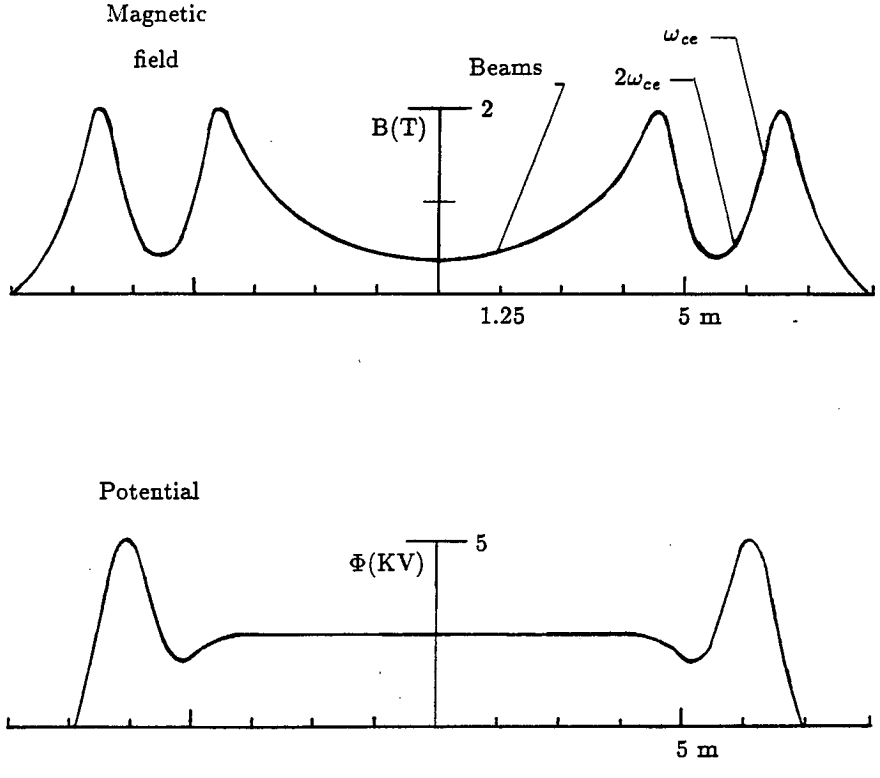

Fig. 3.1. Magnetic field, density and potential profiles projected to be achieved in TMX-U.

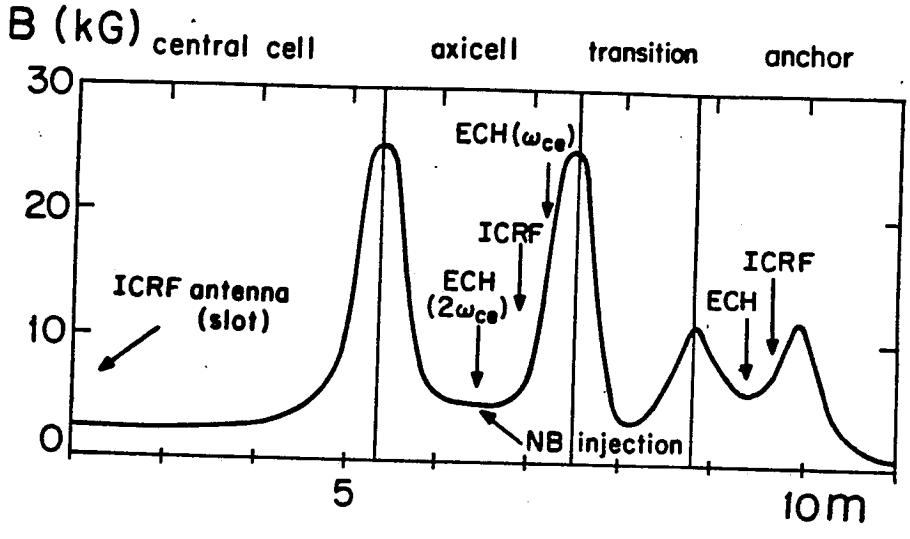

Fig. 3.2. Magnetic configuration and heating arrangement in TARA.

Table I. Typical TMX-U Parameters

Central – cell	
Magnetic field, B_c(T)	0.3
Limiter radius, r_L(m)	0.24
On-axis potential, ϕ_0(KV)	1.0
Perpendicular ion temperature,† $T_{c\perp}$(KeV)	0.1 to 1.0
Plasma length,† L_c(m)	5.0 to 2.5
Pressure Gaussian radius, r_p(m)	0.128
Central-cell density, $n_c(\mathrm{m}^{-3})$	10^{18}
End – cellanchor	
Magnetic field, B_a(T)	0.5
Hot-electron length, L_h(m)	1.0
Hot-electron Gaussian radius, r_{he}(m)	0.2
Anchor vacuum curvature,$\kappa/r(\mathrm{m}^{-2})$	0.5
Hot-electron energy, E(KeV)	300
Hot-electron density, $n_{he}(\mathrm{m}^{-3})$	1×10^{17}
Hot-electron diamagnetism, M_A (A·m)	2×10^3
Sloshing-ion length, L_{si}(m)	2
Sloshing-ion Gaussian radius, r_{si}(m)	0.12

Sloshing-ion energy, E_{si}(KeV)	3.5
Sloshing-ion density, $n_{si}(\mathrm{m}^{-3})$	10^{17}
Total midplane electron density, $n_A(\mathrm{m}^{-3})$	10^{18}

†Without central-cell heating, the temperature is lower and the ions are more isotropic; therefore, the length is longer.

Several heating schemes can be on or off depending on experimental contexts. As one purpose, the ion heating in the central cell is to prevent too many ions to fill the thermal barrier. In the anchor cells, there are two Electron Cyclotron Heating frequencies, one is ω_{ce} and another $2\omega_{ce}$. The heating serves dual purposes: the diamagnetic current created by hot electrons may provide essential stabilization and higher electron temperature can lower the density requirement in the anchor regions. And, there are "sloshing" ions injected into the anchor cells which are hopefully to obtain the "thermal barrier operation".

Fig. 3.3a shows an example of the effect of the observed modes on central-cell density buildup following plugging, when sloshing beams are turned on. The increase in the line-average density is abruptly terminated at $27.5ms$. Fig. 3.3b shows the density on an expanded time scale with the on-axis microwave interferometer and 13cm radially offset interferometer. Note the presence of the low-frequency oscillations, especially in the off-axis interferometer. Also note that when the density buildup is terminated, the two line-integral measurements are nearly equal, indicating a broad radial profile that suggests large radial transport.

In Fig. 3.4, it is shown that the hot electron ring seemingly tends to be pushed out of the axis of the machine, which lowers the effectiveness of stabilization.

Fig. 3.5 shows the similar oscillation occurs in the TARA machine. Note that the mode frequency is close to that in TMX-U.

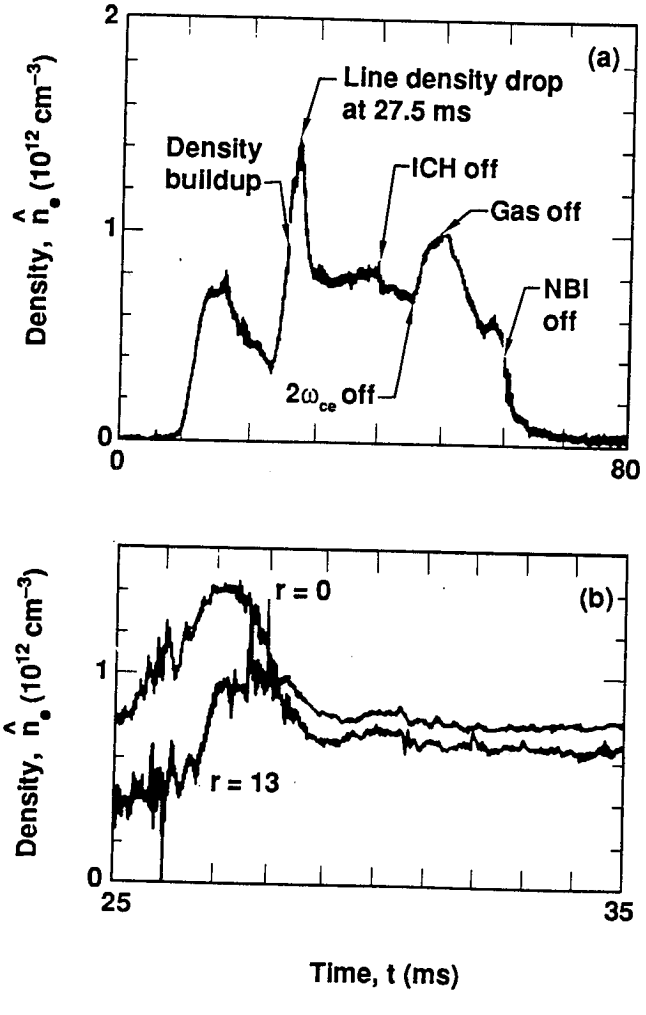

Fig. 3.3. (a) Microwave-measured, central-cell line-averaged density as a function of time. (b) Expanded time scale of the central-cell line-averaged density for interferometer channels at $r = 0$ and $r = 13$cm.

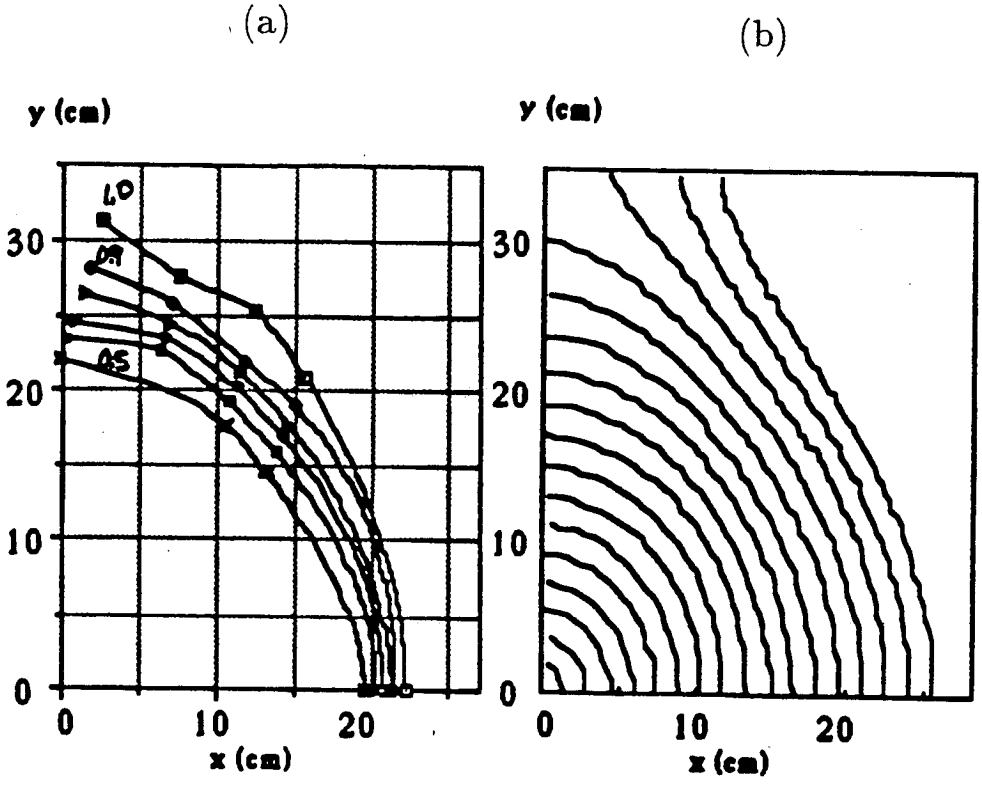

Fig. 3.4. (a) Measurement of hot-electron scrape-off contours. (b) Magnetic curvature drift surfaces in the anchor region.

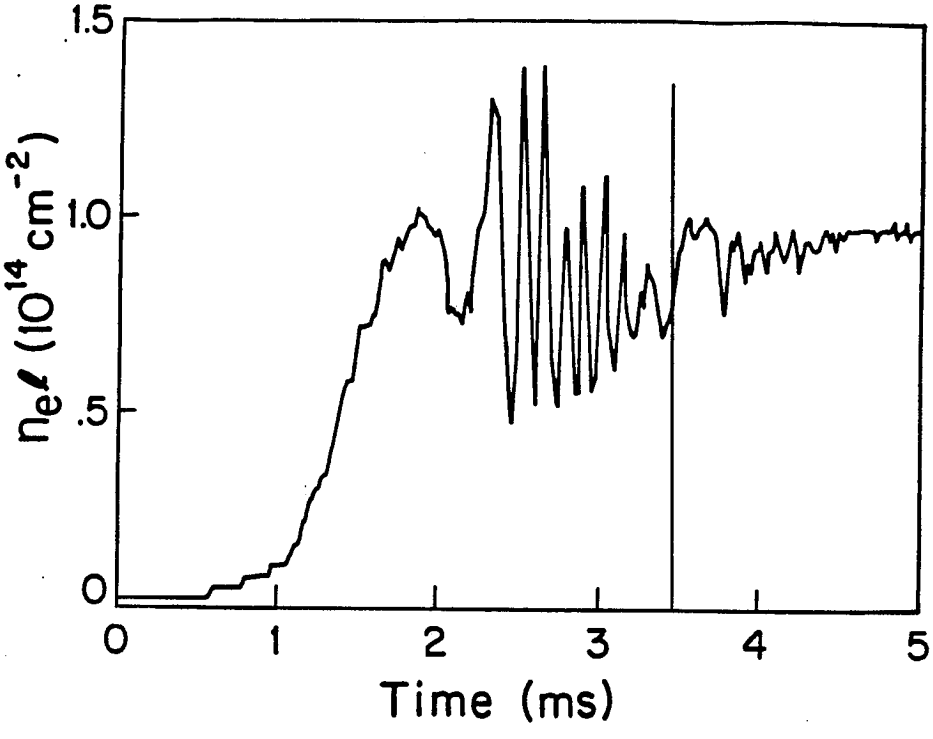

Fig. 3.5. Density fluctuation in unstable situations of TARA operation.

III.3 Preliminaries for Numerical Studies

In this section we evaluate quantities in the dispersion relation Eq. (2.5.21) based on TMX-U data. However, for simplicity of the analysis, we use the tandem mirror model configuration shown in Fig. 3.6.

A. Profile of the Equilibrium

A common model that is used to describe the equilibrium of a system is to employ a Gaussian profile for the density $n_j(r)$ and pressure $p_j(r)$. The potential is asssumed to yield a uniform electrostatic field toward to the wall of the machine. Thus, one has

$$\begin{aligned} n_j &= n_{0j}(s)\exp\Big(-\frac{\alpha}{B_0 r_p^2}\Big) \\ p_j &= n_{0j}(s)T_j\exp\Big(-\frac{\alpha}{B_0 r_p^2}\Big) \\ \Phi &= \Phi_0\Big(1-\frac{2\alpha}{B_0 r_L^2}\Big), \end{aligned} \tag{3.3.1}$$

where α is defined as the magnetic flux with a factor 2π and r_L is the limiter radius. The evaluation for the parameter r_p according the Gaussian model can be related to the customary parabolic profile used by TMX-U experimentalists as follows

$$\int dl = (2\pi)^{\frac{1}{2}} r_p = \frac{4}{3} r_L$$

$$r_p = \frac{4r_L}{3(2\pi)^{\frac{1}{2}}} = 0.53 r_L = 0.128m. \tag{3.3.2}$$

Then, according to the model used here, the density at the edge of the limiter is

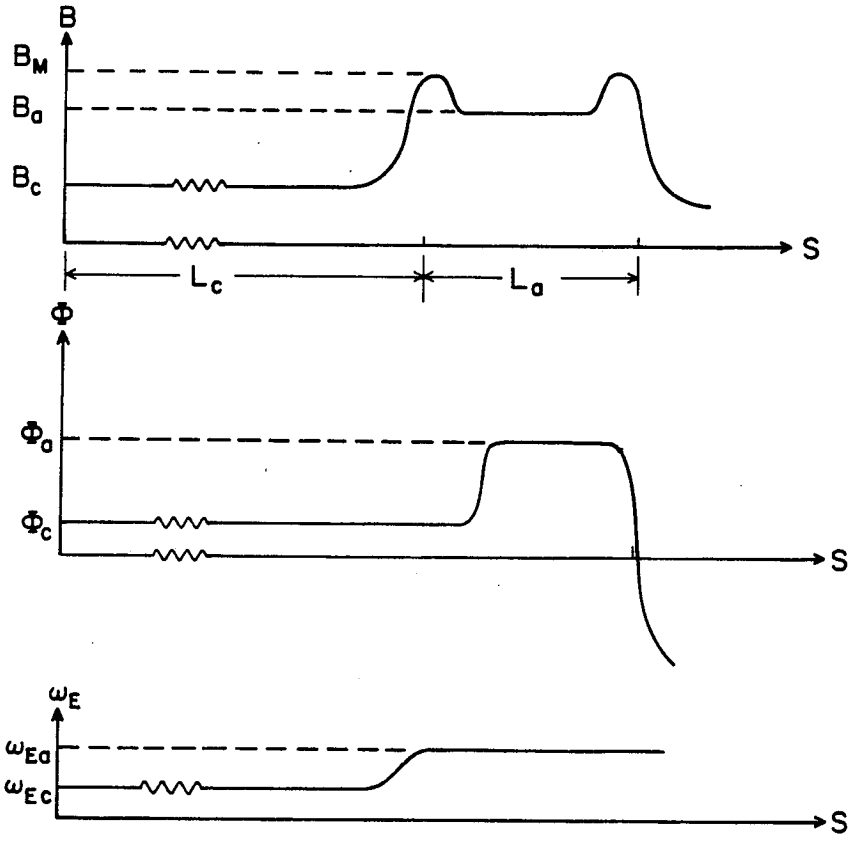

Fig. 3.6. Axial variation of magnetic field, ambipolar potential, and electric field rotational frequency about the midplane of a model tandem mirror configuration.

$$n = n_0 \exp\left(-\frac{1}{2(0.53)^2}\right) = 0.17 n_0,$$

which is reasonably consistent with the measurement.

B. $E \times B$ Rotation Frequency

An important instability driving force in our study is $E \times B$ drift. According to the model for the radial profile of the potential Eq. (3.3.3), we have the following drift frequency for the equilibrium

$$\omega_E = \frac{1}{Br}\frac{\partial \Phi}{\partial r} = -\frac{2\Phi_0}{Br_L^2}, \tag{3.3.3}$$

where Φ_0 is the ambipolar potential of the axial line in the machine. For $B = 0.3T$, $r_L = 0.24m$ and $\Phi_0 = 1KV$ as given in Table I, we have

$$\omega_E = 1.15 \times 10^5 \Phi_0(KV) s^{-1} = 1.15 \times 10^5 s^{-1} = 2\pi \times 18KHz.$$

C. End-cell Hot-electron Grad-B Rotation Frequency

The effective curvature in the end cells has to take into account of the contribution from the hot electrons. From Table. I we find that $\kappa/r = 0.5m^{-1}$ for the TMX-U anchors. Then the grad-B drift rotation frequency is

$$\omega_\kappa = \frac{1-\gamma^2}{2\gamma}\frac{c^2\kappa}{\omega_{ceo}r}. \tag{3.3.4}$$

For $300KeV$ electrons, typical of TMX-U, $\gamma = 1 + E/511 \approx 1.6$ so that

$$\omega_\kappa = 2.6 \times 10^5 s^{-1} = 2\pi \times 42KHz.$$

This frequency is several times higher than the observed instability frequency, which means, in the standard mentioned in the last chapter, the hot electrons are decoupled from the core plasma and justifies our treatment in which the hot electron ring is seen as a rigid non-interactive diamagnetic current.

D. Diamagnetic Drift Frequency

The ion diamagnetic drift frequency in Eq. (2.5.23b) can be calculated in the two different situations shown in Table I. In the first example when the central cell is isotropic ($L_c = 5m$) and not heated ($T_{c\perp} 0.1KeV$), we have

$$\omega_i^* = 1.85\frac{T_{c\perp}}{B_c r_p^2} = 3.8 \times 10^4 s^{-1} = 2\pi \times 6KHz.$$

In the second example with central-cell heating ($L_c = 2.5m$ and $T_{c\perp} = 1KeV$), we have

$$\omega_i^* = 0.8\frac{T_{c\perp}}{B_c r_p^2} = 1.6 \times 10^5 s^{-1} = 2\pi \times 26KHz.$$

E. Charge Uncovering Term

The charge uncovering term is approximately given by:

$$\Theta h \equiv \left(\int_{-\infty}^{\infty} \frac{ds}{B^2}\frac{n_i m_i}{B r_p^2}\right)^{-1} \bar{\Theta}_h = \frac{2r_p^2}{a_i^2}\frac{\frac{B_c}{B_a} n_h L_h}{n_c L_c + 2\sum_j \frac{n_j T_j L_j B_c}{T_c B_a^2}},$$

where the summation is over the species j in the anchors and a_i is the central-cell ion gyro-radius, $a_i = 0.014 T_c^{\frac{1}{2}} m$ with T_c in KeV. Using the

typical TMX-U values from Table I, we find that when ions in the central cell are isotropic and $L_c = 5m$,

$$\Delta Q = \frac{2}{T_c + 0.1}.$$

When the central-cell heatng results in a nonisotropic ion distribution and $L_c = 2.5m$,

$$\Delta Q = \frac{4}{T_c + 0.2}.$$

F. Eigenvalue m^*

The eigenvalue m^* has been evaluated by B. et al.[50] In Fig. 3.7, we show their results. In TMX-U, we have

$$\frac{r_L^2}{r_p^2} = \frac{0.24^2}{0.128^2} = 3.5$$

Then we find that $m^* = 2, 6$, and 10 for tha azimuthal modes $m = 1, 2$, and 3.

G. MHD Drive $\Gamma^{\dagger}_{\mathrm{MHD}}$

The MHD drive $\Gamma^{\dagger}_{\mathrm{MHD}}$ is defined

$$\Gamma^{\dagger}_{\mathrm{MHD}} \equiv \left(\int_{-\infty}^{\infty} \frac{ds}{B^2} \frac{n_i m_i}{B r_p^2} \right)^{-1} (\hat{\gamma}_c^2 + \hat{\gamma}_a^2),$$

which has been calculated with the TEBACO code[51] to obtain

$$\Gamma^{\dagger}_{\mathrm{MHD}} = \frac{0.63 \times 10^{31} a_c \beta_c - 1.26 \times 10^{31} \beta_{eff} (1 + \beta_{si\|0}/\beta_{si\perp 0})}{n_c},$$

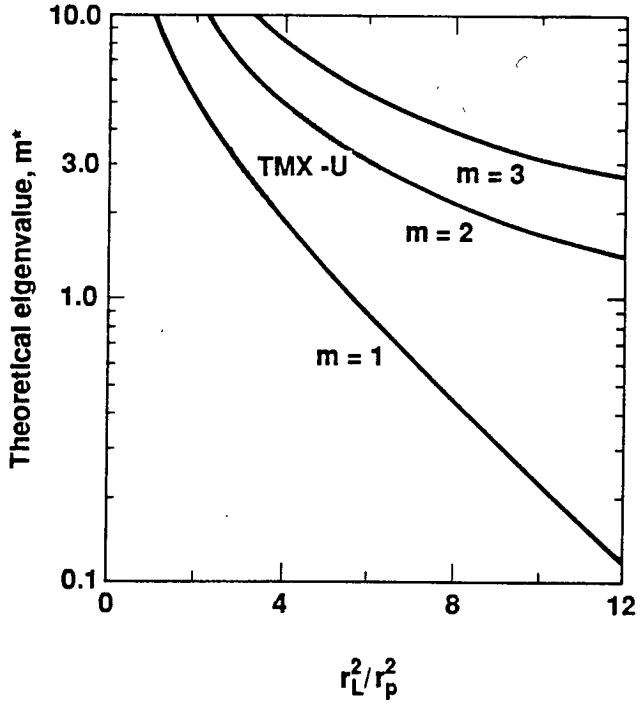

Fig. 3.7. Theoretical eigenvalue m^* as a function of r_L^2/r_p^2. This figure is from Ref. 50, but have been renormalized to the units of this work.

where a_c, a measure of the cetral-cell isotropy, is 1.0 for an isotropic central-cell plasma and 0.2 for a highly nonisotropic central-cell plasma. Following the calculation in Ref. 31, we find

$$\Gamma^{\dagger}_{\rm MHD} = 10^{10} \times [2.8 a_c T_c - 13.2 \frac{n_{si}}{n_c}(1 + 2.5 \times 10^{-4} M_A)],$$

where M_A is hot electron diamagnetism.

III.4 Numerical Studies of Instabilities

III.4.1 Review of Instability Branches

Before we start with the numerical investigation of the two major instabilities, it is useful to review the dispersion relation and find the solution branches. By identifying their branches and studying their typical behaviors, we can better understand our numerical results.

The quadratic dispersion relation obtained in the last chapter is

$$-Q(\omega) = R\psi_c^2 + S\psi_a^2 + W\Delta\psi^2, \qquad (3.4.1)$$

where R, S and W are defined there.

By taking the variations in Eq. (3.4.1) with respect to ψ_a and ψ_c, we obtain two equations

$$(R + W)\psi_c - W\psi_a = 0$$

and

$$-W\psi_c + (S + W)\psi_a = 0.$$

These equations lead to the dispertion relation

$$RS + W(R + S) = 0. \tag{3.4.2}$$

The equation (3.4) implies that the eigenfunctions ψ_a and ψ_c satisfy

$$\frac{\psi_a}{\psi_c} = \frac{R + W}{W} = \frac{W}{S + W}. \tag{3.4.3}$$

(1) If $|W| \gg |R|, |S|$, then the dispertion relation Eq. (3.4) reduces to the following form

$$R + S = 0. \tag{3.4.5}$$

This mode is to lowest order independent of the collision properties and gives the usual MHD predictions for the flute interchange modes. The finite W, which contains the contributions from passing particles, collisional effects and ion Landau-damping, will yield the following correction

$$\delta\omega = RS\big(W\frac{\partial}{\partial\omega}(R + S)\big)^{-1}, \tag{3.4.6}$$

where the differential is taken at $\omega = \omega_0$ which is solution of Eq. (3.4.5).

It is clear that when the valus of W is large the ratio

$$\left|\frac{\psi_a}{\psi_c}\right| \approx 1$$

holds true, which is typical behavior of the flute mode.

(2) If $|S| \gg |R|$, then the dispersion Eq. (3.4.2) becomes another form

$$R + W = 0. \tag{3.4.7}$$

According Eq. (3.4.3), the mode eigenfunction satisfies

$$\left|\frac{\psi_a}{\psi_c}\right| \approx 0$$

which gives a typical trapped particle mode having perturbations basicly inside the central cell where the curvature is unfavorable.

The finite S yields a correction which can be analytically expressed as follows

$$\delta\omega = -\frac{R+S}{RS\dfrac{\partial W}{\partial \omega}} \approx -(R\frac{\partial W}{\partial \omega})^{-1}, \tag{3.4.8}$$

which can be used to check the numerical results.

In certain situations, when the value of $|R|$ is relatively small, Eq. (3.4.7) can be further simplified to

$$W \approx 0$$

without introducing a large error. Then, the solution can be analytically obtained in several limits. For instance, when $\nu_p \gg \tilde{\Phi}^2\Omega_a$, we have a collision term as

$$-2N_a\Omega_a\lambda_{1a} = \frac{2N_c\Omega_c N_a\Omega_a[(\omega-\omega_e^*+\eta\tilde{\Phi}_c\omega_e^*)(\omega-\langle\omega_E\rangle)+\Omega_c\eta\omega_e^*\tilde{\Phi}N_c/N]}{N[(\omega-\langle\omega_E\rangle)^2+4\tilde{\Phi}^2N_c\Omega_cN_a\Omega_a/(3N^2)]\omega_e^*}. \tag{3.4.9}$$

Combining it with the expressiom of W in Eq. (2.5.22), we have four roots for the dispersion relation

$$\omega = \omega_{Ea}, \quad \omega = \omega_{Ec}$$

and

$$\begin{aligned}\omega = \langle\omega_E\rangle + \frac{1}{2}(\omega^*_{enc}\frac{N_a}{N} + 2\omega^*_{enc}\frac{N_a}{N} + \eta\tilde{\Phi}\omega^*_e\frac{N_c - 2N_a}{N}) \\ \pm [(\omega^*_{enc}\frac{N_a}{N} + 2\omega^*_{enc}\frac{N_a}{N} + \eta\tilde{\Phi}\omega^*_e\frac{N_c - 2N_a}{N})^2 \\ - \frac{8N_cN_a}{N^2}\eta\omega^*_e\tilde{\Phi}(\omega_{Ea} - \omega_{Ec})]^{\frac{1}{2}}.\end{aligned} \tag{3.4.10}$$

One observes that there is instability if

$$-\frac{8N_cN_a}{N^2}\eta\omega^*_e\tilde{\Phi}(\omega_{Ea} - \omega_{Ec}) > (\omega^*_{enc}\frac{N_a}{N} + 2\omega^*_{enc}\frac{N_a}{N} + \eta\tilde{\Phi}\omega^*_e\frac{N_c - 2N_a}{N})^2. \tag{3.4.11}$$

Thus in the limit of very high electron collisional frequency one can obtain an instability through the conbination of temperature gradient, axial variation of the $E \times B$ drift and the potential variation along the field line. Those modes were reported in Ref. 52.

III.4.2 Investigation of Flute Modes

As analyzed in the last section, when the absolute value of W is relatively large, there is a mode whose perturbation spreads along the whole field line, which is typical behavior of the flute modes. Since the study of the flute modes in context of this dissertation serves basicly a comparison with the trapped article modes, we take the rather simple approach to assume large $|W|$ and $R+S=0$ to study the mode features.

Thus we have dispersion relation as the following

$$(1+m^*)\Omega^2 + [2\omega_E + \omega_i^*(\Delta Q - m^*)] + \Gamma_{MHD}^{\dagger} + \omega_E^2 = 0, \qquad (3.4.12)$$

where ω_E is assumed to take the same value in the central cell and anchor cells and $\Omega = \omega - m\omega_E$. The other parameters were defined in the last section. Eq. (3.4.12) is an algebraic quadratic equation which has solution

$$\begin{aligned}\omega = \frac{mm^*\omega_E}{1+m^*} - \frac{m\omega_i^*(\Delta Q - m^*)}{2(1+m^*)} + \frac{im}{1+m^*} \\ [m^*\omega_E^2 - \omega_E\omega_i^*(\Delta Q - m^*) \\ - \frac{(\omega_i^*)^2}{4}(\Delta Q - m^*)^2 + (1+m^*)\Gamma_{\mathrm{MHD}}^{\dagger}]^{\frac{1}{2}}.\end{aligned} \qquad (3.4.13)$$

When the value in [ ] is bigger than zero, there is instablity arising. One can observe taht the $E \times B$ drift and the unfavorable curvature in the central cell are definitely instability driving forces. The charge uncovering terms, which are proportional to the $(\Delta Q - m^*)$, usually provide the stabilization.

The instability region can be described by the equation

$$m^*\omega_E^2 - \omega_E\omega_i^*(\Delta Q - m^*) - \frac{(\omega_i^*)^2}{4}(\Delta Q - m^*)^2 + (1+m^*)\Gamma_{MHD}^{\dagger} = 0, \tag{3.4.14}$$

which gives a curve in the parameter space.

In Fig. 3.8 and 3.9, corresponding isotropic ions and nonisotropic ions in the central cell respectively, we plot curves to show the stable region and unstable region in terms of temperature of the central-cell ions and the potential along the axis of the machine. In Fig. 3.9, it is obvious that higher $E \times B$ drift (proportional to the axis potential) or higher ion heating in the central cell will trigger the instability. There are two curves to correspond $m = 1$ modes, one is to assume that the diamagnetic current inside plasma is formed by hot electrons so that the system becomes more stable and one is to assume that the hot electron ring is pushed from inside to the scrape off contours shown in Fig. 3.4 so the stabilizing effect is minimum. The real situation might be somewhere between those two curves and observations in TMX-U appear to be in this region (see the shadowed squre in Fig. 3.9).

In Fig. 3.10 and 3.11, we give the pictures to show more effects of hot electrons. There are two curves to present the change of the threshold due to the different situations. All the curves are ploted in terms of $m = 1$ modes. The curve 1 describe the threshold under assumptions that the hot electron density is $10^{17}m^{-3}$ which is about 10% of the total electron population and that the hot electron ring enhances the effective curvature

of the anchor cell. Without any hot electrons, as the curve 2 shows, the system will be all unstable when the $E \times B$ drift exceeds a certain level (axis potential $\Phi_0 > 0.9KV$), which will be interesting if experiments can confirm that. The curve in Fig. 3.11 shows the change of the real frequency of the modes according to hot-electron population. The figure is drawn in such a way that if the solution curve split into two branches the system has two stable modes; if the two branches merge together one of them is a growing mode ($\gamma > 0$). It is observed that the hot electrons stabilize the system and the predicted mode frequency is little above the observed frequency.

Similar picture in Fig. 3.12 shows the effects of the central cell ion temperature and value of the ambipolar potential on the modes. The real mode frequency is seemingly not very sensitive to those parameters, though the system is much easy to be unstable when the two destabilizing factors are up.

Since the parameter m^* is determined by the machine geometry as well as the operation condition (profile), we allow them to have a small variation. The results are shown in Fig. 3.13 and 3.14. The decrease of the value m^*, which means that the plasma has deeper density gradient, will destabilize the system. In Fig. 3.14, we try to squeeze more information in one figure. However, it shows the small m^* gives better frequency prediction.

Several conclusions are:

1) The mode frequency of the flute instability obtained by this approach is about the upper limit of the observed one.

2) The stability threshold is predicted higher than that in the TMX-U experiments if the hot electron enhancement of the anchor-cell curvature is present. If the pressure gradient of the hot electrons is not significant, which may be possible, the stability condition is close to the observation.

3) Destabilizing effects of the central-cell heating and $E \times B$ drift are confirmed.

4) Higher frequency and higher m-modes detected in the experiments are also predicted.

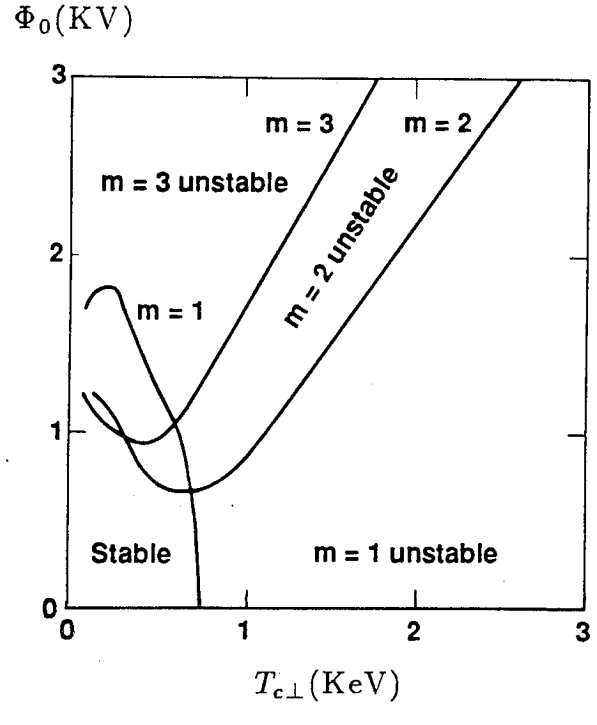

Fig. 3.8. Flute instability threshold as a function of central-cell perpenticalar ion temperature and potential for azimuthal modes $m = 1, 2,$ and 3, when ions are considered isotropic.

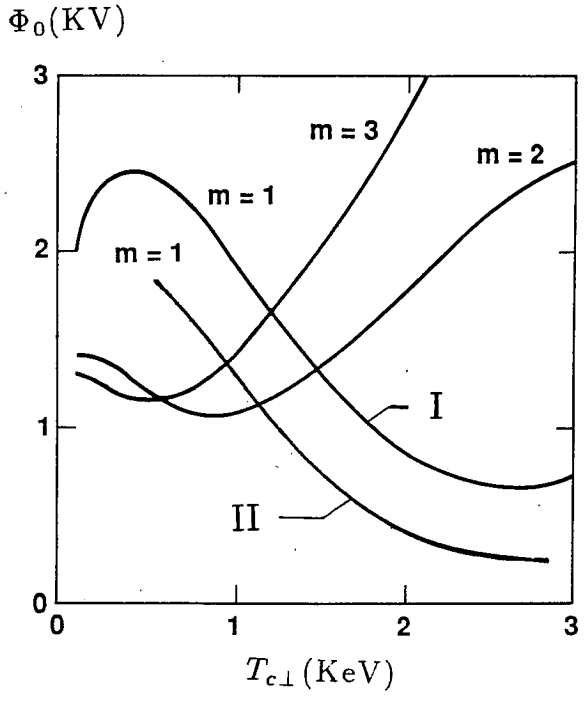

Fig. 3.9. Flute instability threshold as a function of central-cell perpenticalar ion temperature and potential for azimuthal modes $m = 1, 2,$ and 3, when ions are considered nonisotropic ($a_c = 0.2$).

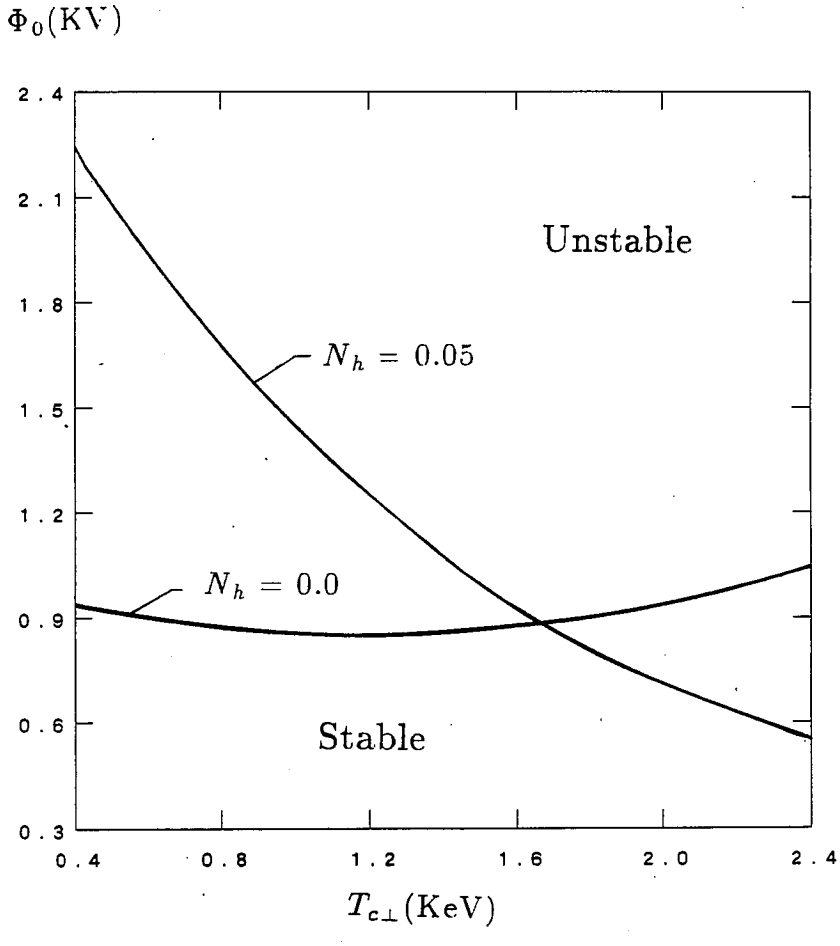

Fig. 3.10. Flute instability threshold as a function of different hot-electron density ($N_h \equiv n_h/n_c$).

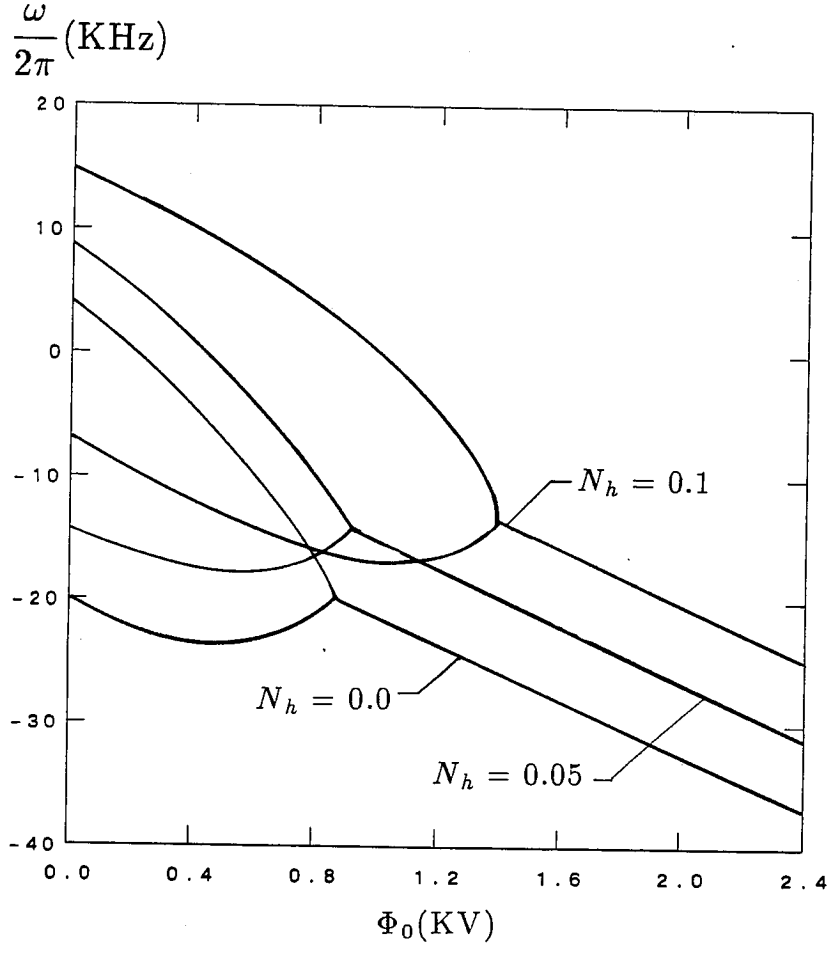

Fig. 3.11. Real frequency as a function of N_h. As two curves merge together, the system goes to instability.

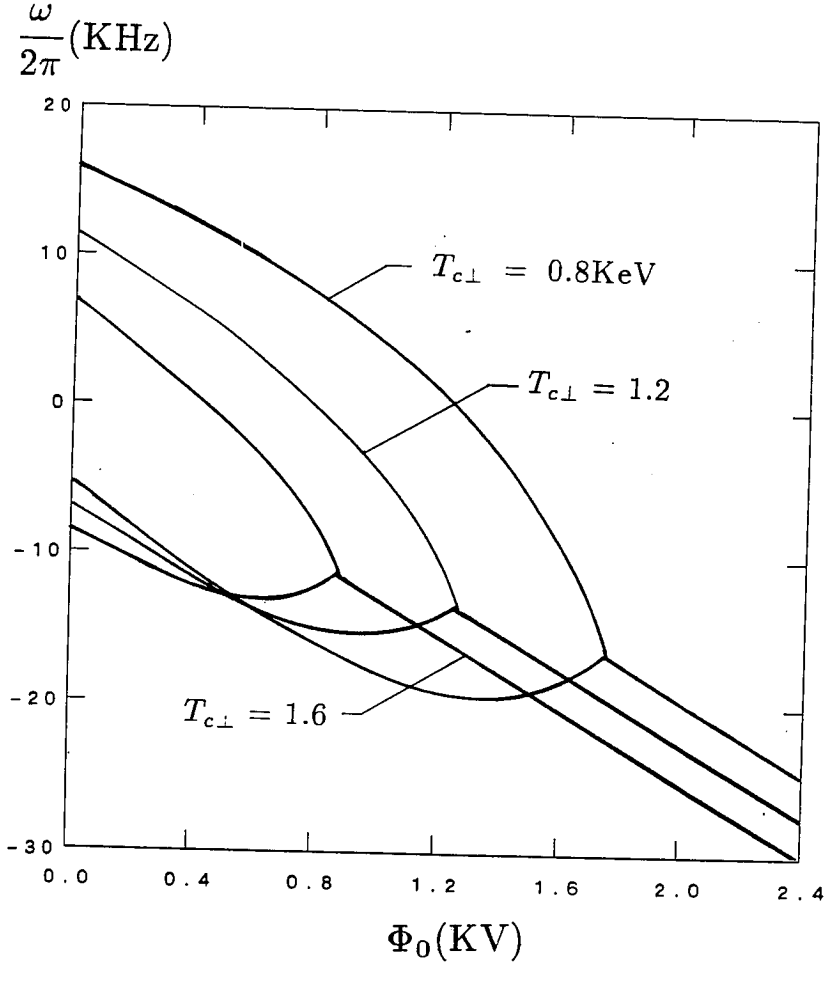

Fig. 3.12. Real frequency as a function of $T_{c\perp}$.

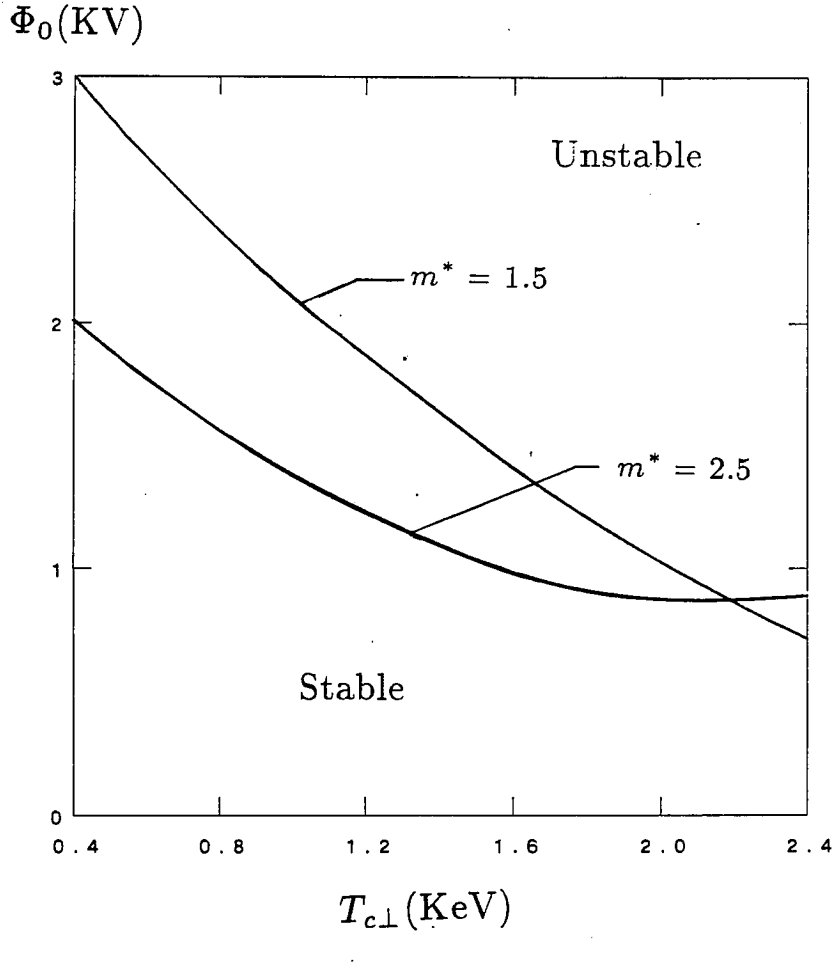

Fig. 3.13. Flute instability threshold as a function of different m^*.

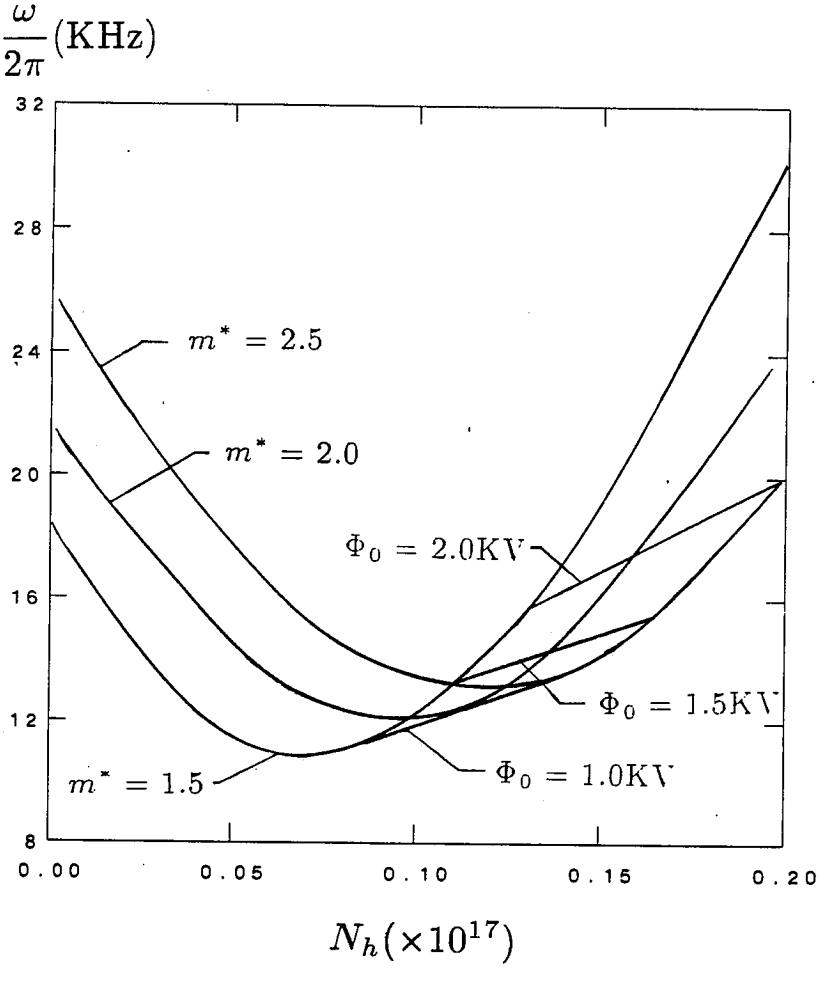

Fig. 3.14. Real frequency as a function of various parameters.

III.4.3 Trapped Particle Instability

We start our numerical analysis on the trapped particle modes at the collisionless and rotationless limits. To find the mode branches, we first set $|S| \to \infty$ and achieve the mode branch whose eigenfunctions have the typical features of the trapped particle modes $|\psi_a/\psi_c| = 0$. Then, the value of $|S|$ is slowly lowered down to the realistic one. In such a way, we try not to mix the trapped particle modes with the flute modes.

It turns out there are two branches of the trapped particle modes, which are shown in Figs. 3.15 and 3.16, where

$$N_{i\text{passing}} = \frac{\int n_{i\text{passing}} ds/B^2}{\int n_{\text{total}} ds/B^2} \tag{3.4.15}$$

In light of their behavior under the collisions, they can be recongnized as the negative-energy wave and the positive-energy wave as those in Ref. 33. At the collisionless and rotationless limit, the imaginary parts of the two modes are symmetric: one grows at the same rate as another damps.

When we put collision effects into account, the two modes respond differently. In Fig. 3.17, for the positive-energy mode, the growth rate goes down when the collision coefficient increases. While the growth rate goes up sharply when the collisional effect is introduced in Fig. 3.18. However, after the coefficient reaches near its realistic value the growth rate falls down slowly, which means there is too much dissipation for the mode.

On the other hand, in Figs. 3.15 and 17, we observe that the two modes can be stabilized when the population of the passing ions is increasing. The figure particularly shows that when the passing ions are less than a certain level (5%-6%), the plasma is susceptible to fast-growing trapped particle modes, which was reported in Ref. 32.

As another feature, the perturbation is not limited in the central cell, because the passing particls carry the perturbed information along the field line. It turns out that all the trapped particle modes discussed in this section do not have isolated perturbations as long as the realistic parameters are employed.

The numerical work also shows that, provided the population of the passing particles are adequate, the two modes are both stable even when moderate rotation is introduced (Φ_0 is less than $0.8KV$), the modes can still be stable.

Ion Landau-damping term is put into effects in Fig. 3.19. The results are opposite to those of the collision effects in the nearby region (compare to Fig. 3.17). It is suggested that if the collision term is reduced by increasing the electron temperature in the central cell, those two effects can be approximately canceled each other and the system may stabilized. Compared Fig. 3.17 and 3.19, we expect that the electron temperature should be raised by factor 3. In Fig. 3.20, we show that the trapped particle modes will be unstable, when the $E \times B$ drift goes higher (about half of the observed value).

Now we investigate the behaviors of the trapped particle modes at the situation that all the parameters in the dispersion take the values observed in the TMX-U experiments or calculated in Sec. III.3 except one that varies in a reasonable range. In such a way, we hope that the results may be assessed more easily in experiments. In Fig. 3.21, with increasing the $E \times B$ drift, which is marked by the potential Φ_0 along the axis, the mode frequency becomes higher, the growth rate goes up and ratio ψ_a/ψ_c approaches to unity. The results show that the $E \times B$ drift has rather strong destabilizing effects and that when the mode is strongly destabilized the mode perturbation spreads into the anchor region as if it is the flute mode.

In Fig. 3.22, we plot the effects of hot electrons on the mode. As we did in examining the flute mode in the last section, we assume full credit for stabilizing effects of hot electrons, suggesting that both curvature enhancement and charge uncovering machenism are considered. The results show that the system is stabilized to a certain degree, though the growth rate is still rather large. We have not shown that the system can be completely stabilized merely by hot electrons according to this study.

In Fig. 3.23, we present the effects of the potential difference $\tilde{\Phi} \equiv (\Phi_a - \Phi_c)/T$ between the the central cell and anchor cells. When the potential difference goes up, the growth rate of the mode is higher. In Fig. 3.24, the central-cell heating increases the growth rate. In Fig. 3.25, more collisions gives smaller growth rate. In Fig. 3.26, the bigger size of

the machine gives a little impovement on the stability property.

Several conclusions are

1) Factors such as the better central-cell curvature and the hot electron ring, which stabilize the flute modes, also stabilize the trapped particle mode. The situation is similar for the destabilizing factors such as the $E \times B$ drift. However, effectiveness of the stabilizing factors is not strong when allowance is made for non-flutelike perturbations.

2) In certain parameter regimes, where the plasma rotation is not too strong, the effect of the collision term is opposite to that of the ion Landau damping term which helps stabilize the system.

3) The trapped particle mode can be stabilized by reducing $E \times B$ rotation by factor 2. However, the theory of this mode gives a pessimistic prediction on stability feature of tandem mirrors.

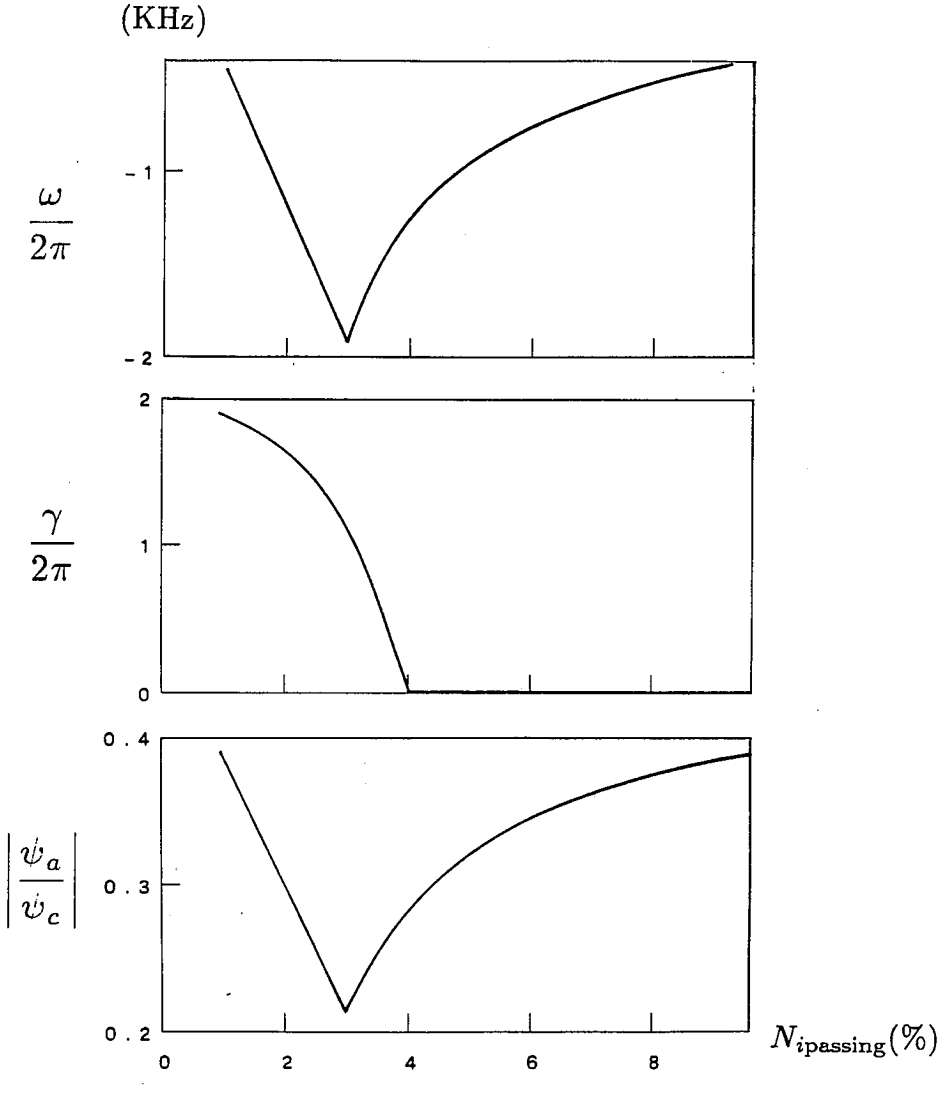

Fig. 3.15. Trapped-particle mode features as a function of the density N_{passing} of passing ions.

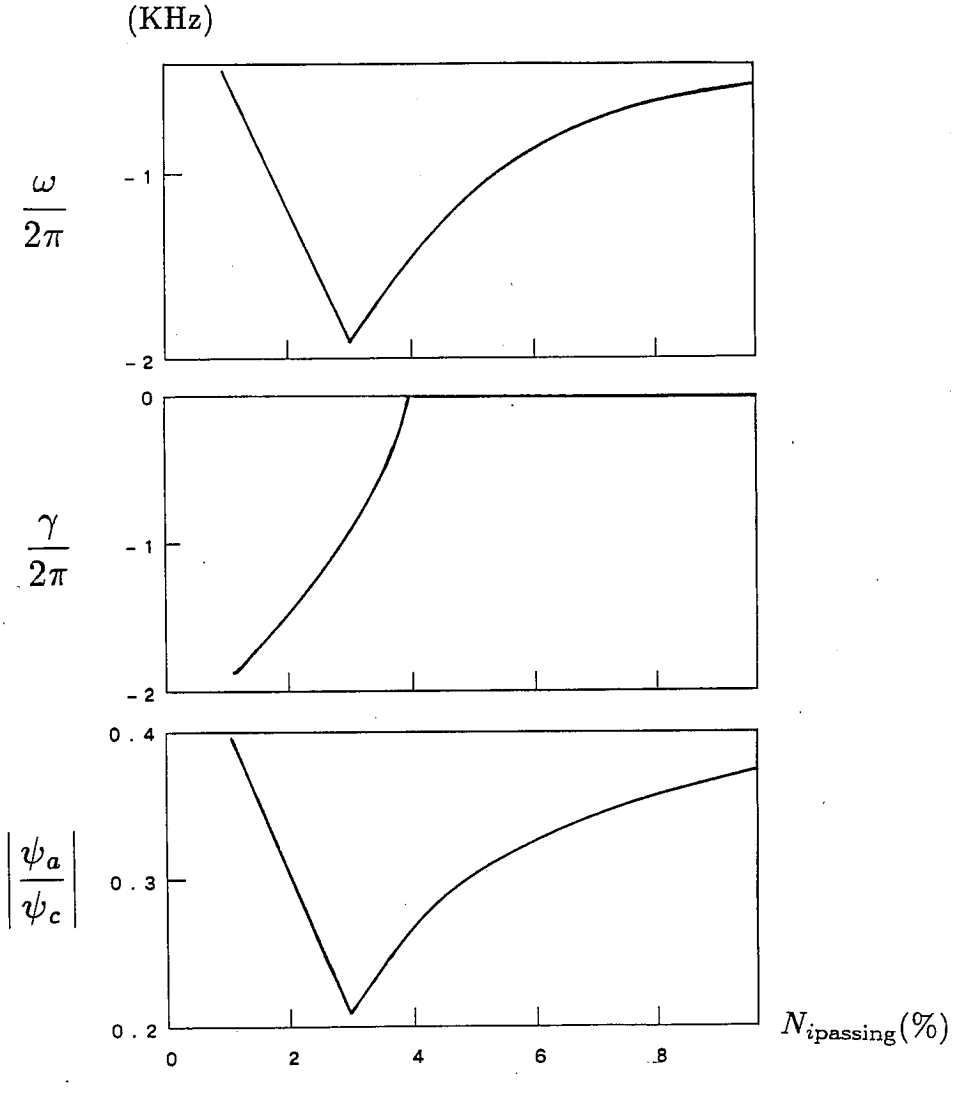

Fig. 3.16. Trapped-particle mode features as a function of the density N_{passing} of passing ions.

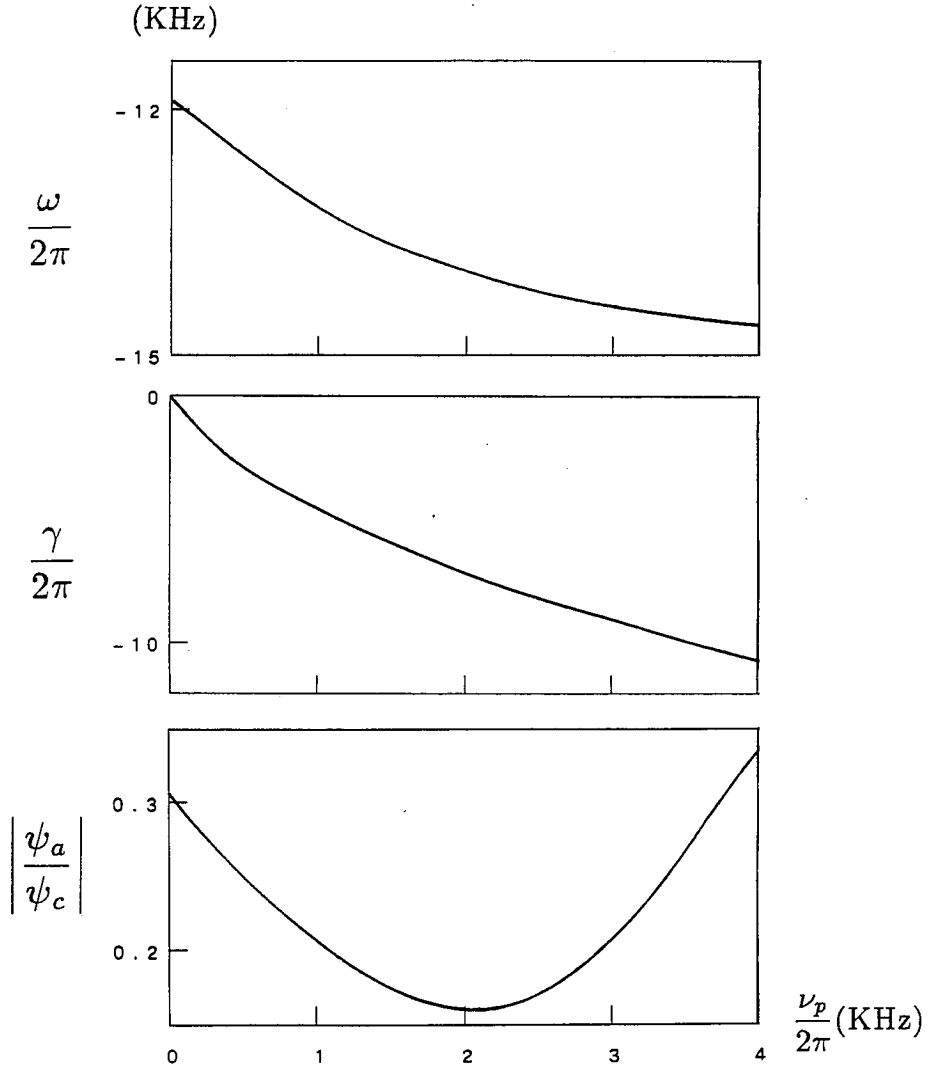

Fig. 3.17. Features of one dissipative trapped-particle mode (positive-energy) as a function of the Pastukhov scattering coefficients ν_p.

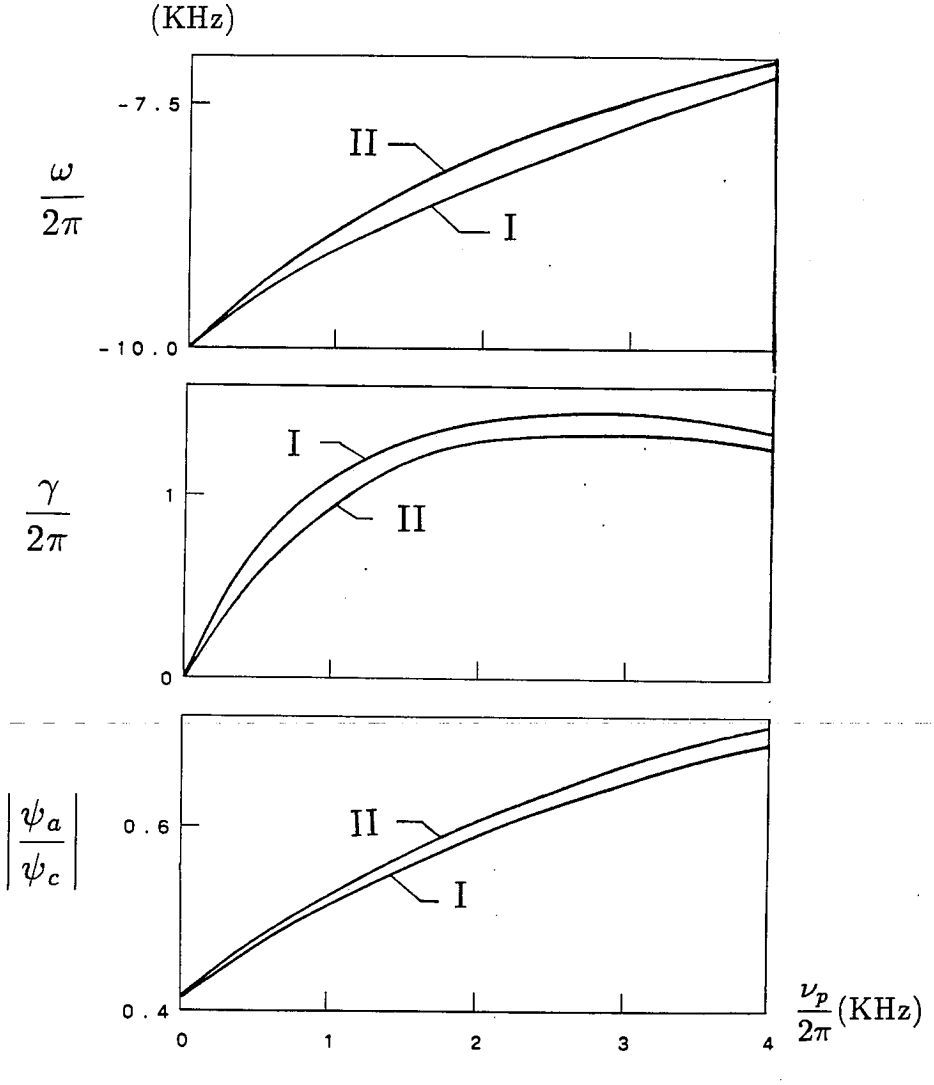

Fig. 3.18. Features of one dissipative trapped-particle mode (negative-energy) as a function of the Pastukhov scattering coefficients ν_p. The curves I and II are the numerical solutions for short anchor cells and arbitrary anchor cells (see Sec. 2.6.1 and 2.6.2) respectively.

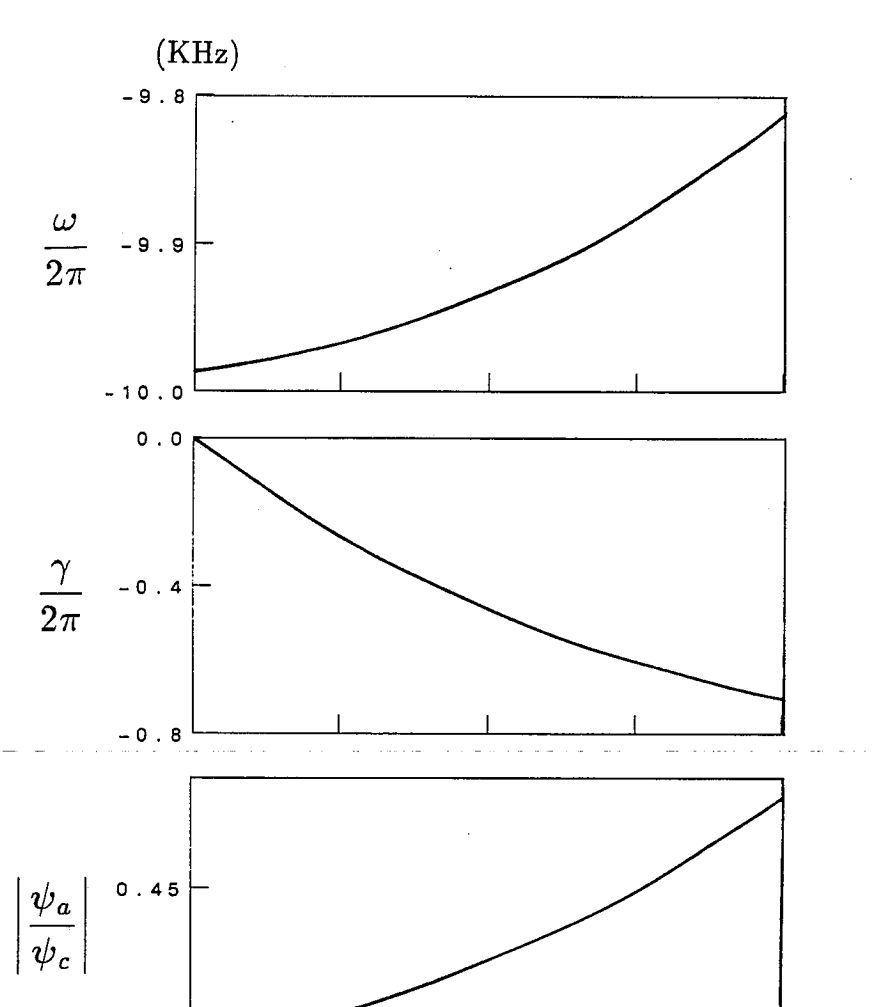

Fig. 3.19. Features of the trapped-particle mode as a function of the ion Landau-damping term (The term is gradually introduced; as $\sigma = 1.0$, full credit of the Landau damping term is considered).

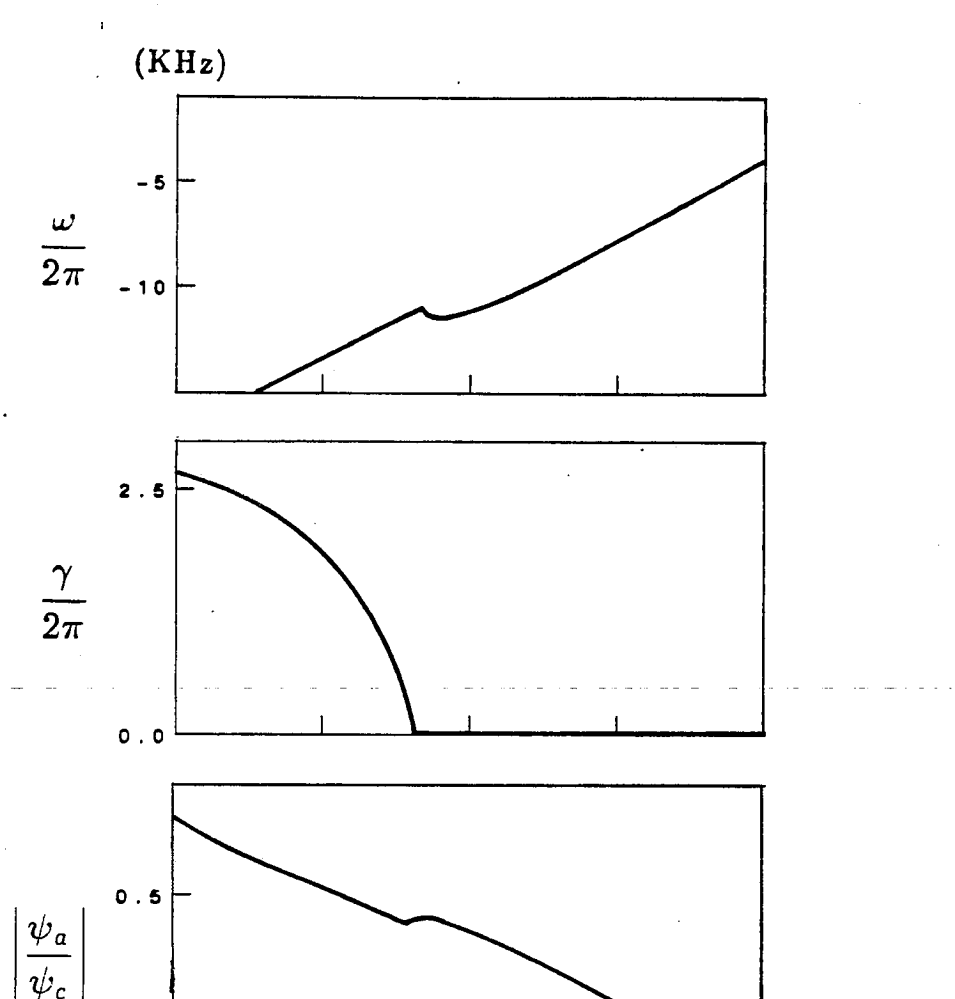

Fig. 3.20. Features of the trapped particle modes as a function of the $E \times B$ drift. The system goes unstable when the axial potential approaches 0.5KV (about half of the observed value).

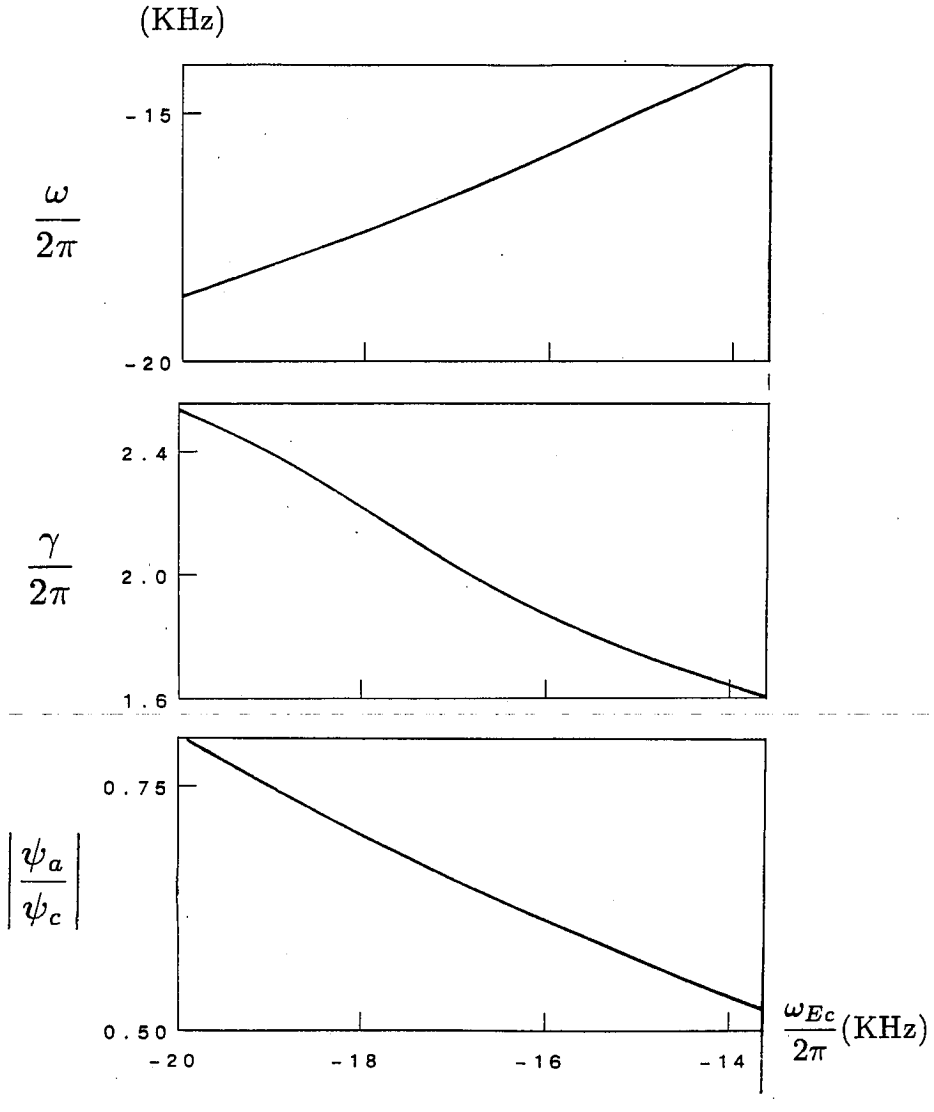

Fig. 3.21. Feature of the trapped-particle mode as a function of the electric field rotational frequency.

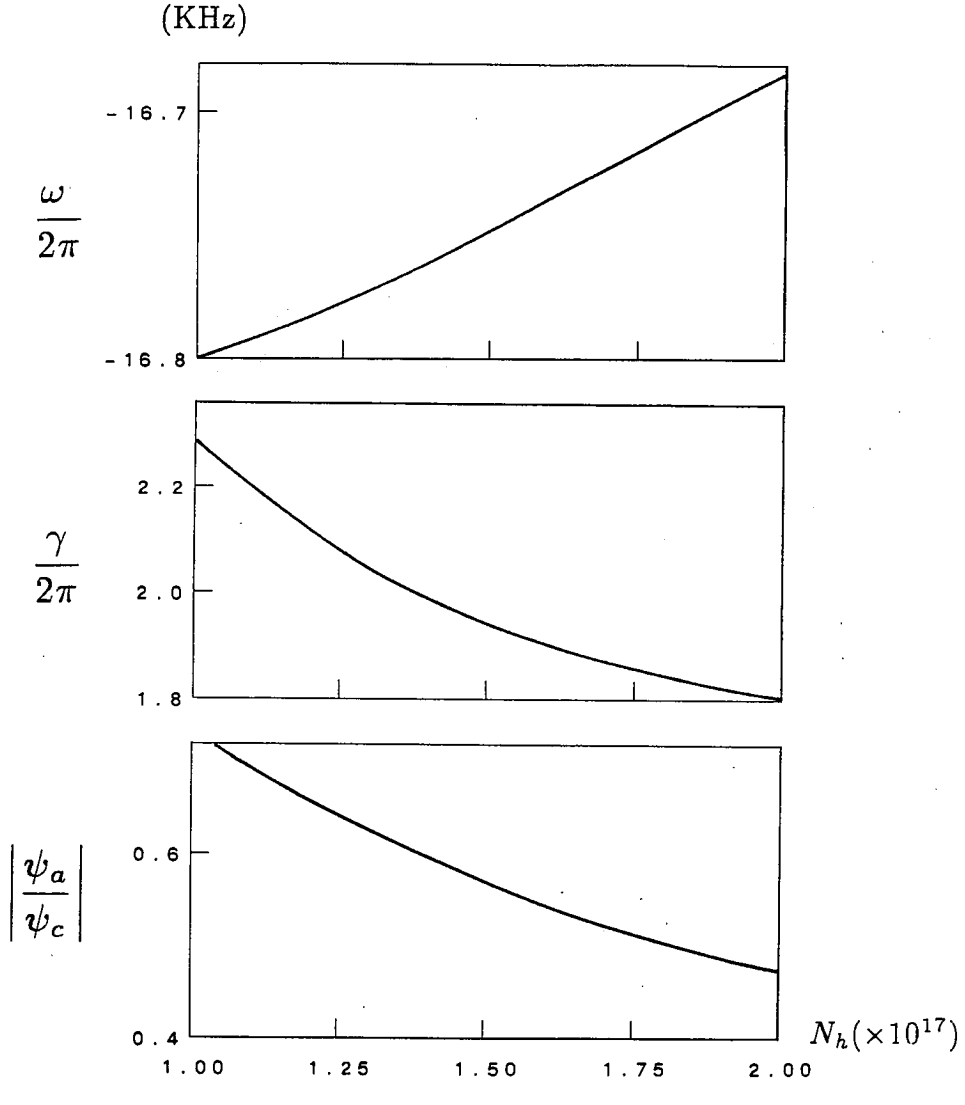

Fig. 3.22. Feature of the trapped-particle mode as a function of hot-electron density.

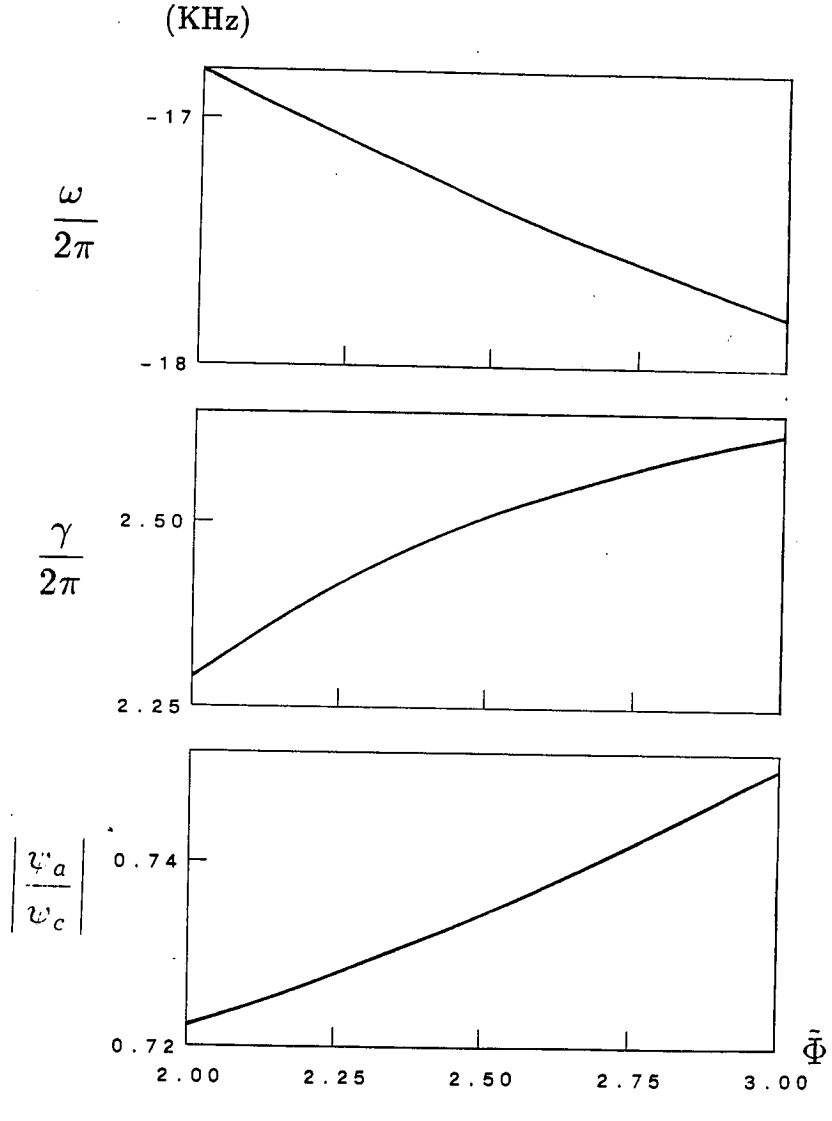

Fig. 3.23. Feature of the trapped-particle mode as a function of the ambipolar-potential difference.

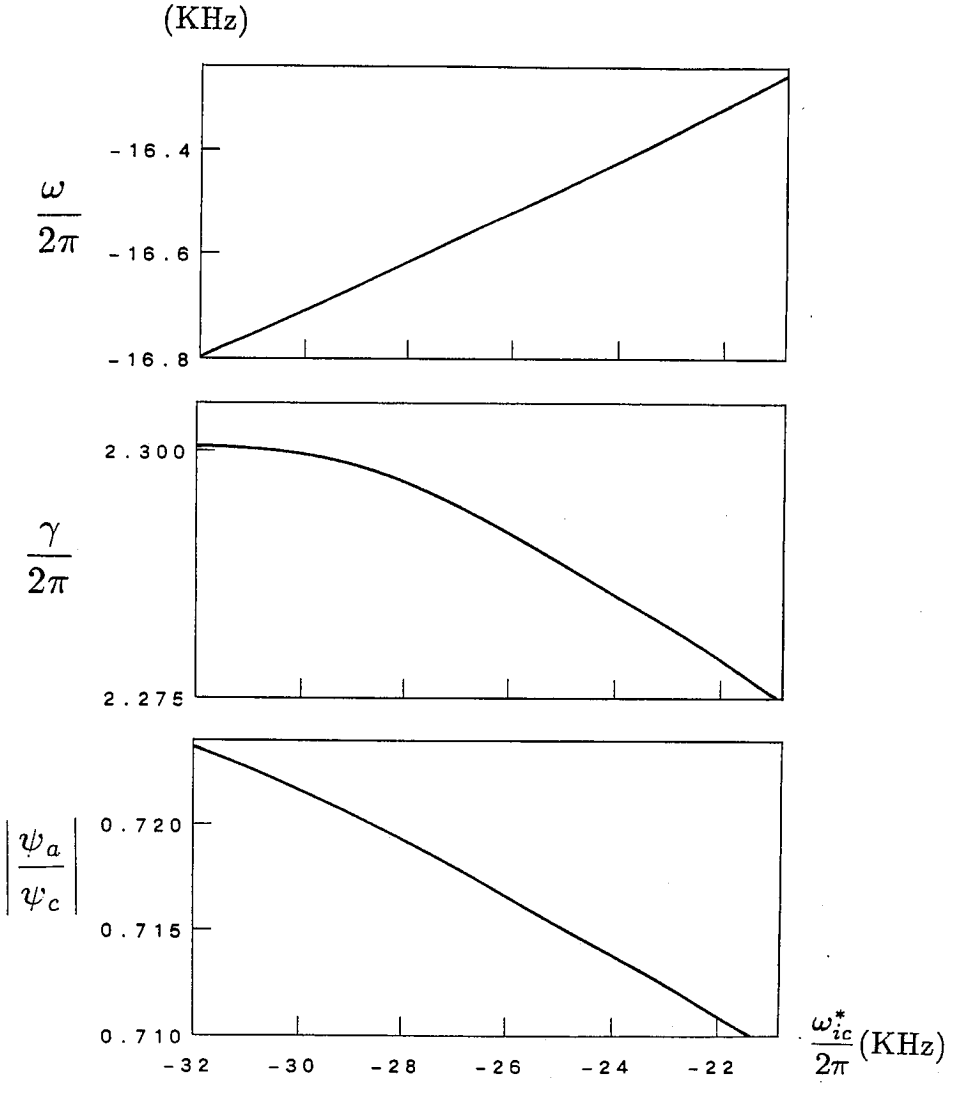

Fig. 3.24. Feature of the trapped-particle mode as a function of the ion diamagnetic frequency.

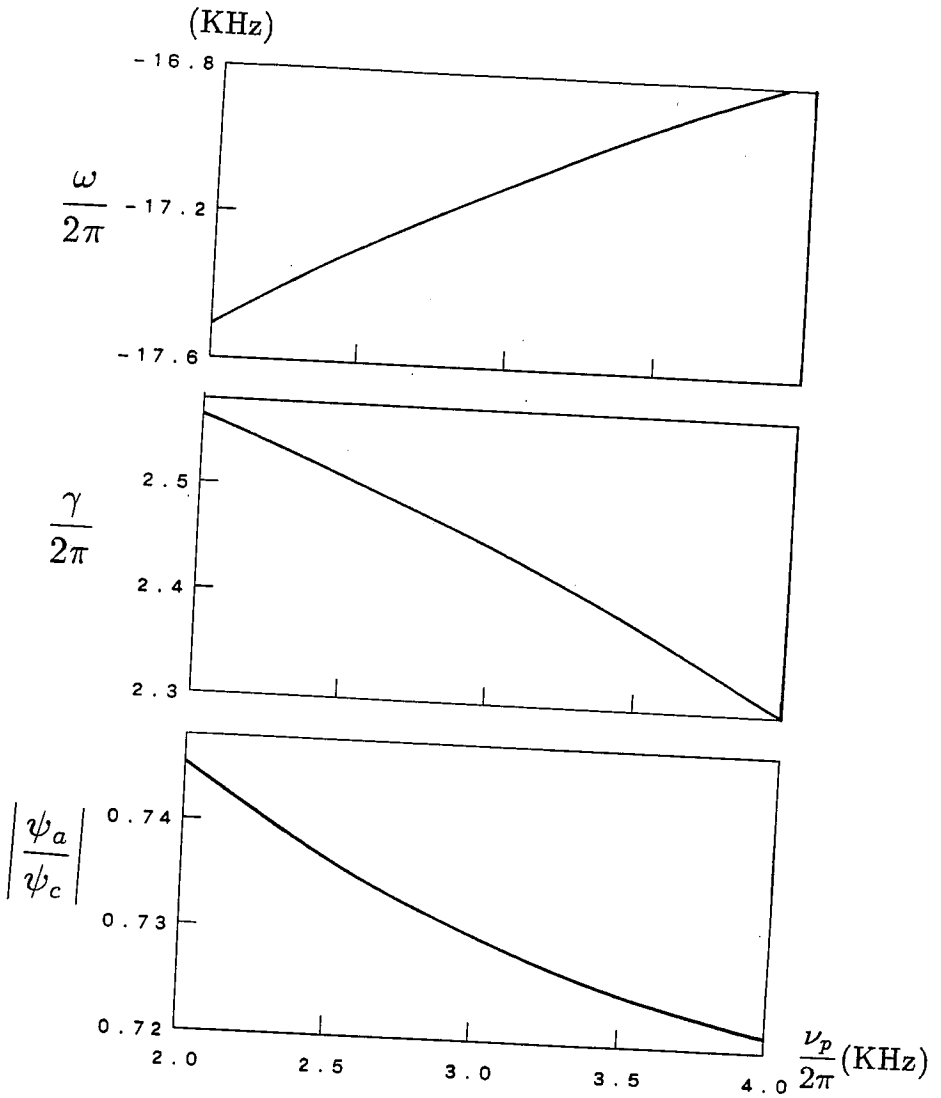

Fig. 3.25. Feature of the trapped-particle mode as a function of the Pastukhov coefficients.

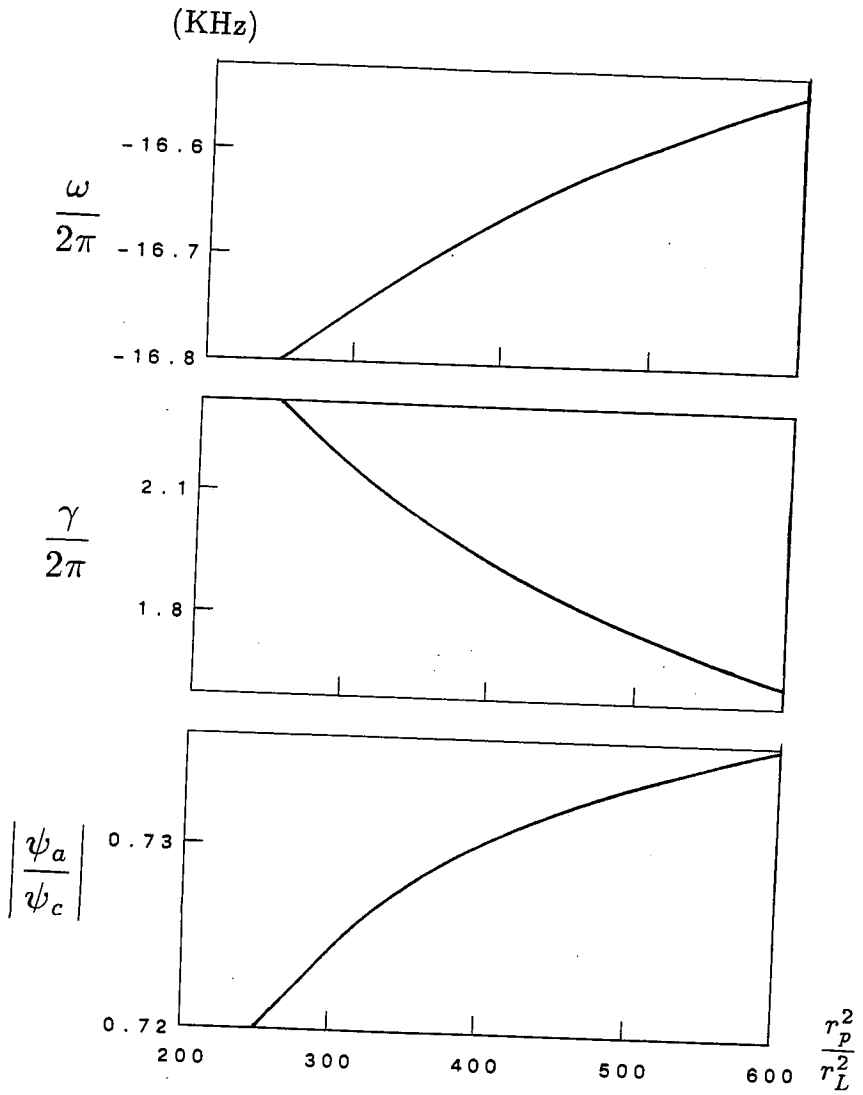

Fig. 3.26. Feature of the trapped-particle mode as a function of the system scale.

III.5 Summary

In this section we have investigated two major instabilities: the trapped particle modes and the flute modes. they are likely to affect the confinement of the tandem mirrors. The results are summarized and discussed as the follows.

From the intuitive points of view, one can expect some similarities between those two modes. Factors like the unfavorable curvature in the central cell and the $E \times B$ drift destabilize the flute mode as well as the trapped particle mode. And, the hot electron current, when it acts like a rigid noninteractive ring, provides stablizing effects on both the modes.

The real part of the frequency ω predicted by both approaches do not show significant difference. The reason probably lies on the fact that both modes are low frequency in nature and the frequency calculated here and observed in the experiments is greatly affected by "Doppler effects".

Trapped particle modes are supposed to appear only in the central cell where the curvature is not favorable. However, in our numerical studies, the mode are throughout the whole machine though the perturbation in the anchor regions may be slightly smaller. Those similarities may serve an explanation of the difficulty to distinguish the two modes in the experiments.

However, there is still some hope to make the things somewhat clearer. Theoretically, as our numerical work suggests, raising the potential of the anchor cells definitely will stimulate the trapped particle

mode and the experiments in TMX-U shows that the instability tends to be strong as ambipolar potential goes higher, which seemingly already confirm the interpretation. Unfortunately, the results are not so conclusive, since the parameters in the experiments are usually interrelated with each other, so there is a possibility that some other factors affect the stabilities.

The flute mode study in our work gives a more optimistic prediction on the instability threshold while the trapped particle mode study gives a pessimistic one. It appears that the instability persists in the region where the flute mode is supposed to be suppresed by lowering the $E \times B$ drift and limiting the central-cell beta. The trapped particle mode theory, though having difficulties to obtain exact onset of the instability, may serve a better explanation and features of the trapped particle mode revealed by this study can be a hint to understand the experimental observations.

Chapter IV. Conclusion

In this part of the disertation, we have construct a quadratic dispersion relation, in which various MHD and kinetic effects like ion diamagnetism, electron diamagnetism, electron-electron electron-ion collisions, ion Landau-damping, $E \times B$ drift and energetic particles are included and treated in a systematic way. The numerical study in which we use the formalism to investigate the two most likely instabilities in tandem mirror machines produced many quantitative and qualitative results about the two modes.

In Chapter II, we discussed the general formalism of the variational form and then we derive a concise form which is more suitable to discuss the instability problem in tandem mirrors.

Particular attention has been paid to how to calculate the collision term. Since the passing particles equilibriate, by collisions, the distribution of the trapped particles in both the cells, they are essentially related to the collision term. After employing the Pastukhov solution, we were able to evaluate the contribution from the passing particles as well as the collision term. Other physical effects like those of ambipolar potential and hot energetic particles were also discussed since they have significant impact on the stability properties of tandem mirrors. It is shown that the collisional effect on the instability is not very sensitive to the length of the anchor cells, although the analysis for the short anchors is easier acomplished.

In Chapter III, we investigated two instabilities: flute mode and trapped particle mode. The numerical work on the flute mode gives optimistic prediction on the system's stabilities, while the work on the trapped particle mode gives pessimistic one. In summary of those results, the trapped particle mode may serve explanation for the observed instabilities.

The investigation of the observed mode is by no means finished. In particular, the explanation about why the trapped particle modes can be stabilized in usual situations may provide the subject for future work.

Part B:

Scale Closure Scheme

In Alfven Wave Turbulence

Chapter V Introduction

It is generally believed that the renormalized turbulence theories[53-58] present a most promising way to deal with fluid as well as plasma turbulences. The essence of these theories could be schematically expressed in a simple equation54

$$\epsilon_k \phi_k = \tilde{\phi}_k, \tag{5.1.1a}$$

or equivalently

$$|\epsilon_k|^2 |\phi_k|^2 \equiv |\epsilon_k|^2 I_k = |\tilde{\phi}_k|^2, \tag{5.1.1b}$$

where $k = (\mathbf{k}, \omega)$ is the wave four component vector, ϕ_k is the fluctuating quantitiy whose spectrum $I_k = |\phi_k|^2$ we wish to obtain, ϵ_k is the renormalized propagator (response function, dielectric function in appropriate cases), and $\tilde{\phi}_k$ is generally referred to as the incoherent source term. Equation (5.1.1) is generally derived by splitting the nonlinear interaction into two parts: the coherent part which modefies (renormalizes) the linear propagator to yield the nonlinear response function ϵ_k, and the incoherent part $\tilde{\phi}_k$ which accounts for the remainer. Equation (5.1.1) can be viewed as representing a driven system with the incoherent source acting as an external driver. One must however remember that this analog with an external souce is essentially formal (barring some special cases where

the turbulence may be externally driven) because the incoherent source comes purely from the interaction of those very waves whose spectrum is the object of concern.

The simplicity of Eq. (5.1.1) is quite superficial: both ϵ_k and $\tilde{\phi}_k$ are functionals of the spectrum I_k (and, in general, functionals of higher order correlations). However, Eq. (5.1.1) does serve as a basis for constructing an unending chain of equations in which an n-th order correlation is determined in terms of higher order correlations. This feature is, of course, common with the unnormalized theories.[59-60] One of the primary tasks of turbulence theory is to propose a suitable closure scheme to truncate this infinite set of equations. For example, the assumption of quasi-normality[59] has been often used to affect the closure in unrenormalized fluid theories (These fluid theories suffer from overshoot problems, and other theoretical difficulties, and were thus abandoned.).

A major advance in fluid turbulence was the Direct Interaction Approximation [53] (DIA) initiated by Kraichman which led to an essentially renormalized theory that contains the lowest nonlinear correction to the linear response function. The treatment of the incoherent source (IS) terms, however, was still a problem. In the DIA application to plasma theory known as DIAC[57] (coherent approximation to DIA), the incoherent term is very conveniently set equal to zero. However, the validity of such an assumption is questionable.

It seems clear that a proper understanding of turbulence theories will

only come with a deeper undertanding of the incoherent source. At the very least, one must make reasonable assumptions (to be verified a posteriori) about the nature of the incoherent source, and develop a closure scheme based on these assumptions. We must mention that the treatment of the IS is a very active field of research, and several authors[61-62] have set up two-point correlation theries to handle the problem. This, however, is a subject of much complexity, and our main interest here is to propose a physically motivated simple closure schems which treats the incoherent source adequately.

In the linear theory, the right-hand side of Eq. (5.1.1) goes to zero, giving rise to a point spectrum $\omega = \omega(\mathbf{k})$ obtained as a solution of $\epsilon^{\text{linear}}_{\mathbf{k},\omega} \equiv \epsilon^{l}_{\mathbf{k},\omega} = 0$. The dielectric response function $\epsilon^{l}_{\mathbf{k},\omega}$ contains the entire information about the linear modes. For nonlinear situations, the right-hand side of Eq. (5.1.1), i.e., the incoherent source term, is not zero and could acquire an arbitrary magnitude as the mode amplitudes build up. Setting $\tilde{\phi}_{\mathbf{k},\omega} = 0$ under such conditions (as is done in DIAC) is at best a fairly poor approximation. This approximation further leads to the so called nonlinear dispersion relation $\epsilon_{\mathbf{k},\omega} = 0$ which is then solved to obtain complex $\omega(\mathbf{k})$ giving the nonlinear growth or damping rates. There is still a unique complex ω for a given $\mathbf{k}$. This approach is simply an extension of the linear concepts, and is probably an adequate description only in the transient state immediately following the linear state. By no means, we could safely extend this to describe fully developed turbulence where

$\tilde{\phi}_{\mathrm{k},\omega}$ is quite arbitrary, and the spectrum $I_{\mathbf{k},\omega}$ is to be determined for real ω and k; there being no growth or damping of modes in the steady-state turbulence. For fully developed turbulence the equation $\epsilon_{\mathbf{k},\omega} = 0$ becomes meaningless, because $|\tilde{\phi}_{\mathbf{k},\omega}| \neq 0$ leads to singular amplitudes at the zeros of $\epsilon_{\mathbf{k},\omega}$. The dielectric response function $\epsilon_{\mathbf{k},\omega}$, however, still contains a wealth of information: linear as well as nonlinear coherent response of the medium. It is now pertinent to ask what determines the detailed nature of the wave spectrum $I_{\mathrm{k},\omega}$; is it the coherent nonlinear behavior of the medium which sustains the waves? or is it the character of the nonlinear source which is obtained by interminable scattering of waves by one another? For several problems of physical interest, we are concerned with determining the properties of the medium (plasma) in the presence of turbulence, for example, the anomalous electron transport in a tokamak plasma which is supposed to be driven by low-frequency microinstabilities. We now argue that if the turbulence were to strongly affect the medium, i.e., to appreciably change $\epsilon_{\mathbf{k},\omega}$ from its linear value, then the turbulence (i.e., the turbulence spectrum) must also be strongly affected by $\epsilon_{\mathbf{k},\omega}$. Thus, in a steady state self-consistent interaction, the properties of $\epsilon_{\mathbf{k},\omega}$ and $I_{\mathbf{k},\omega}$ are strongly linked to each other. Under these conditions the nonlinear source, though arbitrary in magnitude, will not determine the detailed structure of $I_{\mathbf{k},\omega}$. We further note that in strong turbulence the linear modes are broadened, and are constantly interacted with each other. These constant interactions, when summed up to give

the incoherent source terms, are expected to be quite flat in ω and $\mathbf{k}$.

The preceding considerations suggest that a non-perturbative approximation scheme based on a scale-separation hypothesis between $|\epsilon_{\mathbf{k},\omega}|$ and $|\tilde{\phi}_{\mathbf{k},\omega}|$ (comparatively structureless in ω and $\mathbf{k}$) could make a good starting point for determining the spectrum of steady-state turbulence in situations where we expect the medium properties to be strongly affected by the turbulence. It is proposed that the fine structure of the steady-state turbulence spectrum is controlled by the nonlinear response function $|\epsilon_{\mathrm{k},\omega}|$ alone; the incoherent source $|\tilde{\phi}_{\mathbf{k},\omega}|$, slowly varying in ω and $\mathbf{k}$, determines only the magnitude of the turbulence level. Based on those considerations, the incoherent contribution can be approximated by a constant source term which characterizes the strength of the turbulence itself and a numerically solvable closure scheme is developed. Detailed discussion, in particular the analysis of the incoherent source terms, is presented in Chapter VI.

To demonstrate the application of the theory to realistic problems, we study in Chapter VII a simplified model of Alfven wave turbulence as a test case. After deriving an appropriate nonlinear wave equation, we employ our closure scheme to calculate the Alfven wave spectrum. The numerical results reveal interesting features of the renormalized turbulence theories in general, and of the Alfven wave turbulenc in particular. The k-spectrum for the Alfven wave turbulence is observed to obey a power law $I_k \sim k^{-2}$, which is consistent with the results obtained by a theory

based on renormalization group techniques[11]. We also find that the form of the spectrum power law is almost independent of the strength of the turbulence, dampling mechanism or system size. These observations are basicly consistent with the experimental facts. The wave-broadening and the frequency shift are explicitly evaluated and numerically confirmed.

Finally, we summarize our work in Chapter VIII.

Chapter VI Scale Separation Closure

VI.1 Background of Renormalized Theory

In the Fourier space, one may describe a nonlinear wave system (plasma or fluid) by the following equation[63]

$$\epsilon_k^l \phi_k = \sum_{k'} V_{k,k'} \phi_{k'} \phi_{k-k'}, \tag{6.1.1}$$

where $k = (\mathbf{k}, \omega)$ is four-component wave vector, $V_{k,k'}$ is the nonlinear coupling coefficient and ϵ_k^l is the linear response function of the system, ϕ_k is the fluctuating quantitiy whose spectrum is the major concern of the turbulence theories.

The very essential part of the renormalized turbulence theories[53-54] is to separate the nonlinear terms into two parts: the coherent and the incoherent. By a straightforward substitution Eq. (6.1.1) into itself, one finds a nonlinear wave equation

$$(\epsilon_k^l + C_k)\phi_k \equiv \epsilon_k \phi_k = \tilde{\phi}_k. \tag{6.1.2a}$$

where

$$C_k = -2 \sum_{k'} \frac{V_{k,k'} V_{k-k',k}}{\epsilon_{k-k'}} |\phi_{k'}|^2 \tag{6.1.3}$$

represents the coherent part of the nonlinear term, and renormalizes the linear propagator ϵ_k^l to $\epsilon_k = \epsilon_k^l + C_k$. The propagator renormalization takes care of the divergence problem which arises in the theories using

the bare propagator ϵ_k^l. The incoherent source terms, symbolicly denoted as $\tilde{\phi}_k$, are obtained from the relation

$$\begin{aligned}\tilde{\phi}_k &= \sum_{k'} V_{k,k'}\phi_{k'}\phi_{k-k'} - \text{Coherent Part} \\ &= \sum_{k'} V_{k,k'}\phi_{k'}\phi_{k-k'} + 2\sum_{k'} \frac{V_{k,k'}V_{k-k',k}}{\epsilon_{k-k'}}|\phi_{k'}|^2.\end{aligned} \tag{6.1.4}$$

Equation (6.1.2a) is now written in terms of the spectrum I_k

$$|\epsilon_k|^2 I_k = |\tilde{\phi}_k|^2, \tag{6.1.2b}$$

where all the terms are defined in Eqs. (6.1.3) and (6.1.4).

This procedure, which seems to be a simple rearrangement of the initial nonlinear equation, implies a significant progress. Since the coherent wave-broadenning factor has been added to the linear response function, a particular wave in turbulences can no longer be regarded as an isolated wave whose behavior depends solely on the equilibrium medium as a linear wave does. All the wave is now related and their dynamics becomes coupled. The coupling gives a larger effective inertia for each wave with the result that it becomes impossible to excite a particular wave to an arbitrarily high amplitude. This contributes a physical explanation for the removal of divergence by the wave-broadening factor (renormalization).

From Eqs. (6.1.3) and (6.1.4), one sees that the coherent correction C_k to the response function depends (to this order) only on the fluctuating spectrum $|\phi_{k'}|^2$, while the incoherent part $\tilde{\phi}_k$ is considerably more complicated involving lots of unknown correlations between $\phi_{k'}$ and $\phi_{k-k'}$. To proceed further, one needs to understand the nature of $\tilde{\phi}_k$.

The DIAC theory, obviously motivated by the desire to solve the problem, puts $|\tilde{\phi}_k| = 0$. A possible justification could be that for highly dispersive media (as the plasmas are), the strong coupling condition in one dimension ($\mathbf{k} = (0, 0, k)$)

$$\omega(k_1) + \omega(k_2) = \omega(k_1 + k_2) \tag{6.1.5}$$

is not likely to be satisfied, and therefore the interaction term $\phi_{k'}\phi_{k-k'}$ should be neglegible except for the coherent part. This argument is not very convincing, and this procedure is likely to lead to conceptual problems in the description of strong turbulence. The assumption $|\tilde{\phi}_k| = 0$ automatically leads to $|\epsilon_k| = 0$, which is very much like the linear eigenvalue problem. Although the dielectric now has a nonlinear correction, the solution would still be an unique, albeit complex, ω for a given $\mathbf{k}$. Thus, the waves grow or damp in the turbulence background, but the waves do not interact incoherently with each other. A definite correspondence between ω and $\mathbf{k}$ really conflicts with the concept of mode-broadening which should be one of the main features of a strong turbulence theory.

In fact, one finds that the incoherent wave-wave interaction is more responsible for transporting energy from one mode to another mode than the coherent interaction. In three dimensions, the quasilinear three wave coupling condition

$$\omega(\mathbf{k}_1) + \omega(\mathbf{k}_2) = \omega(\mathbf{k}_1 + \mathbf{k}_2) \tag{6.1.6}$$

can always be satisfied no matter what kind of dispersion relation the wave might have. We further notice that even in one dimension, the four wave interaction condition

$$\omega(k_1) + \omega(k_2) + \omega(k_3) = \omega(k_1 + k_2 + k_3) \tag{6.1.7}$$

can also be satisfied easily as long as ω can be negative as well as positive. The contribution to IS term from this four-wave coupling process is given by $\phi_{k'}\phi_{k''}\phi_{k-k'-k''}$ which is precisely the same order as the coherent part.

It should be stressed that the preceding discussion is valid in the quasilinear regime. For the fully developed turbulences, the waves are broadened implying that the dispersion curves are not lines but bands in the parameter space. This broadenning allows a larger number of wave-interactions to contribute effectively to the incoherent source. The measure of these wave-interactions should be much larger than the measure of wave-interactions contributing to the coherent part. Thus we can safely conclude that setting IS= 0 can not be justified for a turbulence system.

We now try to motivate the scale-separation or the band separation argument to deal with the incoherent source. Based on the previous arguments, the IS terms can be written as

$$\begin{aligned} \tilde{\phi}_k &= \sum_k V_{k,k'}\phi_{k'}\phi_{k-k'} - \text{coherent part} \\ &\sim \sum_k V_{k,k'}\phi_{k'}\phi_{k-k'}, \end{aligned} \tag{6.1.8}$$

because the coherent terms really form a very small subset of all the nonlinear terms. Since the IS is obtained by summing over the entire spectrum range, a possible granular structure in the spectrum can not yield similar structure in IS source. We expect that the structure of the IS will be smeared out in k (where $k = \mathbf{k}, \omega$) particularly when the spectrum is already broadened by nonlinear effects. The following process will lead more smearing out. A typical turbulence spectrum is broad with a width Δk around some k. Since $\Delta\omega$ and $\Delta\mathbf{k}$ are generally large (in the drift-wave turbulence, $\Delta\omega \sim \omega^{64}$), these neighboring waves of comparable amplitude will generate a strong and wide low k band. This low k band, beating with any possible peak of the wave spectrum, will produce a spreaded incoherent source terms.

Thus, we can expect that the spectrum of the incoherent source, which is not observable though, would be quite flat in the vicinity of the broadened nonlinear wave spectrum. This picture helps us to develop an adequate approximation procedure to close the chain of equations contained in Eq. (6.1.2), and achieve a relatively simpler set.

VI.2 Closure Scheme

Within the context of the proceding discussion, we make the following assumptions

(1) Microstructure of turbulence is mainly determined by the nonlinearly renormalized response function $\epsilon_k = \epsilon_k^l + C_k$. This assumption is justified 'a posterior' by the results obtained in the approarches which predict the details of the spectrum by analyzing the renormalized response function only.

(2) The incoherent source term does not have a fine structure like ϵ_k. As a result, this term is approximated, to leading order, by a constant which reflects the strength of the turbulence.

Making use of these assumptions, we rewrite Eq. (6.1.2) as

$$|\epsilon_k^l + C_k|^2 |\phi_k|^2 \equiv |\epsilon_k|^2 I_k = S_0, \tag{6.2.1}$$

and the equation for the renormalizing factor as

$$C_k = C_k(I_k, C_k) = -2 \sum_{k'} \frac{V_{k,k'} V_{k-k',k}}{\epsilon_{k-k'}^l + C_{k-k'}} |\phi_{k'}|^2, \tag{6.2.2}$$

which form a closed set.

To obtain the spectrum of steady-state turbulence (I_k), we must find a way to solve Eq. (6.2.1) and (6.2.2) with the proviso that $k = (\mathbf{k}, \omega)$ must be real. Thus the scale-separation argument has led us to a relatively simple set of closed equations which describe steady-state turbulence. Notice that ϵ_k^l and, $V_{k,k'}$ contain all the information about the medium and the basic wave motion around which the turbulence is built. We believe that the above formalism should be applicable to a broad range of plasma and fluid phenomena.

Equations (6.2.1) and (6.2.2), though comparatively simple are still too difficult to be solved analytically for the spectrum I_k. However, a numerical iteration procedure can be developed, which can be shown as the following:

$$\begin{aligned} \epsilon^{(0)}_{\mathbf{k},\omega} &= \epsilon^{l}_{\mathbf{k},\omega} \\ \epsilon^{(1)}_{\mathbf{k},\omega} &= \epsilon^{l}_{\mathbf{k},\omega} + C^{(0)}_{\mathbf{k},\omega} \end{aligned} \tag{6.2.3a}$$

($C^{(0)}_{\mathbf{k},\omega}$ can be rather arbitrarily chosen as long as all the symmetries of the system are satisfied)

$$\begin{aligned} |\phi^{(1)}_{\mathbf{k},\omega}|^2 &= \frac{S_0}{|\epsilon^{(1)}_{\mathbf{k},\omega}|^2} \\ C^{(1)}_{\mathbf{k},\omega} &= -2\sum_{k'} \frac{V_{k,k'}V_{k-k'}}{\epsilon^{l}_{\mathbf{k},\omega} + C^{(0)}_{\mathbf{k},\omega}} |\phi^{(1)}_{\mathbf{k},\omega}|^2 \\ &\cdots\cdots \\ |\phi^{(n)}_{\mathbf{k},\omega}|^2 &= \frac{S_0}{|\epsilon^{(n)}_{\mathbf{k},\omega}|^2} \\ C^{(n)}_{\mathbf{k},\omega} &= -2\sum_{k'} \frac{V_{k,k'}V_{k-k',k}}{\epsilon^{l}_{\mathbf{k},\omega} + C^{(n-1)}_{\mathbf{k},\omega}} |\phi^{(n)}_{\mathbf{k},\omega}|^2 \end{aligned} \tag{6.2.3b}$$

In the next chapter, we shall employ numerical method to solve the problem of Alfven wave turbulence. Now we take a digression to show some aspects of the problem of plasma heating by externally excited waves which can be analytically tackled within the framework developed in this section.

VI.3 Plasma Turbulence Heating

In the initial stage, the wave heating[65] (externally driven) of plasma can be viewed as a linear problem. But as the amplitude of the excited wave increases, nonlinear effects will become important, and the generation and interaction of wave modes could easily lead to a turbulent situation. The situation is, of course, quite similar to the turbulent system we have dealt with in this Chapter, but with the difference, that now the source terms must contain the effects of the external source in addition to the incoherent soure. The basic equation describing the spectrum $I_k = |\phi_k|^2$ in this case is

$$|\epsilon_k|^2 I_k = |\tilde{\phi}_k^{\text{ext}} + \tilde{\phi}_k|^2, \tag{6.3.1}$$

where $\tilde{\phi}_k^{\text{ext}}$ represents the incoherent effects of the external driving source. The problem will reduce to the linear driven case if $\tilde{\phi}_k = 0$, and $\epsilon_k = \epsilon_k^l$. Clearly for large amplitude waves (high power heating), the characteristics of the waves in the plasma are bound to be quite different from its linear characteristics. Therefore to understand the mechanism as well as efficiency of high power heating, we need to study the fully nonlinear

system schematically represented by Eq. (6.3.1). As outlined earlier, our attempt here is again to determine the struture of I_k, the range or band in which it is significantly different from zero.

A very intergral part of our approximation is the scale separation between the renormalized nonlinear response function ϵ_k and the incoherent source. We have given arguments to show that the source terms are expected to satisfy several conditions. We believe that similar arguments are valid even for $\tilde{\phi}_k^{\text{ext}}$, because the coherent aspects of the source (which may have strong peaks in the linear limit) will become a part of ϵ_k, and $\tilde{\phi}_k^{\text{ext}}$ due to multiple incoherent interactions will be quite broad in $k(\mathbf{k},\omega)$.

With this argument, we can achieve interesting and useful consequences of our theory. For simplicity, we deal with an one-dimensional problem, i.e., $k = (\mathbf{k},\omega) = [(0,0,k),\omega]$. Schematically, the essence of Eq. (6.2.1) is

$$I_{k,\omega} = \frac{S_0}{|\epsilon_{k,\omega}|^2}, \tag{6.3.2}$$

where S_0 is independent of k and ω, and is nonzero. We could now proceed formally and deduce that for a given k, the spectrum $I_{k,\omega}$ will peak at that value of $\omega = \omega_0$ for which $|\epsilon_{k,\omega}|^2$ is minimum, i.e., the solution of

$$\left[\frac{d}{d\omega}|\epsilon_{k,\omega}|^2\right]_{\omega=\omega_0} = 0, \tag{6.3.3}$$

for fixed k, determines the maximum value of the fluctuation spectrum. It must, of course, be borne in mind that the analysis is meaningful only

for real k and ω, and we must admit only the real roots of Eq. (6.3.3). Notice that $|\epsilon_{\mathbf{k},\omega}| = 0$ leading to complex ω or $\mathbf{k}$ is not admissible, because it yields 1) $I_{\mathbf{k},\omega} \to \infty$ since $S_0 \neq 0$, and 2) the turbulence will be nonstationary if ω is complex. Using Eq. (6.3.3), we can write Eq. (6.3.2) as

$$I_{k,\omega} = \frac{\bar{S}_0}{\Delta^2 + (\omega - \omega_0)^2}, \tag{6.3.4}$$

where

$$\Delta^2 = \left[\frac{1}{2}\frac{d^2}{d\omega^2}|\epsilon_{k,\omega}|^2\right]^{-1}_{\omega-\omega_0} |\epsilon_{k,\omega_0}|^2$$

and

$$\bar{S}_0 = S_0 \cdot \left[\frac{1}{2}\frac{d^2}{d\omega^2}|\epsilon_{k,\omega}|^2\right]^{-1}_{\omega-\omega_0}.$$

Thus, to leading order, we obtain a lorentzian spectrum peaked at $\omega = \omega_0$, and with a width Δ. As expected, the general shape of the spectrum is independent of S_0, although the peak value is $I_k \sim S_0/\Delta$. We must, however, point out that Eq. (6.3.4) is purely formal, because both ω_0 and Δ are functions of $\epsilon_{\mathbf{k},\omega}$, which is itself a function of $I_{k,\omega}$, the principal object of interests.

Chapter VII Alfven Turbulence and Numerical Methods

VII.1 Basic Equation

In this section, we demonstrate that the theoretical methods developed in the last Chapter can be applied to realistic turbulence problem. We choose a simplified model of Alfven waves turbulence as a test case. We deal with a cylindrical plasma of radius r and axial length $2\pi R$ (to simulate a torus of radius R) within the framework of ideal magnetohydrodynamics (MHD). The basic renormalized equations are derived in Appendix A, and are ($\mathbf{k}$ and ω dependence is explicitly displayed in this section)

$$|\epsilon_{\mathbf{k},\omega}|^2|U_{\mathbf{k},\omega}|^2 = |F_{\mathbf{k},\omega} + C_{\mathbf{k},\omega}|^2|U_{\mathbf{k},\omega}|^2 = |\tilde{U}_{\mathbf{k},\omega}|^2, \tag{7.1.1}$$

and

$$C_{\mathbf{k},\omega} = \sum_{\mathbf{k}-\mathbf{k}'\neq 0,\omega-\omega'\neq 0} \frac{\omega(\omega-\omega')(k_\theta^2 - k_\theta'^2 - k_\theta k_\theta')}{F_{\mathbf{k}-\mathbf{k}',\omega-\omega'} + C_{\mathbf{k}-\mathbf{k}',\omega-\omega'}} \frac{|U_{\mathbf{k}',\omega'}|^2}{V_A^4} \tag{7.1.2a}$$

or

$$C_{\mathbf{k},\omega} = \sum_{\mathbf{k}'\neq 0,\omega'\neq 0} \frac{\omega\omega'(-k_\theta^2 - k_\theta'^2 + 3k_\theta k_\theta')}{F_{\mathbf{k}',\omega'} + C_{\mathbf{k}',\omega'}} \frac{|U_{\mathbf{k}-\mathbf{k}',\omega-\omega'}|^2}{V_A^4}, \tag{7.1.2b}$$

where Eq. (7.1.2b) is obtained from Eq. (7.1.2a) by simply letting $\mathbf{k}' \to \mathbf{k} - \mathbf{k}'$ and $\omega' \to \omega - \omega'$. In Eqs. (7.1.1) and (7.1.2), U_θ is the azimuthal component of the velocity field, and the linear response function $F_{\mathbf{k},\omega}$ is

$$F_{\mathbf{k},\omega} = \frac{\omega^2}{V_A^2} - k_z^2, \tag{7.1.3}$$

with

$$k_z = n/R, \quad k_\theta = m/r$$

where m and n are respectively the azimuthal and axial wave numbers, $V_A = B_0/(4\pi\rho_0)^{1/2}$ is the Alfven speed, ρ_0 is the plasma density and B_0 is the equilibrium axial magnetic field, $C_{\mathbf{k},\omega}$ is the coherent wave-broadenning factor, and $\tilde{U}_{\mathbf{k},\omega}$ is the incoherent nonlinear source term.

Notice that Eqs. (7.1.1) and (7.1.2) are exactly the same form as Eqs. (6.1.1) and (6.1.2) implying that the closure can be achieved by putting the incoherent term

$$|\tilde{U}_{\mathbf{k},\omega}|^2 = S_0, \tag{7.1.4}$$

where S_0 is independent of $\mathbf{k}$ and ω. The set of Eqs. (7.1.1) to (7.1.4) is numerically solved in Sec. VII.3. In the next section, we show how we can extract some useful information out of these equations for a special heating problem by using the method developed in the last Chapter.

VII.2 Frequency Shift in Alfven Wave Heating

In wave heating of plasmas, electromagnetic waves of a given description are generated in an antenna located near the edge of the plasma. These modes are converted to the appropriate natural oscillation modes of the plasma, and then can impart energy to the plasma (by resistivity or by Landau damping, etc.). Since the dominant modes in the plasma must, in general, correspond to the modes driven by the antenna, one has a prior knowledge of the wave numbers from a knowledge of the antenna structure. Now for a given set of wave numbers, the heating efficiency depends upon the frequency of the wave. In Alfven wave heating, for example, $F_{\mathbf{k},\omega} = \omega^2/V_A^2 - k_z^2 = 0$ (the linear dispersion relation of the wave) is the condition for maximum efficiency in the linear regime. For higher power or heating in the nonlinear regime, the optimum heating frequency must depend upon the wave energy I_k of the excited wave. This was essentially the content of Chapter VI, where we derived a formula for the frequency ω_0 at which I_k peaks.

Let us consider an idealized Alfven wave experiment where the antenna generates waves of $m = \pm 1$ and $n = \pm 1$ only. The best driving frequency for this case in the linear regime is obviously $\omega_l = \pm V_A/R$. However, we are interested in finding the optimum frequency ω_0 in the nonlinear regime. Let us assume that the steady state nonlinear stage is already set up, then ω_0 will obviously be the solution of Eq. (6.3.3). Because of the peculiar choice of the antenna, we could assume that the

principal part of the excited spectrum is at $\omega = \pm\omega_0$. Thus the excited spectrum is

$$|U_{\mathbf{k},\omega}|^2 = |U_{m,n,\omega}|^2 = \begin{cases} U_0^2, & \text{if } m = \pm 1,\ n = \pm 1,\ \omega = \pm\omega_0; \\ 0, & \text{otherwise.} \end{cases} \tag{7.2.1}$$

Of cource, the excited spectrum will have a width, which can be calculated from Eq. (6.3.4). However, as long as the width is small compared to $|\omega_0|$, the spectrum given in Eq. (7.1.1) will give approximately correct results. Making use of Eqs. (7.1.2) and (7.2.1), it is clear that (we propose to calculate ω_0 for $m = 1$, $n = 1$)

$$C_{1,1,\omega} = \left(\frac{U_0}{V_A}\right)^2 \frac{1}{r^2 V_A^2}\left[\frac{\omega(\omega-\omega_0)}{F_{2,2,\omega-\omega_0} + C_{2,2,\omega-\omega_0}} + \frac{\omega(\omega+\omega_0)}{F_{2,2,\omega+\omega_0} + C_{2,2,\omega+\omega_0}}\right], \tag{7.2.2}$$

because only $n' = n \pm 1$, $m' = m \pm 1$, $\omega' = \omega \pm \omega_0$ can contribute to the sum in Eq. (7.2.2). Notice that we are using the notation $C_{\mathbf{k},\omega} = C_{m,n,\omega}$. Equation (7.2.2) indicates that in order to calculate $C_{1,1,\omega}$ we need to calculate $C_{2,2,\omega\pm\omega_0}$, and of course to calculate $C_{2,2,\omega\pm\omega_0}$ we would need higher $C_{m,n,\omega}$'s. But to make analytical progress, we must make further approximations. In most cases of interest $U_0/V_A = \delta$ is a small quantity. We exploit this property $\delta \ll 1$ to propose the ordering $C_{m,n,\omega} \sim \lambda_{mn}\delta/rR$, where λ_{mn} is a number we cannot determine by analytical theory. Notice that this ordering solves Eq. (7.2.2) provided the denominator $F_{2,2,\omega\pm\omega_0} + C_{2,2,\omega\pm\omega_0} \sim \delta/rR$. This will indeed turn out to be true.

Within the context of the preceding discussion, we have

$$\epsilon_{1,1,\omega} = \frac{\omega^2}{V_A^2} - \frac{1}{R} + \frac{\delta^2}{r^2}\left[\frac{\omega(\omega-\omega_0)}{(\omega-\omega_0)^2 - 4(V_A^2/R^2) + \lambda_2\delta V_A^2/rR} + \frac{\omega(\omega+\omega_0)}{(\omega+\omega_0) - 4(V_A^2/R^2) + \lambda_2\delta V_A^2/rR}\right]. \tag{7.2.3}$$

where $\lambda_2 \equiv \lambda_{22}$ and $\epsilon_{1,1,\omega} = F_{1,1,\omega} + C_{1,1,\omega}$. Since $\epsilon_{1,1,\omega}$ is real for this simple case, Eq. (6.3.3) is equivalent to $d\epsilon_{1,1,\omega}/d\omega$. Further we have stipulated that the peaks are at $\omega = \pm\omega_0$.

Either of the equations $(d\epsilon_{1,1,\omega}/d\omega)_{\omega=\pm\omega_0} = 0$ can be used to obtain optimum frequency ω_0. Differentiating Eq. (7.2.3) and equating its value to zero at ω_0, we obtain

$$\frac{2\omega_0}{V_A^2} + \frac{\delta^2}{r^2}\left[\frac{\omega_0}{-4\dfrac{V_A^2}{R^2} + \dfrac{\lambda_2\delta V_A^2}{rR}} + \frac{3\omega_0}{D} - \frac{2\omega_0^2[2\omega_0 + \dfrac{\delta V_A^2}{rR}\dfrac{\partial\lambda_2}{\partial\omega_0}]}{D^2}\right] = 0, \tag{7.2.4}$$

where

$$D = 4\left(\omega_0^2 - \frac{V_A^2}{r^2}\right) + \lambda_2\frac{\delta V_A^2}{rR}. \tag{7.2.5}$$

Since the assumed ordering requires $D \sim \delta$, the dominant balance in Eq. (7.2.4) comes from

$$\frac{2\omega_0}{V_A^2} - \frac{\delta^2}{r^2}\frac{4\omega_0^3}{D^2} = 0, \tag{7.2.6}$$

where both terms are of order unity. Eq. (7.2.5) can be rewritten in the form

$$D = 2^{1/2}\delta\omega_0\frac{V_A}{R}, \tag{7.2.7}$$

which can be approximately solved to obtain

$$\omega_0^2 = \frac{V_A^2}{R^2} + \frac{\delta V_A^2}{4r^2}\left[2^{1/2} - \frac{\lambda_2 r}{R}\right] \tag{7.2.8}$$

showing that the correction to the linear dispersion relation $\omega_l^2 = V_A^2/R^2$ $(m = 1, n = 1)$ is of order

$$\delta \sim U_0/V_A \tag{7.2.9}$$

rather than δ^2, which would be the quasilinear or the weak turbulence result. We must state that it is not possible to determine the value of λ_2 by this simple analytic method. However, we have already obtained a very interesting strong turbulence result that the frequency shift scales linearly with the strength of the turbulence.

The spectrum width Δ can be readily obtained using Eq. (6.3.4) to be

$$\Delta = \lambda \frac{\delta V_A}{2^{3/2} r}, \tag{7.2.10}$$

where λ is a number of order unity. We notice that both the frequency shift and spectrum width are of order δ.

VII.3 Numerical Solution

In this section we numerically investigate the Alfven wave turbulence with our closure scheme and Eqs. (7.1.1) and (7.1.2).

Reality of the wave field or the fluid velocity imposes the universal sysmmetry

$$C_{\mathbf{k},\omega} = C^*_{-\mathbf{k},-\omega}, \tag{7.3.1}$$

where the notation $*$ stands for the complex conjugation. Additional symmetries will, of course, depend upon the special properties of the system under consideration. For our problem, we could deduce further symmetries from Eqs. (7.1.1)-(7.1.3). Before doing this we must mention that the linear response function $F_{\mathbf{k},\omega}$ in Eq. (7.1.3), in general, has an imaginary part (due to resistivity or Landau damping , for instance) proportional to ω.[66] This imaginary part is quite important to insure convergence of the numerical iteration and is retained in our work, although we do not display is explicitly in Eq. (7.1.3). The existence of this imaginary part proportional to ω implies $F_{\mathbf{k},\omega} = F^*_{\mathbf{k},-\omega}$, which coupled with Eq. (7.3.1) leads to

$$C_{\mathbf{k},\omega} = C^*_{\mathbf{k},-\omega}. \tag{7.3.2}$$

Eqs. (7.3.1) and (7.3.2) trivially yield

$$C_{\mathbf{k},\omega} = C_{-\mathbf{k},\omega}. \tag{7.3.3}$$

With help from Eq. (7.3.2) and (7.3.3), we can systematically solve Eq. (7.1.1) and (7.1.2). The iteration procedure has been shown in

Sec. VI.2. However, we must point out that the calculation of $C^{(n)}_{\mathbf{k},\omega}$ using the method is tantamount to doing a complicated multiple integral, and one can indeed run into convergence problem. We have been able to avoid convergence problems by 1) introducing a small imaginary part into the nonlinear response function which effectively damps very high k_z modes, and 2) making the iteration procedure relatively slow, that is, the quantities $C_{\mathbf{k},\omega}$ are varied slowly from one iteration cycle to another $[C^{(n)} = (jC^{(n-2)} + C^{(n-1)})/(j+1)]$, and 3) adding an extra positive number to the denominator and dismissing it cycle by cycle till it is zero.

These computing techniques seem a bit artificial, but they very effectively take care of oscillation problems which may be encountered in the usual procedure.

In our numerical calculations, we have further simplified the problem by concentrating on waves with $m = \pm 1$, thus effectively reducing the problem to a two-dimensional problem in $k_z(n/R)$ and ω.

In Fig. 6.1, we display the spectrum $I_{k,\omega}$ as a function of k and ω on a two-dimensional plot. The spectrum is broad in both k and ω clearly indicating the fundamental difference between a turbulent and a linear spectrum.

After integrating the spectrum $I_{k,\omega}$ over all ω, we obtain the spectrum I_k, which is displayed in Fig. 6.2 as a function of k. To make the k-dependence more perspicuous, we have plotted in Fig. 6.3 a graph of $\ln I_k$ versus $\ln k$ for the intermediate range (inertial range) of k. We no-

tice that the curve is essentially a staight line implying that the Alfven wave spectrum obeys a power law

$$I_k \propto k^{-\alpha} \tag{7.3.4}$$

with the exponent $\alpha = 2$. This is similar to the Kolmogorov spectrum in hydrodynamical turbulence but with a different exponent; the exponent in hydrodynamical turbulence equals 1.67.

To reveal more turbulence features, we vary several conditions to see their effects on the spectrum curves. In Fig. 6.4, we change the system scale length by putting more restrictions on the low-k modes, which reduce amplitude of these modes. Curves representing two different situations vary slightly, and the behavior of the inertial range is unchanged (the two curves are separated purposely). In Fig. 6.5, the high-k damping terms are varied. In Fig. 6.6, different strengthes of S_0 are employed. These pictures show that the turbulence spectrum in the inertial regime is clearly unaffected by these variations. This fact is consistent with the experimental observations on most turbulence systems. In Fig. 6.7, we plot the k-spectrum for a given ω. The curves in the figure represent three situations with different strength levels of turbulence. In Fig. 6.8, we plot these three curves on the same amplitude scale. One sees that curve 3, which corresponds to the strongest turbulence, gives the widest wave-broadening and the biggest frequency shift. Similar effects can be seen in Figs. 6.9 and 6.10 where ω is smaller than that in Fig. 6.9.

Finally we plot the curve for the total incoherent part in Fig. 6.11 based on calculation of the following expression

$$|\tilde{\phi}_k|^2 \sim |\sum_{k'} V_{k,k'}\phi_{k'}\phi_{k-k'}|^2, \tag{7.3.5}$$

which, though not really accurate, serves as a good estimate. Clearly, $|\tilde{\phi}_k|^2$ is relatively flat in the k-spectrum.

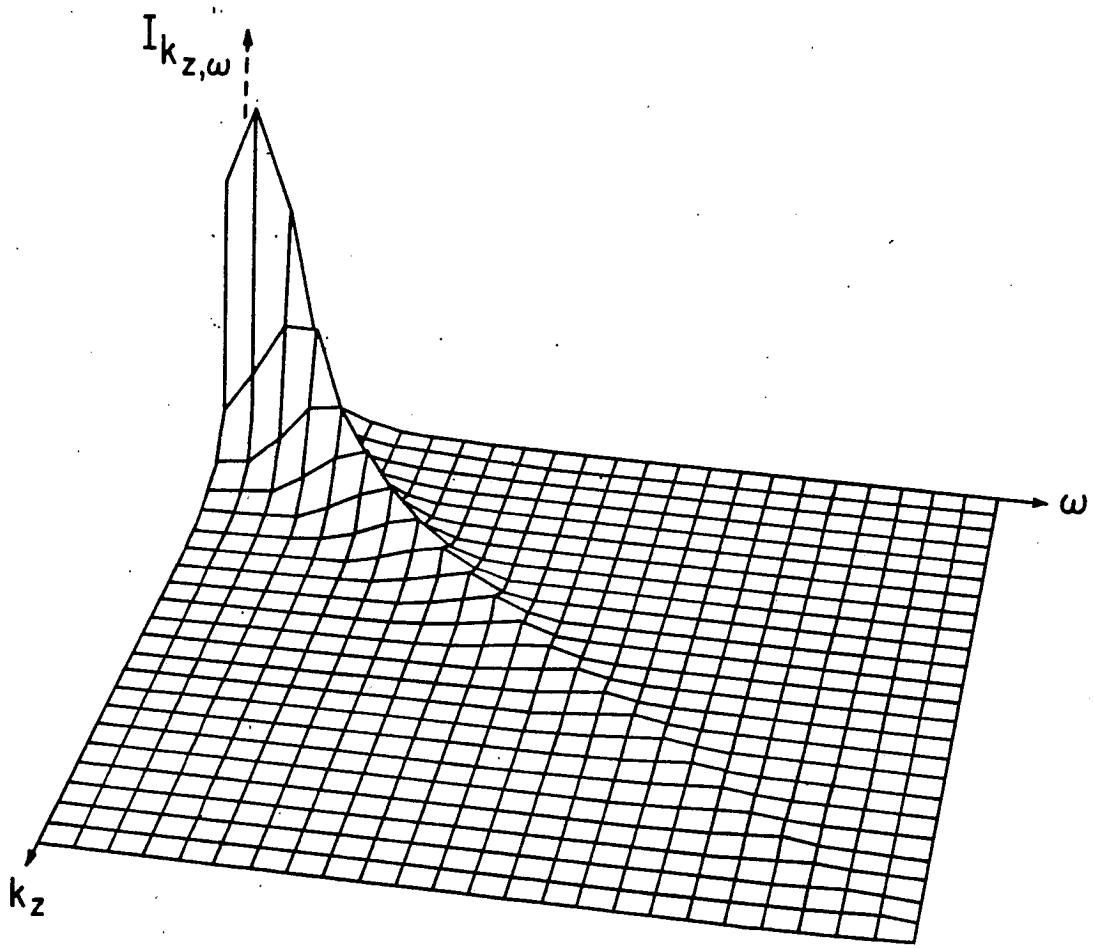

Fig. 6.1. Alfven wave turbulence spectrum $I_{k_z,\omega}$ as a function of k_z and ω on a two dimensional plot with ω being normalized by Alfven speed $V_A = B_0/(4\pi\rho)^{1/2}$.

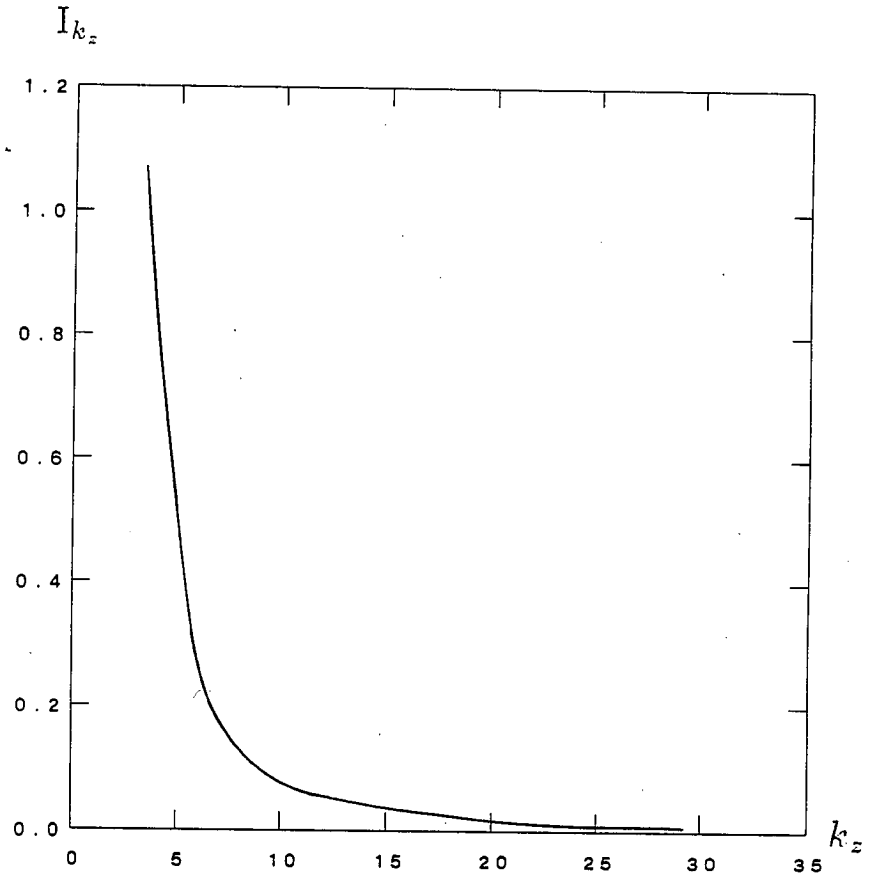

Fig. 6.2. A plot of frequency-integrated spectrum $I_{k_z} = \int d\omega I_{k_z,\omega}$ versus k_z.

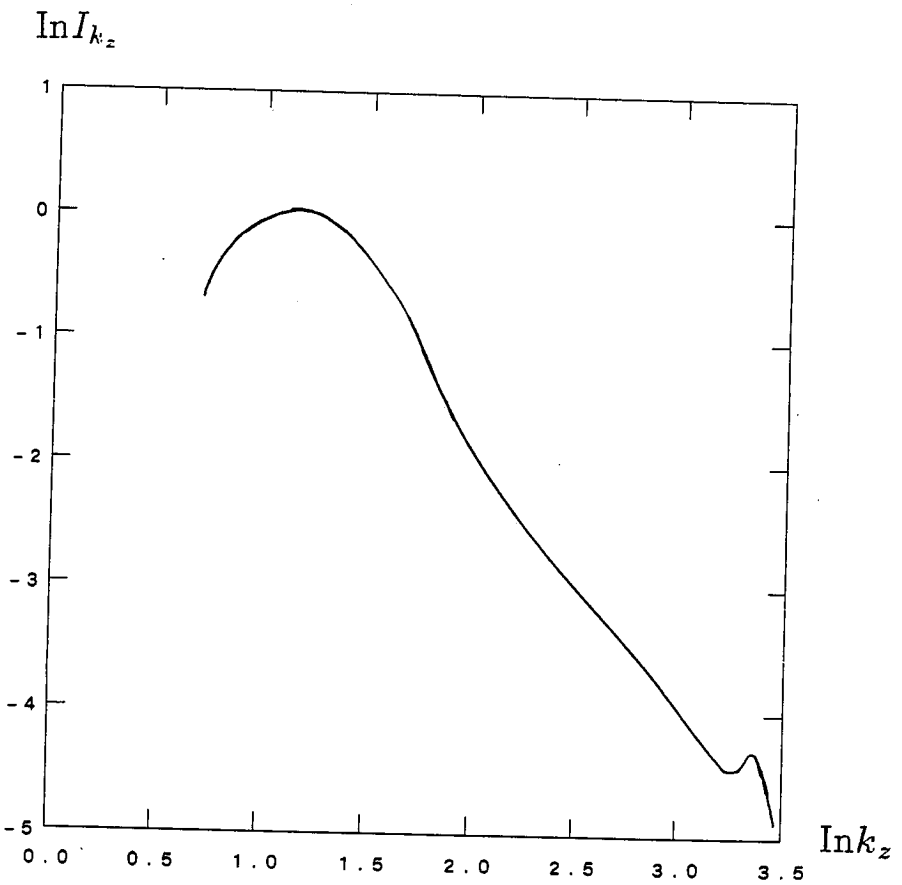

Fig. 6.3. A plot of ln I_{k_z} versus ln k_z in the intermediate range (initial range) of k_z; the straightline has a slope approximately equal to two.

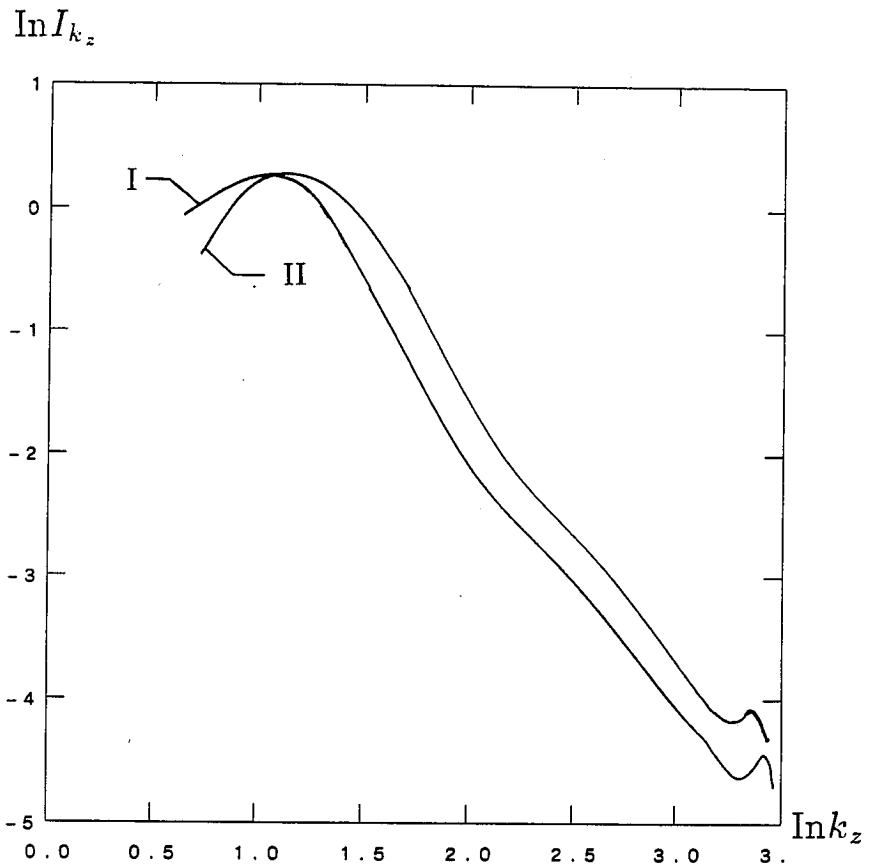

Fig. 6.4. $\ln I_{k_z}$ versus $\ln k_z$ with different space restriction (long-wave-length modes suppressed). Note that only amplitudes of low-k_z modes changed (curves I and II are artificially separated).

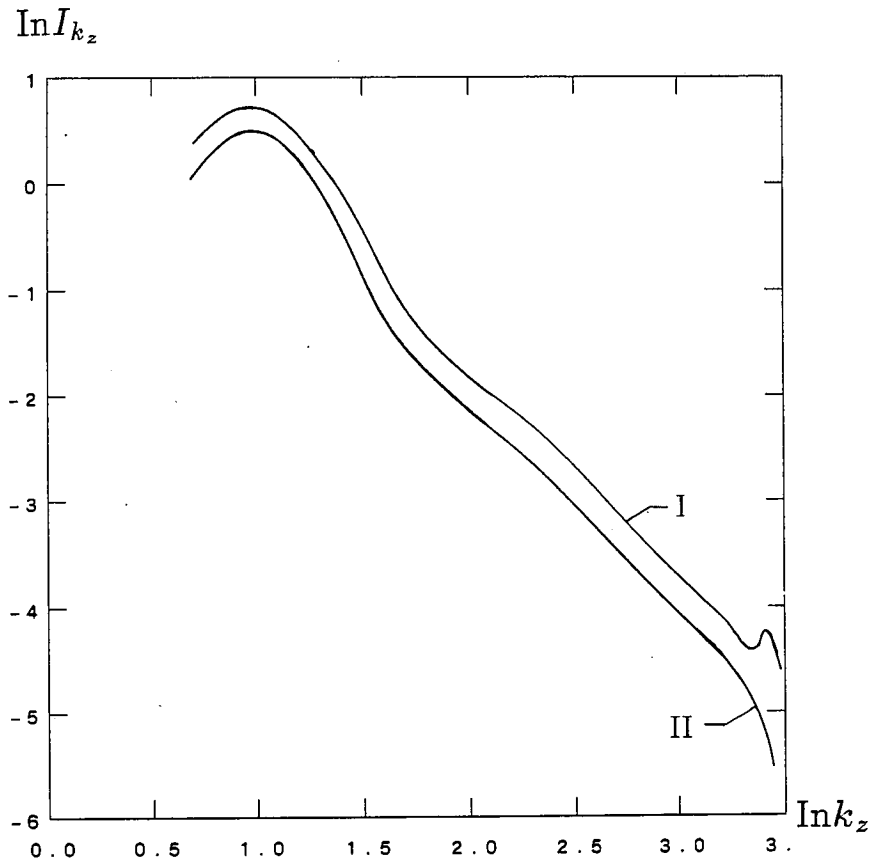

Fig. 6.5. A plot of $\ln I_{k_z}$ versus $\ln k_z$ with different high-k damping conditions (curves I and II are artificially separated).

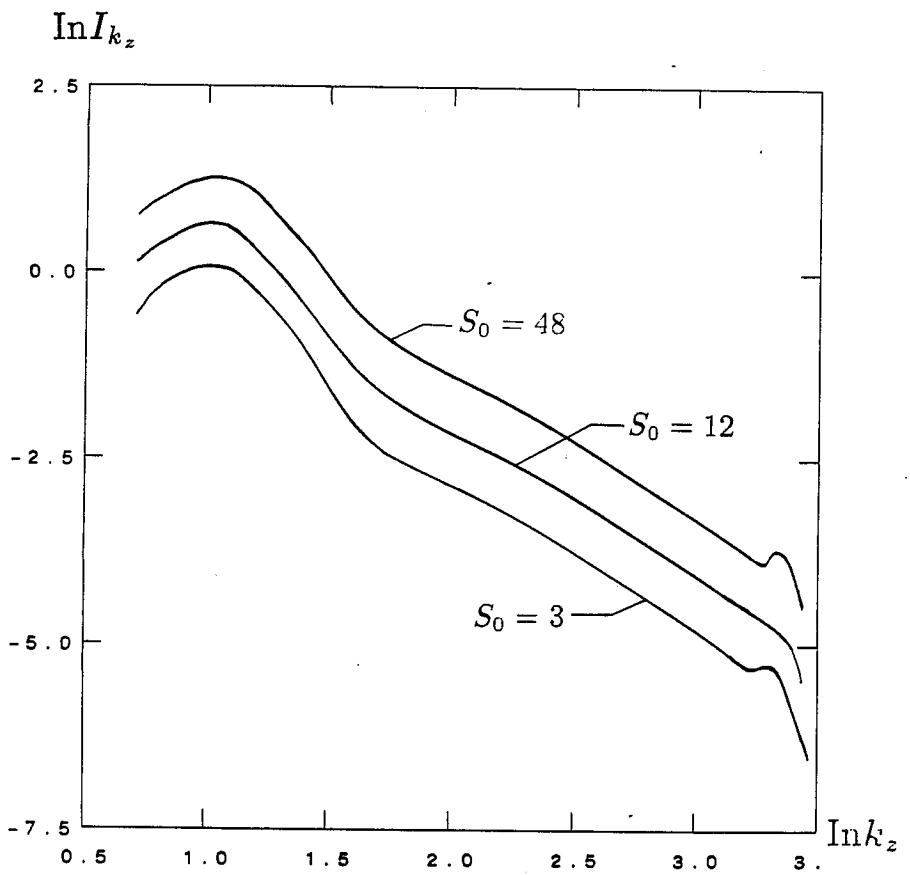

Fig. 6.6. A plot of $\ln I_{k_z}$ versus $\ln k_z$ with different-strength sources ($S_0 = 3, 12, 48$).

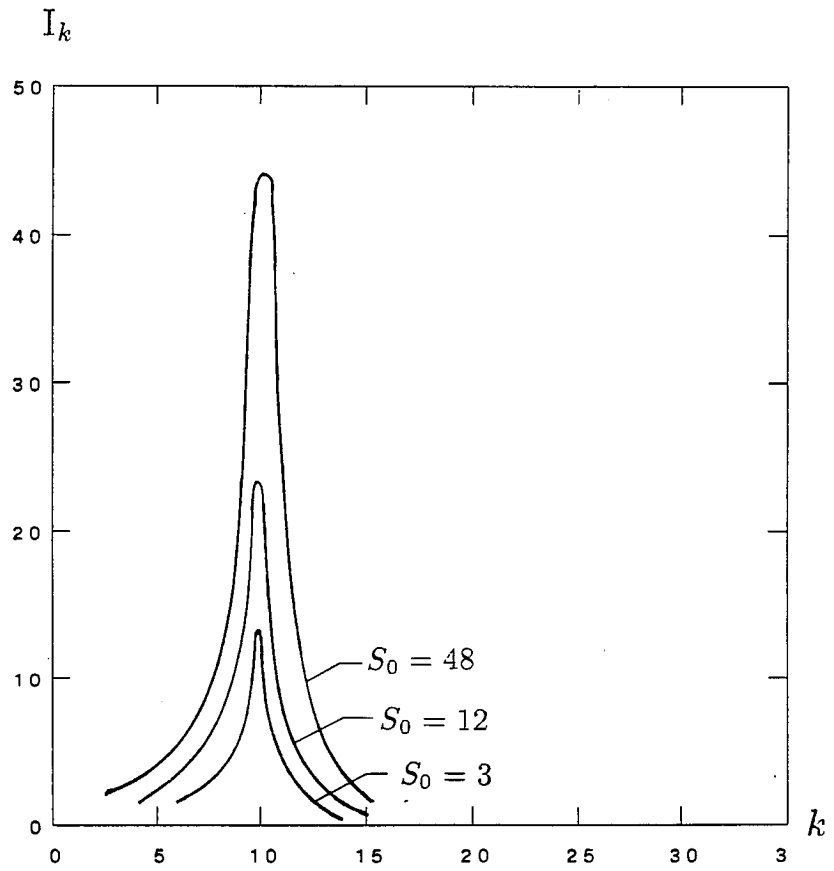

Fig. 6.7. A plot of k-spectrum ω is fixed ($\omega = 10.0 \times V_A$). The three curves correspond different sources ($S_0 = 3, 12, 48$).

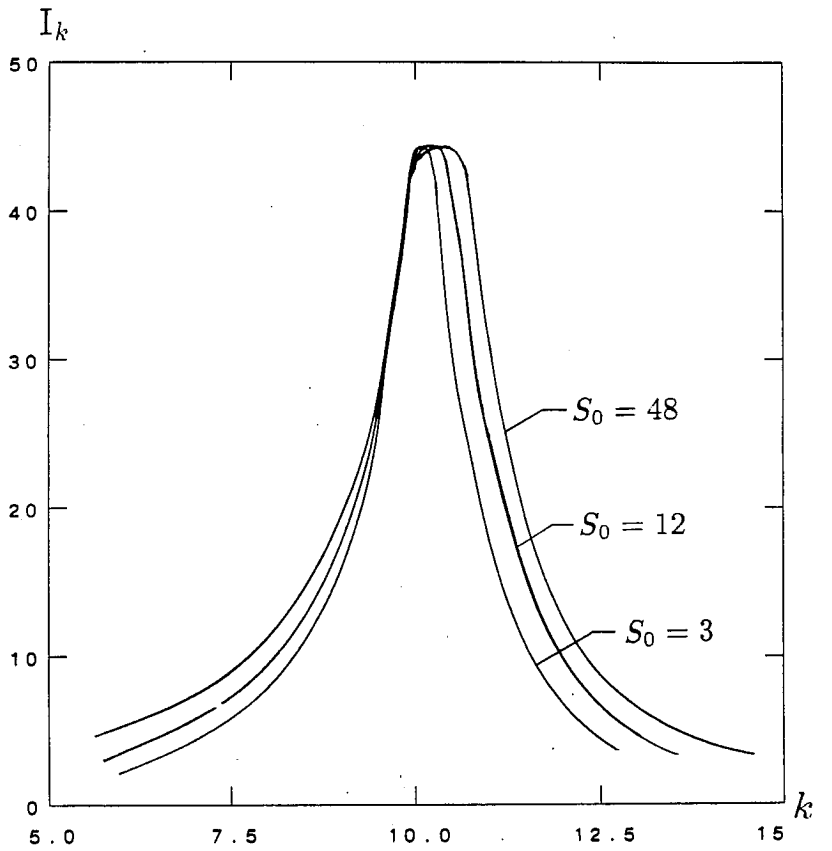

Fig. 6.8. Putting the three curves of Fig. 6.7. in the same scale of amplitude.

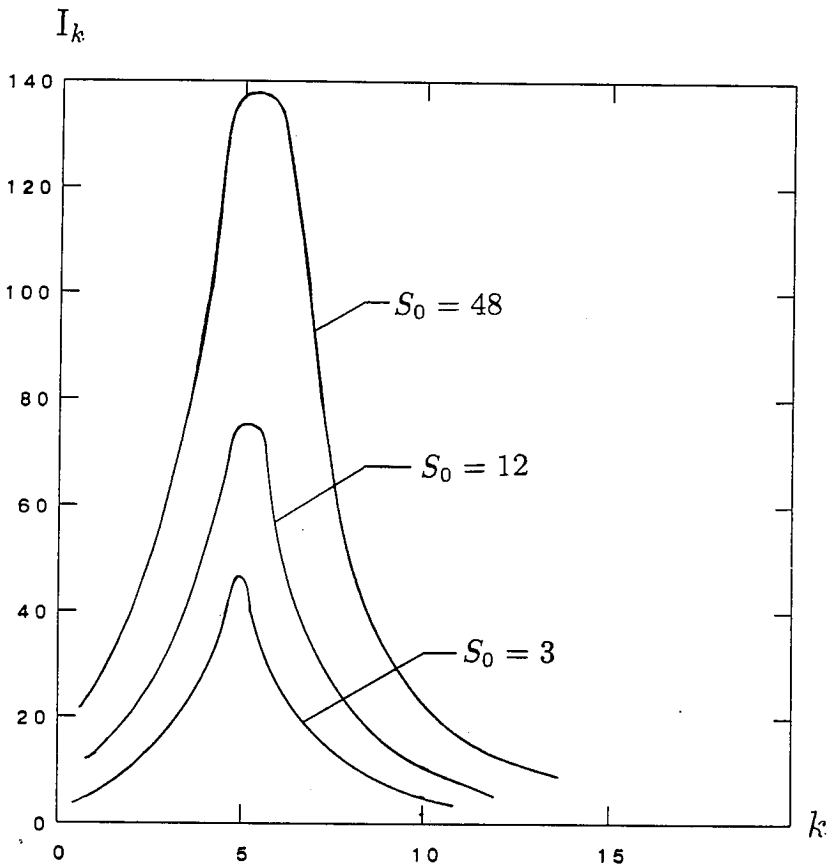

Fig. 6.9. A plot of k-spectrum as ω is fixed ($\omega = 5.0 \times V_A$).

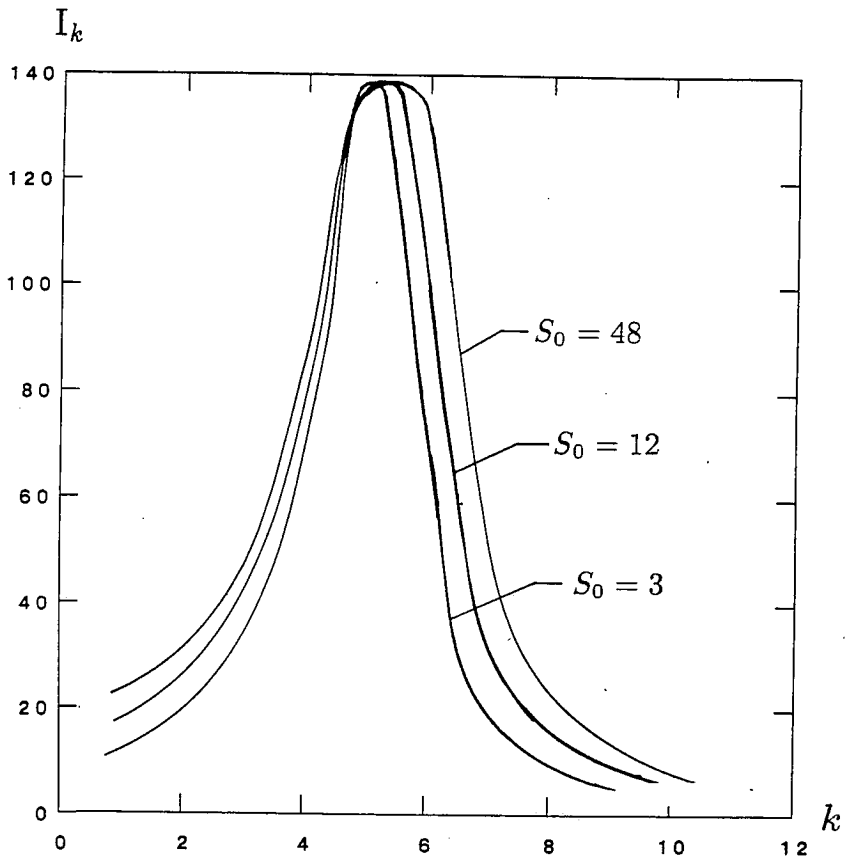

Fig. 6.10. Putting the three curves of Fig. 6.9. in the same scale of amplitude.

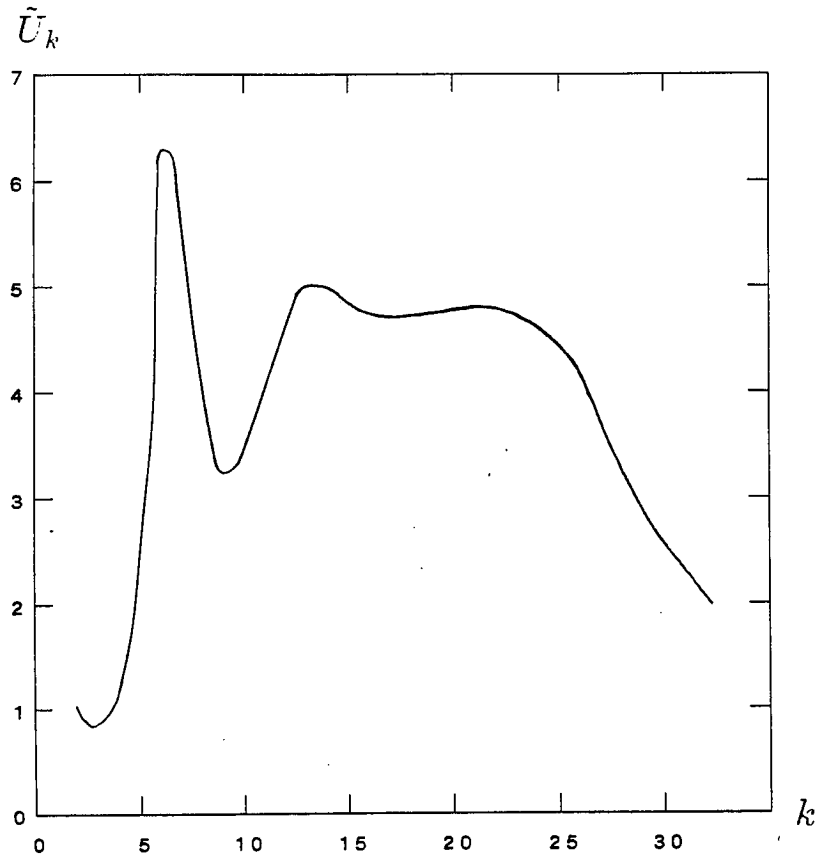

Fig. 6.11. A plot of k-spectrum for the incoherent source term (as an estimate).

Chapter VIII. Summary and Conclusion

We have proposed a physically motivated, non-perturbative closure scheme to deal with some problems in plasma or fluid turbulence. The scheme is based on a scale separation assumption; the structure (in $\mathbf{k}, \omega$) of the turbulent spectrum is essentially determined by the structure of the nonlinear coherent response function $\epsilon_{\mathbf{k},\omega}$, and not by the structure of the incoherent source which is assumed to vary on a much larger scale in $\mathbf{k}$ and ω. This allows us to obtain a comparatively simple closed set of equations which can, in principle, be always solved.

After discussing a few simple analytically tractable applications, we have applied our formalism to a model problem: the shear-Alfven turbulence. The problem is readily solved numerically to obtain the turbulent spectrum with the following features

(1) The calculated spectrum has explicit frequency shift from the linear theory as well as explicit band-broadening in $\mathbf{k}, \omega$ space.

(2) The frequency integrated spectrum obeys a power law in the intermediate k range, i.e., $I_k \sim k^{-\alpha}$, where α approaches the value 2 in the case we studied.

(3) The form of the power law is hardly influenced by changing low-k, high-k damping effects, or by changing the strength of the turbulence.

It is very encouraging that this closure scheme is capable of producing essential features associated with a turbulence spectrum. We hope to be able to compare our results with experimental studies of shear-Alfven

turbulence, when the experimental results become available. We believe that our methods should prove quite useful in studying a broad class of turbulent phenomena.

Appendix A

Our starting point, the ideal cold magnetohydrodynamic (MHD) equations are

$$\begin{aligned}
&\frac{\partial \bar{\rho}}{\partial t} = \nabla \cdot (\bar{\rho}\mathbf{U}) = 0 \\
&\bar{\rho}\left[\frac{\partial}{\partial t} + \mathbf{U}\cdot\nabla\right]\mathbf{U} = \frac{1}{4\pi}(\nabla \times \mathbf{B}) \times \mathbf{B} \qquad (A1) \\
&\frac{\partial \mathbf{B}}{\partial t} = \nabla \times (\mathbf{U} \times \mathbf{B}),
\end{aligned}$$

where $\bar{\rho}$ is the plasma density, $\mathbf{U}$ is the velocity and $\mathbf{B}$ is the magnetic field. We now separate the average (equilibrium) and the fluctuating quantities, i.e., $\bar{\rho} = \rho_0 + \rho$, $\mathbf{B} = (4\pi)^{1/2}(\mathbf{B}_0\hat{e}_z + b)$, $\mathbf{U} = \mathbf{U}$, where $(4\pi)^{1/2}B_0$ is the strong ambient axial magnetic field, ρ_0 is the average density, and ρ, $(4\pi)^{1/2}b$ and $\mathbf{U}$ are respectively the fluctuating density, magnetic field, and velocity. Evolution of ρ, $\mathbf{b}$ and $\mathbf{U}$ is determined by

$$\frac{\partial \rho}{\partial t} + \rho_0 \nabla \cdot \mathbf{U} = -(\mathbf{U}\cdot\nabla)\rho - \rho\nabla\cdot\mathbf{U}, \qquad (A2a)$$

$$\begin{aligned}
\rho_0 \frac{\partial \mathbf{U}}{\partial t} - B_0\left(\frac{\partial \mathbf{b}}{\partial z} - \nabla b_z\right) &= -\rho\frac{\partial \mathbf{U}}{\partial t} \\
&\quad - \rho_0(\mathbf{U}\cdot\nabla)\mathbf{U} + (\mathbf{b}\cdot\nabla)\mathbf{b} - \frac{\nabla b^2}{2},
\end{aligned} \qquad (A2b)$$

and

$$\begin{aligned}
-\frac{\partial \mathbf{b}}{\partial t} + B_0\left(\frac{\partial \mathbf{U}}{\partial z} - \hat{e}_z\nabla\cdot\mathbf{U}\right) &= -(\mathbf{b}\cdot\nabla)\mathbf{b} \\
&\quad + \mathbf{b}(\nabla\cdot\mathbf{U}) + (\mathbf{U}\cdot\nabla)\mathbf{b},
\end{aligned} \qquad (A2c)$$

where we have put the nonlinear terms on the right-hand side of Eq. (A2). We now consider a cylindrical plasma of axial length $2\pi R$ (to possibly

simulate a torus). Azimuthal and axial symmetry allow us to expand the fluctuating quantities as

$$f(r,\theta,z,t) = \sum_{m,n,\omega} f_{m,n,\omega}(r)\exp(i\omega t + ik_\theta r\theta + ik_z z), \qquad (A3)$$

where

$$k_z = \frac{n}{R}, \quad k_\theta = \frac{m}{r}$$

are the axial and azimuthal components of the wave-vector, and n and m are respectively the wave numbers. Making use of Eq. (A3), Eq. (A2) can be cast in the form

$$\begin{aligned} F_k\left([mu_{rk} + i\frac{\partial}{\partial r}ru_{\theta k}\right) &= -\frac{\omega}{B_0^2}\frac{\partial}{\partial r}(rN_{\theta k}) \\ &- \frac{k_z}{B_0}\frac{\partial}{\partial r}(rM_{\theta k}) + \frac{im}{B_0^2}N_{rk} + \frac{ik_z m}{B_0}M_{rk}, \end{aligned} \qquad (A4)$$

where

$$k = (m,n,\omega) = (k_\theta r, k_z R, \omega),$$
$$F_k = \frac{\omega^2}{V_A^2} - k_z^2$$

is the linear dispersion function, and $N_{\theta k}$ (N_{rk}), and $M_{\theta k}$ (M_{rk}) are respectively the Fourier transforms of the nonlinear terms of $\theta(r)$- components of Eqs. (A2b) and (A2c). Although Eq. (A4) can be subjected to the usual renormalization treatment, (and will be done at a large stage) we make a set of simplifying assumptions so that we can deal with a more perspicuous system and hence show the working of our proposed closure scheme. Some of these assumptions are a bit artificial, but we

make them for simplicity and clarity. Since we are dealing with shear Alfven turbulence, we ignore the effects of compressibility. We also assume that $|U_\theta| > |U_r|$, so that the principal nonlinearity comes from $N_{\theta k}$. We neglect all other nonlinear terms. For this model problem, Eq. (A4) reduces to

$$F_k U_{\theta k} = \frac{i\omega}{B_0^2}\rho_0 \sum_{k'} k'_\theta U_{\theta(k-k')} U_{\theta(-k')} \qquad (A5)$$

can be renormalized in a straightforward fashion to yield

$$\epsilon_k U_{\theta k} \equiv (F_k + C_k) U_{\theta k} = \tilde{U}_{\theta k} \qquad (A6)$$

and

$$C_k = \sum_{k'} \frac{\omega(\omega - \omega')(k_\theta^2 - k_\theta'^2 - k_\theta k'_\theta)}{V_A^4 (F_{k-k'} + C_{k-k'})} |U_{\theta k'}|^2,$$

where $\tilde{U}_{\theta k}$ is nonlinear incoherent source, C_k is the coherent renormalizing modification of the linear response function F_k, and $|U_{\theta k}|^2 \equiv I_{\theta k}$ is the spectrum of turbulence.

1. D. Baldwin, Rev. of Modern Phys. **49**, 1317 (1977).

2. I.B. Bernstein, E.A. Frieman, M.D. Kruskal and R.M. Kulsrud, Proc. Roy. Soc. **A224**, 17 (1958).

3. M.N. Rosenbluth and C.L. Longmire, Annals of Phys. **1** 120 (1957).

4. M.S. Loffe, R.I. Sobolev, V.G. Telkovskii, E.E. Yushmanov, Zh. Eksperim Theor. Fiz. **40**, 40 (1961) [English trans. JETP **13**, 27 (1961)].

5. C.C. Damm, J.H. Foote, A.H. Futch, Jr., A.L. Gardner, F.J. Gordon, A.L. Hunt, and R.F. Post, Phys. of Fluids **8**, 1472 (1965).

6. A.H. Futch, J.P. Holdren, J. Killeen, and A.A. Mirin, Plasma Phys. **14**, 211 (1972).

7. G.I. Dimov, V.V. Zakaidakov, and M.E. Kishinevsky, Fiz. Plasmy **2**, 597 (1976).

8. T.K. Fowler and B.G. Logan, Comments Plasma Phys. Controlled Fusion **2**, 167 (1977).

9. D.D. Ryutov, G.V. Stupakov, Pis'ma Zh. Ehksp. Teor. Fiz. **26**, p.186 (1977) [JETP Lett. **26**, p.174].

10. D.D. Ryutov and G.V. Stupakov, Fiz. Plasmy **4**, p.501, (1978) [Sov. J. Plasma Phys. **4**, p.278 (1978)].

11. D.D. Ryutov and G.V. Stupakov, Dokl. Akad. Nauk SSSR **240**, P.1086 (1978) [Sov. Phys. Dokl. **23**, p.412 (1978)].

12. N.C. Christofilis in *Proceedings of the Second United Nations International Conference on the Peaceful Uses of Atomic Energy* (United

Nations, Geneva, Switzerland, 1958) vol. 32, p.279.

13. J.J. Bzura, T.J. Fessenden, H.H. Fleischman, D.A. Phelps, A.C. Smith, and D.M. Wooldall, Phys. Rev. Lett **29**, 256 (1972).
14. J. Kesner, R.S. Post, D.K. Smith, D.E. Boldwin, and Y.C. Lee, Nucl. Fus. **22**, p.577, (1982).
15. G. Benford, D.L. Book, N.C. Christofilis, T.K. Fowler, V.K. Neil, and L.D. Pearlstein, *Proceedings of Plasma Physics and Controlled Fusion*, (IAEA, 1969) Vol. I, p.981.
16. D.B. Nelson and C.L. Hedrick, Nucl. Fusion **19**, 283 (1979).
17. N.A. Krall, Phys. Fluids **9**, 820 (1966).
18. H.L. Berk, Phys. Fluids **19**, 1255 (1976).
19. J.W. Van Dam and Y.C. Lee, *Proceedings of the EBT Ring Physics Workshop* (ORNL, Oak Ridge, 1979) Conf. 791228, p.471.
20. D.B. Nelson, Phys. Fluids **23**, 1850 (1980).
21. J.M. Greene and B. Coppi, Phys. fluids **8**, 1745 (1965).
22. H.L. Berk, Emerging Synthesis in Science.
23. R.F. Post, Phys. Fluids **4**, 902 (1961).
24. D.J. BenDaniel, Plasma Phys. **3**, 235 (1961).
25. E.E. Yushmanov, Sov. Phys. [JETP] **22**, 409 (1966).
26. D.E. Baldwin and B.G. Logan, Phys. Rev. Lett. **43**, 1318 (1979).
27. T.A. Casper, in *Summary of TMX-U Results* in 1984, Vol. 2, Chapter 6, Lawrence Livermore National Laboratory, Livermore, CA, UCID-20274 (1984).

28. K. Brau, B. Lane, J. Casey, S. Horne, J. Kesner, S.N. Golovato, J.H. Irby, R.S. Post, E. Sevillano, and D.K. Smith, Nucl. Fus.

29. J. Marilleau, T.A. Casper, E.B. Hooper, A.W. Molvik, and A.K. Sen, Bull. Am. Phys. Soc. **29**, 1393 (1984).

30. A. Sen, in *Summary of TMX-U Results* in 1984, Vol. 2, Chapter 6, Lawrence Livermore National Laboratory, Livermore, CA, UCID-20274 (1984).

31. T.C. Simonen, H.L. Berk, T.A. Casper, and C.Y. Chen, Submit to Nucl. Fusion.

32. H.L. Berk, M.N. Rosenbluth, H.V. Wong, T.M. Antonsen, and D.E. Baldwin, Fiz. Plasmy **9**, 176 (1983) [Sov. J. Plasma Phys. **9**, 108 (1983)].

33. H.L. Berk, M.N. Rosenbluth, R.H. Cohen, and W.M. Nevins, **28** 2824 (1985).

34. R.H. Cohen, W.M. Nevins, and H.L. Berk, Phys. Fluids **29**, 1578 (1986).

35. H.L. Berk and B.G. Lane, Phys Fluids **29**, 1076 (1986).

36. H.V. Wong, Phys. Fluids **25**, 1811 (1982).

37. H.L. Berk and C.Y. Chen, Phys. Fluids **31**, 137 (1987).

38. J.P. Freidberg, Rev. of Modern Phys. **54**, 801 (1982).

39. V.P. Pastukhov, Nucl. Fusion **14**, 3 (1974).

40. R. Hazeltine, Private communication.

41. J.W. Van Dam, M.N. Rosenbluth, and Y.C. Lee, Phys. Fluids **25**,

1349 (1982).

42. See, for instance, B.R. Suydam, in *Proceedings of the Second United Nations International Conference on the Peaceful Uses of Atomic Energy* Vol. 31, p.157.

43. R.R. Domingues and H.L. Berk, Phys. Fluids **27**, 1142 (1984).

44. T.M. Antonsen, Jr. and B. Lane, Phys Fluids **23**, 1205 (1980).

45. P.J. Catto, W.M. Tang, and D.E. Boldwin, Plasma Phys. **23**, 639 (1981).

46. L. Spitzer, *Physics of Fully Ionized Gases*, Interscience, New York (1962).

47. L.D. Landau, Physik, Z. Sowjetunion **10**, 154 (1936),

48. M.N. Rosenbluth, W.M. MacDonald, and D.J. Judd, Phys. Rev. **107**, 1 (1959).

49. K. Miyamoto, *Plasma Physics For Nuclear Fusion*, MIT, Massachusett (1980)

50. B.I. Cohen, R.P. Freis, and W.A. Newcomb, Phys. Fluids **29**, 1558 (1986)

51. L.D. Pearlstein, T.B. Kaiser, and W.A. Newcomb, Phys. Fluids **24**, 1326 (1981).

52. B. Lane, W.M. Nevins, R.H. Cohen, J.A. Byers, and H.L. Berk, Bull. Am. Phys. Soc. **29**, 130 (1984).

53 R.H. Kraichnan, J. Fluids Mechanics **5**, 497 (1959).

54 T.H. Dupree and D.J. Tetreault, Phys. Fluids **21**, 425 (1978).

55 P.C. Martin, E.D, Siggia, and H.A. Rose, Phys. Rev. **A8**, 423 (1973)

56 J.A. Krommes, *Handbook of Plasma Physics*, Vol. 5, ed. by A.A. Galeev and R.N. Sudan (North Holland Physics Puublishing, 1984), pp. 183, and references therein.

57 J.A. Krommes and R.G. Kleva, Phys. Fluids **22**, 2168 (1979).

58 D.F. Dubois and M. Espedal, Plas. Phys. **20**, 1209 (1978).

59 S.A. Orszag, J. Fluid Mech. **4**, 363 (1970).

60 I. Proadman and W.H. Reed, Phil. Trans. R. Soc. **A247**, 167 (1954).

61 T. Boutros-Ahali and T.H. Dupree, Phys. Fluids **24**, 1839 (1981).

62 P.W. Terry and P.H. Diamond, Phys. Fluids **28**, 1419 (1985)

63 See, for example, B.B. Kadomtsev, *Plasma Turbulence*, Academic Press, London and New York, pp. 49 (1965).

64 E. Mazzucato and A. Semet, Bull. Am. Phys. Soc. **26**, 981 (1981).

65 D.W. Ross, G.W. Chen, and S.M. Mahajan, Phys. Fluids **25**, 652 (1982)

66 S.M. Mahajan, Phys. Fluids **27**, 2238 (1984).